Neurochemical Measurements in Animal Models of Neurodegeneration and Neurotoxicity

by

Sam V. Kaplan

Submitted to the graduate degree program in Chemistry and the Graduate Faculty of the University of Kansas in partial fulfillment of the requirements for the degree of Doctor of Philosophy

_____

Chairperson: Michael A. Johnson, Ph.D.

_____

Susan M. Lunte, Ph.D.

_____

Richard S. Givens, Ph.D.

_____

Heather Desaire, Ph.D.

_____

Jeffrey Krise, Ph. D.

Date Defended: July 9, 2015

The Thesis Committee for Sam V. Kaplan

certifies that this is the approved version of the following thesis:

Neurochemical Measurements in Animal Models of Neurodegeneration and Neurotoxicity

_____

Chairperson: Michael A. Johnson

Date approved: July 9, 2015

Abstract

This dissertation is a compilation of work in which selected analytical methods, including fast-scan cyclic voltammetry at carbon-fiber microelectrodes (FSCV), were used to determine neurotransmitter release and uptake properties in animals that model neurodegenerative disease and neurotoxicity. Alterations in the release and uptake of dopamine (DA), a central nervous system neurotransmitter that plays an important role in motor function and cognition, could contribute to, as well as be a consequence of, abnormal syndromes associated with neurodegeneration and neurotoxicity. First, we describe the application of FSCV to measure DA release and uptake in animals that model post chemotherapy cognitive impairment (PCCI). PCCI is a complication of chemotherapy treatment that is characterized by a general decline in cognition affecting visual and verbal memory, attention, complex problem solving skills, and motor function. It is estimated that one third of patients who undergo chemotherapy treatment will experience cognitive impairment. To investigate how chemotherapy treatment affects these systems, FSCV at carbon-fiber microelectrodes was used to measure dopamine release and uptake in coronal brain slices of the striatum. Here, we report on two PCCI studies with rats treated with carboplatin or a cocktail containing cyclophosphamide, methotrexate, and 5-fluorouracil (CMF), both of which are composed of clinically relevant chemotherapeutic compounds. Measurements were taken from rats treated weekly with selected doses of chemotherapeutic agent and from control rats treated with saline. It was found that DA release in the striatum is attenuated in chemotherapy-treated rats. Nevertheless, overall dopamine content, measured in striatal brain lysates by high performance liquid chromatography, and reserve pool DA, measured by FSCV after pharmacological manipulation, did not significantly

change, suggesting that chemotherapy treatment impairs the dopamine release and uptake processes.

Second, we report on regional differences in DA dysregulation in transgenic Huntington's disease model mice. Huntington's disease (HD) is a fatal, neurodegenerative movement disorder that is characterized by degeneration of the striatum. It has been determined previously that electrically-evoked dopamine (DA) release is severely attenuated in the dorsolateral striatum of R6/2 HD model mice. Here, we have used fast-scan cyclic voltammetry to uncover regional differences of DA release in the striatum of R6/2 mice. We found a dorsal-to-ventral progressive gradient in single pulse DA release in 6 to 14 week-old R6/2 mice. Moreover, when applying a 120 stimulation pulse-train, we found that DA release was only significantly attenuated in the dorsal striatum. In order to see if regional differences of release were caused by the density of viable dopamine terminals, autoradiographic labeling of the dopamine transporter (DAT) with [^{3}H]WIN 35,428 was performed. It was found that the density distribution of DAT is significantly less in R6/2 mice in comparison to their WT controls; however, there were no significant regional differences. These data collectively suggest that the genetic mutation involved in HD leads to the increased vulnerability of the dorsal striatum in comparison to the ventral striatum, therefore providing insight to the disease mechanism

The final project presented here involves the development of a method to combine FSCV measurements with caged compound photo-activation. Caged compounds have been used extensively to investigate neuronal function in a variety of preparations, including cell culture, *ex vivo* tissue samples, and *in vivo*. We describe electrochemical measurements used to determine the extent of caged compound photo-activation while simultaneously measuring DA *in vitro*.

Acknowledgements

I would firstly like to thank the Department of Chemistry and The University of Kansas for providing me the opportunity to be a proud member of the Ralph N. Adams Institute of Bioanalytical Chemistry. I sincerely thank my mentor, Dr. Michael A. Johnson for your support throughout my graduate career. I thank you for your knowledge, your guidance, and your friendship. I would also like to acknowledge my committee members, Susan Lunte, Richard Givens, Heather Desaire, and Jeffrey Krise for their guidance. I would like to personally thank my current group members, of whom include Rachel Gehringer, Mimi Shin, Peter Ruggles, Thomas Field, and Meng Sun. I would also like to acknowledge my past group members including Gregory Osterhaus, Jenny Divis, and Andrea Ortiz. It's truly been a pleasure to work with, guide, and obtain all of your friendships.

To all my extended family and friends, it would be impossible to be here without you, I am very thankful to have your support. I would like to thank my grandparents Ruth and Dave Pollock for their unconditional support and also acknowledge in memory Sam and Jennie Guadagnano and Julius Kaplan. I'd lastly like to dedicate this dissertation to my parents JoAnn and the late Gary Kaplan. Mom, your continued support and unrelenting positivity has been of the utmost importance in me being in the position to complete this program.

Table of Contents

Chapter 1: Introduction

Understanding the detailed mechanisms involved in neurodegenerative disease and neurotoxic events is of critical importance in modern medicine. The ability to detect molecules involved in neuronal signaling has long since been deemed important by the bioanalytical community. For the last 50 years, voltammetry has proven to be a useful method in performing such research. Since its advent, many subsets of voltammetry have been developed to improve the ability to detect and quantify different classes of electroactive biomolecules. Fast-scan cyclic voltammetry at carbon-fiber microelectrodes (FSCV) is one such method that has been developed and has gained the favor of neuroscientists and analytical chemists for its low limits of detection, good chemical selectivity, high spatial resolution, and good temporal resolution.[1–3]

1.1 Electrochemical methods

1.1.1 Voltammetry

Voltammetry is a dynamic electroanalytical method that provides information about an analyte by measuring current as a function of an applied potential to an electrode surface. A voltammetric experiment requires at least two electrodes, a working electrode and reference electrode. As the potential at the surface of the working electrode is varied, a faradaic current response, due to analyte oxidation or reduction, is measured by an ammeter and plotted versus applied potential. A possible complication of carrying out voltammetry measurements with conventionally-sized electrodes is a drop in applied voltage at larger currents (μA or greater) in highly resistive solutions (kOhm or greater). This phenomenon, known as IR drop, is governed by Ohm's Law, E = IR where I is current and R is the solution resistance. The consequence of this potential drop is a distortion in the voltammogram. To diminish the effects of IR drop, a

three-electrode system is typically used when conventional voltammetry measurements are obtained. The three-electrode system uses an auxiliary electrode in addition to the working and reference electrodes. An auxiliary electrode is typically made of chemically inert metal, such as platinum, that allows for current to pass between the working electrode and itself. A schematic of a three electrode system can be seen in Figure 1.

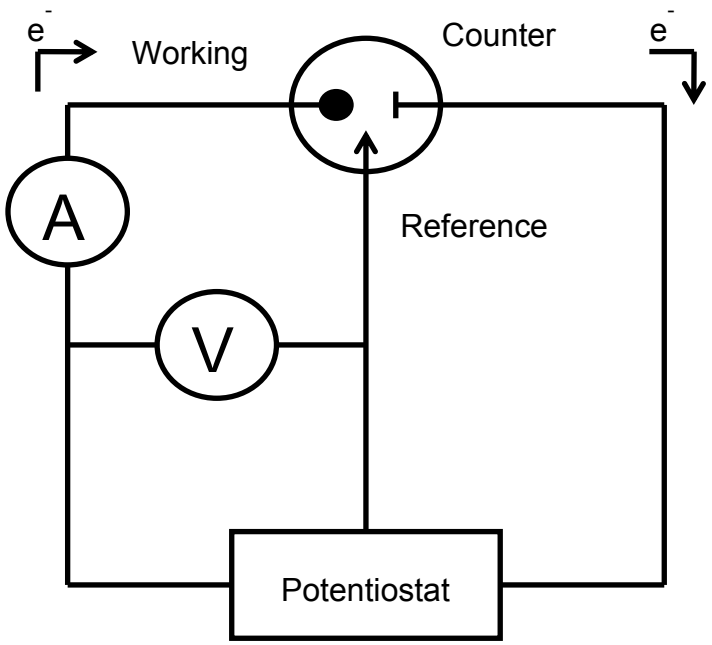

Figure 1. General schematic diagram of a three electrode system. The working, counter and reference electrodes are labeled. *A* represents an ammeter for measuring the current. *V* represents a voltmeter for measuring the voltage difference between the reference and working electrodes.

1.1.2 Cyclic Voltammetry

Cyclic voltammetry is among the most widely used electrochemical techniques and has been extensively applied to the fields of inorganic chemistry, organic chemistry, and biochemistry[4] due to its ability to qualitatively and quantitatively measure redox chemistry at an electrode surface. In cyclic voltammetry, the potential is increased from a holding potential up to the switching potential, seen as the highest voltage point in the waveform in Figure 1, and is then decreased back to the holding potential. This potential at the working electrode surface is controlled by comparison to a reference electrode As the waveform is applied, any redox events can be measured by as a current response. A plot of this current response measured at the working electrode against the applied voltage yields a cyclic voltammogram (CV). A CV provides a researcher with chemical information that includes redox mechanistic information, kinetic information, and can also be used to positively confirm the presence of the analyte of interest.

Two types of faradaic currents are detected using CV: anodic and cathodic. An anodic current is detected when analyte is oxidized as the peak potential in the waveform is approached. A cathodic current is detected during molecular reduction as the holding potential is approached. These two currents have different polarities due to opposing flow of electrons, so they peak on differing sides of the CV.[4] More information will be given on this in section 1.1.3, Fast-Scan Cyclic Voltammetry.

There are four classes of redox reactions that may occur at the electrode surface when performing CV: reversible, quasi-reversible, irreversible, and chemically irreversible reactions. Reversible redox reactions proceed such that there is an equilibrium established between the rate of oxidation and reduction at the surface of the working electrode. Electrochemical reversibility

depends on the rate of electron transfer between the electroactive species and the working electrode. A redox reaction is electrochemically reversible when the electron transfer occurs rapidly ($k_s > 0.02$ cm/s) without thermodynamic barriers.[5] To be considered electrochemically reversible, the observed difference between the oxidation and reduction potentials (as determined by the peaks in the CV) must be less than 0.058 Volts/n, where n is the number of electrons transferred per redox reaction.[5] When rate of electron transfer between the analyte and the working electrode is slow ($k_s < 5 \times 10^{-5}$ cm/s), the reaction is electrochemically irreversible. Redox reactions with intermediate rates of electron transfer are considered to be quasi-reversible.

A reversible reaction taking place at the electrode surface will obey the Nernst Equation.

$$Equation\ 1: E = E^o + \frac{RT}{nF} * \ln(\frac{[ox]}{[red]})$$

The Nernst equation describes how the concentrations of the oxidized and reduced species change as a function of the applied excitatory potential (E) where E^o is the formal reduction potential of the analyte, *R* is the universal gas constant, *n* is the number of electrons per reaction, and *F* is the faraday constant.[4]

$$Equation\ 2: i = \frac{nFAc_j{}^0\sqrt{D_j}}{\sqrt{\pi t}}$$

If the electron transfer of the redox reaction is sufficiently fast, the current measured at the electrode surface in response to the applied potential can be described by the Cottrell equation (Equation 2) where *i* is the current (*A*), *n* is the number of electrons transferred

(equivalents/mol), F is the Faraday constant, A is the area of the electrode, c_j^0 is the initial analyte concentration, D_j is the diffusion coefficient, and t is time.

The ability to stimulate and measure redox reactions as a function of the applied potential at an electrode surface has been of key importance to analytical chemists. To put it simply, the faradaic current response, whether it be oxidative or reductive (depending on the applied waveform), will be directly proportional to the concentration of the species. Cyclic voltammetry therefore provides a means to quantify electrically-active analytes.

1.1.3 Background-Subtracted Fast-scan Cyclic Voltammetry

Fast scan cyclic voltammetry (FSCV) is the most widely used method for the real-time quantification of biogenic amines.[6] Conventional CV experiments typically employ a potential at a scan rate of 100 mV/s while FSCV typically employs a scan rate in the 100-800 V/s range. Like conventional CV, in FSCV a linear sweep triangular waveform is applied to the working electrode with a controlled holding potential, which is the lowest voltage on the waveform, and a switching potential, which represents the highest voltage on the waveform.

The rapid scan rates applied in FSCV offer sub-second temporal resolution, which has made the method applicable to studying the rapid μM concentration changes involved in neuronal signaling. It is this feature, along with the high spatial resolution of microelectrodes, that has led FSCV to be extensively used to measure DA dynamics in neuronal tissue.[6–18] The description of FSCV as applied to the detection of DA will be the focus of this subsequent section. Applications of FSCV have been employed both *in vivo* in awake rats [10,19] and in rodent brain slices.[20–22] The applied waveform can be tailored for the detection of specific analytes. For example, DA oxidizes at approximately 0.6 V,[21] while many other electroactive species (e.g.

adenosine and hydrogen peroxide) oxidize at potentials above 1V.[23,24] Therefore, the waveform chosen goes to a high-enough switching potential to sufficiently oxidize DA while avoiding the oxidation of other possible interferents.

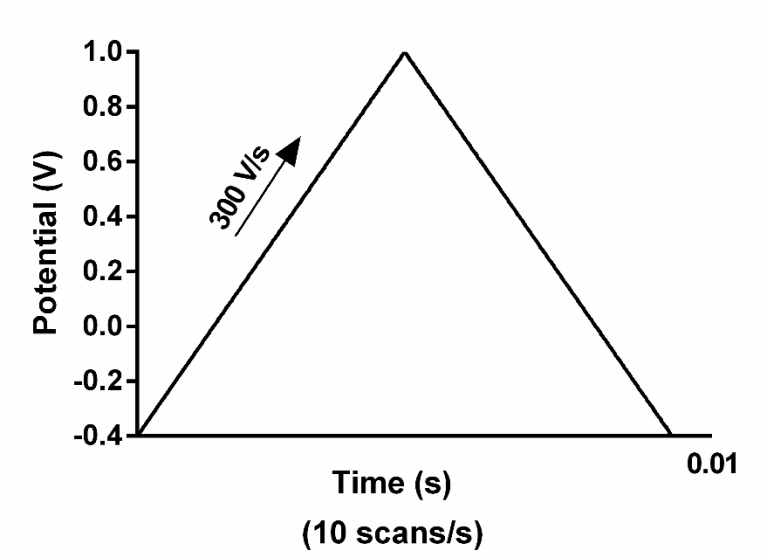

Figure 1: Typical Waveform applied For DA detection via FSCV.

As the potential at the working electrode becomes more positive, the surface becomes increasingly electron deficient. Upon reaching a voltage threshold, typically around +0.6 V (versus Ag/AgCl electrode), DA is oxidized to dopamine-o-quinone. This two-electron oxidation produces a faradaic current that is proportional to the amount of analyte present at the electrode surface. Similarly, a current is produced on the backsweep by the reduction of the dopamine-o-quinone. A typical waveform applied to a carbon-fiber microelectrode when detecting neuronal DA release consists of applying a triangular waveform ranging from -0.4V to +1.0V and back to

-0.4V (Fig. 1). A typical CV obtained for the oxidation and reduction of DA can be seen in Figure 2.

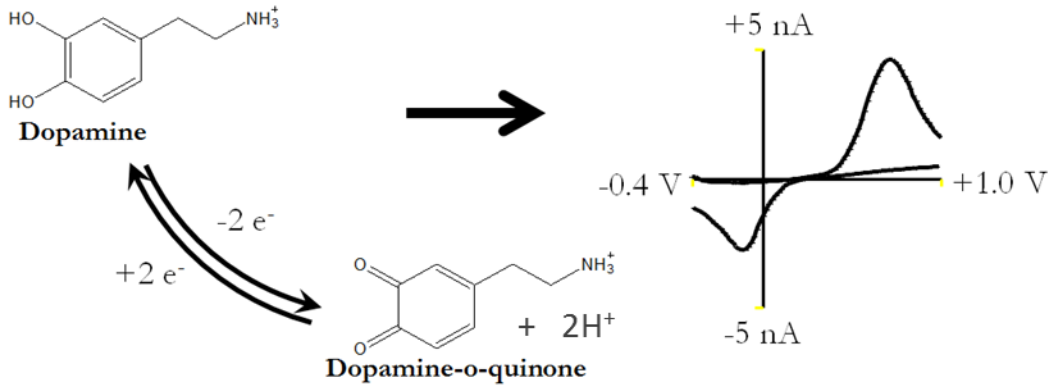

Figure 2: Cathodic and anodic currents measured with FSCV. Top, electrochemical reaction of dopamine oxidation and dopamine-o-quinone reduction. Bottom typical Cyclic voltammogram for DA oxidation and reduction.

Important features of the CV show the oxidation of DA near +0.6 V and the reduction at -0.2 V. This CV is characteristic of DA and is used as a "signature" in order to confirm the presence of DA. Quantification of analyte can be accomplished via flow-cell analysis calibration exploiting the direct relationship between current response and analyte concentration at the electrode surface.

One challenge of FSCV is that the rapid scan rates employed in FSCV lead to a large non-faradaic charging currents that are caused by rapid formation of the electrical double layer.

It is, therefore, imperative to be able to subtract the charging current to adequately reveal the faradaic current of interest within the CV. Fortunately, the charging current is consistent between scans and can be successfully subtracted out, allowing for the quantitative measurement of the faradaic current. Analyte detection and quantification is only possible after successful background subtraction.[4] A representation of this background subtraction can be seen in Figure 3.

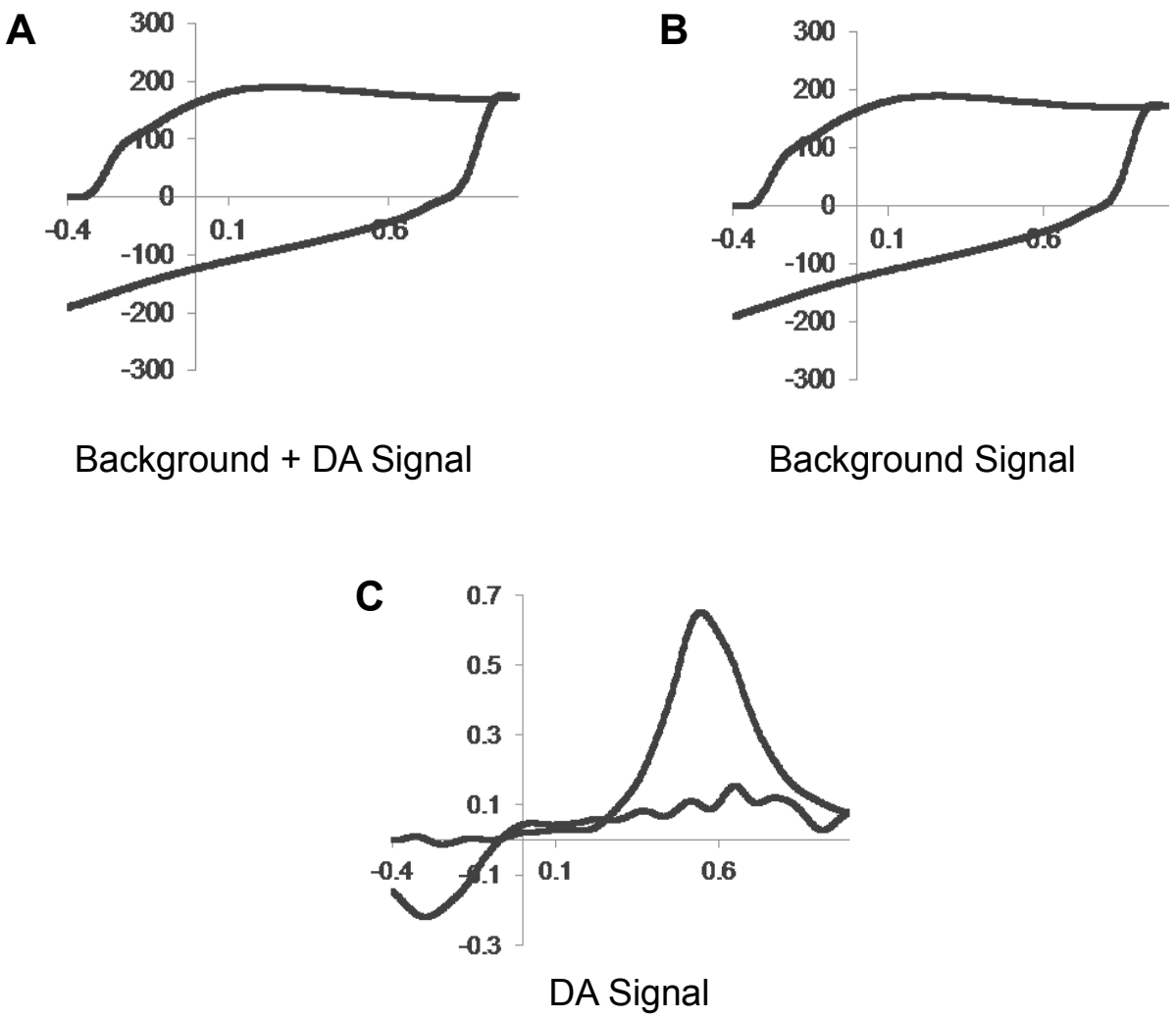

Figure 3: Background subtraction to obtain the cyclic voltammogram of dopamine. Subtracting the background signal (B) from the combined background and DA signal (A) reveals the cyclic voltamogram for DA (C).

1.2 Microelectrodes

A microelectrode is defined as an electrode with an electroactive surface on the μm scale (typically less than 25 μm in diameter).[25,26] Microelectrodes offer several advantages compared to conventional electrodes, including the ability to measure very small currents (below pA range in some instances), a small error contribution due to ohmic drop, minimization of the capacitive current when compared to conventionally "large" electrodes, and a rapid establishment of steady-state mass-transfer. [24] Moreover, the small electrode size minimizes perturbation of biological systems.

Microelectrodes were first used to probe biological systems in the 1940s for the amperometric detection of oxygen in tissues.[27] Despite being successfully used in a wide variety of tissues, their application has been most extensively applied to quantify neurotransmitter levels in neuronal tissue.[9,12,21,28,29]

Microelectrodes have been fabricated using multiple materials and geometries. Some common electrode geometries include cylinders, disks, rings, and bands.[25] Cylindrical and disk electrodes are typically made from metal micro-wires such as gold and platinum or carbon fibers. Band and ring electrodes are typically manufactured via lithography[30] or by the deposition of films and foils.[31,32] Each electrode geometry provides its own advantages and disadvantages. Diffusion is of concern when choosing an appropriate electrode geometry and each option is accompanied with its own rigorous mathematics describing this mass transport.[5] In these studies, we have used cylindrical carbon-fiber microelectrodes..

1.2.1 Carbon-Fiber Microelectrodes

Carbon-fiber microelectrodes (CMFE) have several characteristics that make them useful for obtaining measurements in brain tissue. From our experience, the sides of the carbon-fiber that we used are resistive to electrode fouling. CFMEs also have the possibility of surface modification which is not possible with many other types of materials. This property has been exploited to improve sensitivity, selectivity, and temporal resolution. [35] Another advantage, as touched upon in the previous section regarding general microelectrodes, is that carbon-fibers used for the fabrication of CFMEs are typically between 5-10μm in diameter, which minimally perturb the tissue and provides high temporal and spatial resolution.[33] The electrodes used in these studies are 5 to 7 μm in diameter and are made from carbon-fiber purchased from Goodfellow Cambridge Ltd. (Huntingdon, England). In the subsequent sections and chapters, the unmodified cylindrical CFME will be the primary analytical probe used.

Although a more detailed account of electrode fabrication can be found in the *Materials and Methods* sections of the subsequent chapters, a general fabrication description shall be noted here. CFMEs are made by first aspirating a single carbon fiber into a glass capillary. The glass is then pulled via an electrode puller to form two electrodes. After pulling, the carbon fiber is manually trimmed to a desired length from the end of the glass capillary (typically 30μm). In order to ensure a proper seal, these electrodes are dipped into an epoxy resin solution, dipped in toluene to remove excess epoxy resin, and baked to properly cure and establish a true seal. An electron micrograph of the end of a CFME can be seen in Figure 4.

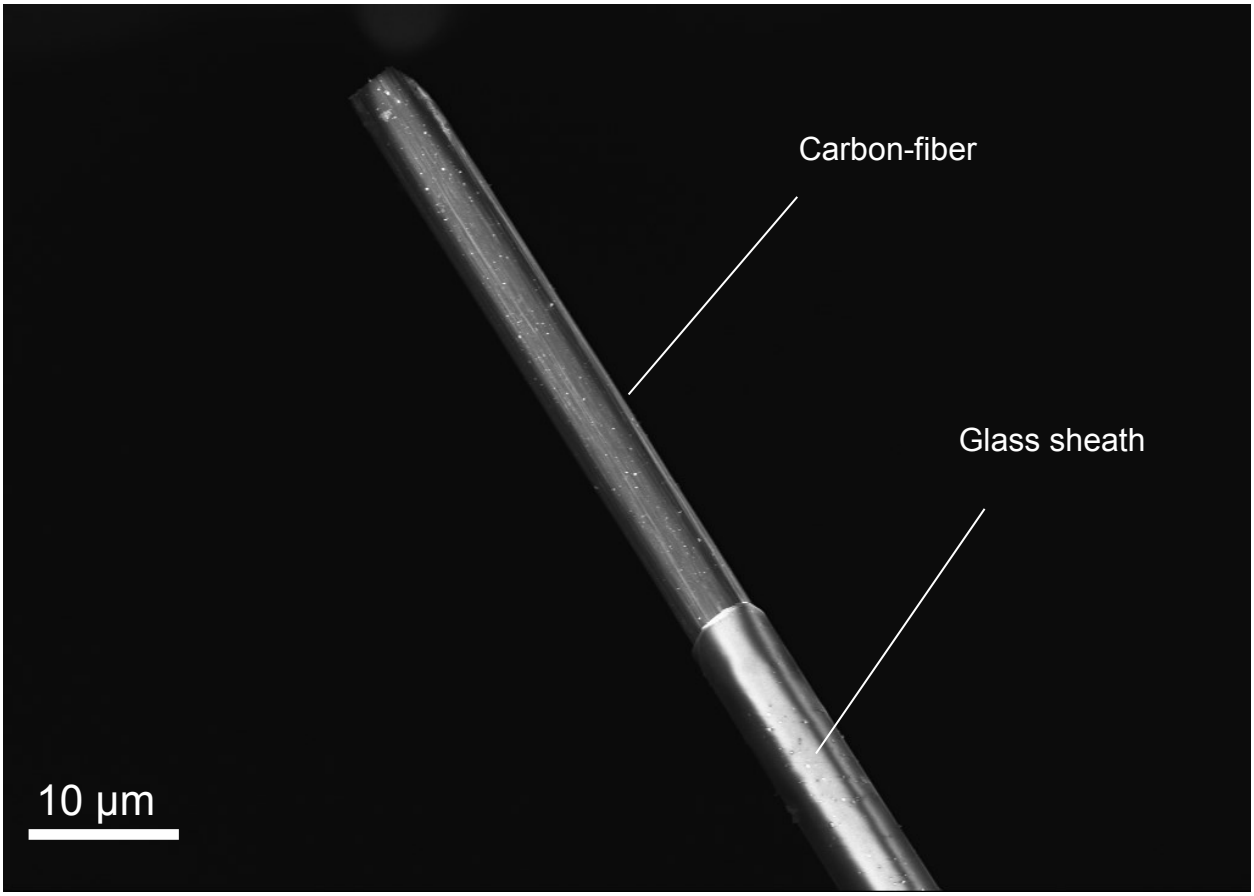

Figure 4. Scanning electron micrograph of a cylindrical CFME.

1.3 Neurotransmission

The application of electrochemical methods for the measurement of electroactive biomolecules in vivo was pioneered by Ralph N Adams at the University of Kansas. This application not only required a sound knowledge of analytical chemistry, but also required the ability to apply it to arguably one of the most complex environments in the universe (please excuse my grandiosity). In order to interpret information obtained from neurotransmitter release measurements, one must first understand the neuron itself. Although neurons vary widely in their overall shape, function, and structural features, these cells, which are responsible for the

collection and relaying of signals, contain certain general features. In the simplest of terms, a neuron contains a cell body and external projections that are used for communication. These projections are dendrites, which surround the cell body and are responsible for receiving input, and axons, which are responsible for signal output. In order to propagate a signal, a neuron's specialized ion channels will open, causing the negatively charged intercellular space to depolarize. If this depolarization crosses a threshold, it will cause an action potential that will rapidly propagate (exceeding 50m/s) along the length of the axon, leading to exocytosis of neurotransmitters into the synaptic cleft.[37] The primary analyte of interest that we measure with FSCV is DA. Upon release into the synaptic clef, DA can either interact with post-synaptic or pre-synaptic receptors, be taken up into the neuron by the DA transporter, or diffuse out of the synaptic cleft. DA that diffuses out of the synaptic cleft is available to be detected electrochemically.

1.4 Dopamine

DA is a central nervous system (CNS) neurotransmitter involved in many neurological processes that play in integral role in reward,[34] cognition,[35] and locomotor control.[35] Alterations in DA system function have been associated with many neurological disorders or outcomes that include chemically induced oxidative insult,[19] genetic modifications that model oxidative stress,[36] and neurodegenerative disease.[19,37–42] The study of how the DA system is altered in neurological disease or toxic events therefore may provide insight into the underlying mechanisms of the disease or disorder. Such insight provides valuable information that may lead to potential points of therapeutic intervention. The rest of this section will be dedicated to the relevant information regarding the dopaminergic system relevant to the studies discussed in the following chapters.

1.4.1 Dopamine Synthesis

DA synthesis occurs in the cytosol of the dopaminergic neuron, where biosynthesis begins from tyrosine. Tyrosine is supplied by dietary protein and makes its way to the brain via the blood stream. Upon crossing the blood-brain-barrier (BBB), tyrosine enters the dopaminergic neuron. Within the cytosol of the dopaminergic neuron, tyrosine is first converted to dihydroxyphenylalanine (L-DOPA) via the enzyme tyrosine hydroxylase (TH). It is important to note that this catalytic conversion is the rate limiting step in the synthesis of DA. L-DOPA is then converted to DA via the enzyme aromatic amino acid decarboxylase (AADC, dopa decarboxylase).[43] The steps listed here are visually represented in Figure 5.

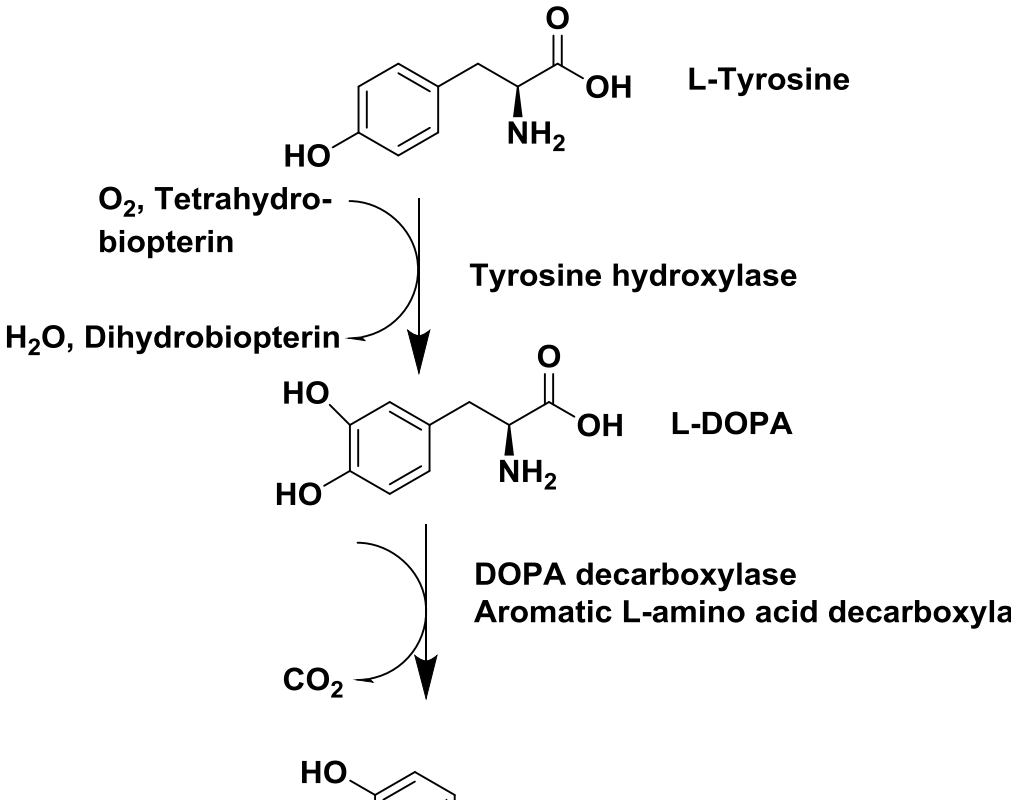

Figure 5. The biosynthesis of DA.

1.4.2 Dopamine Storage, Release, and Reuptake

Cytosolic DA is packaged into synaptic vesicles by the vesicular monoamine transporter (VMAT). Within each vesicle, the concentration of DA is roughly one to three orders of magnitude larger than the concentration within the cytosol (≈ 0.1M).[43] Within the neuron, the synaptic vesicles are held within three different pools. The generalized three-pool model of neurotransmitter-containing vesicles within neurons consists of a readily releasable pool, a recycling pool, and a reserve pool.[44–46] The readily releasable pool contains only 1-2% of vesicles within a neuron.[46] After depleting the readily releasable pool vesicles, they are

replenished by the recycling pool, which accounts for 5-20% of the total number of vesicles within the neuron.[47–49] The reserve pool contains 80-90% of the total number of vesicles within a neuron and is thought to be mobilized in response to increased levels of synaptic activity.[44–46] This three-pool model can be seen in Figure 6.

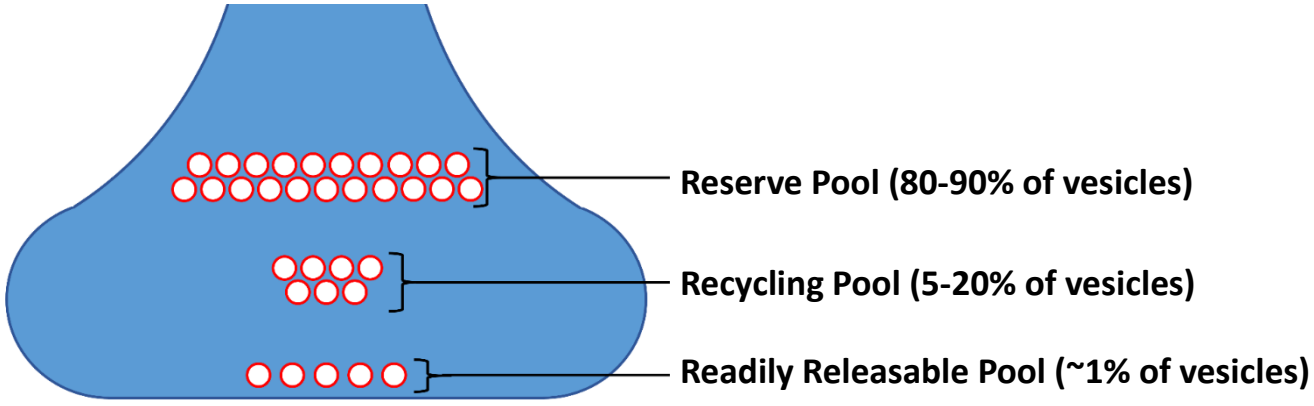

Figure 6. The three pool-pool model of DA vesicular storage

Upon receiving an action potential, the neuron undergoes specific protein conformation changes leading to the influx of Ca^{+} which leads to the release of DA via exocytosis.[43,50] Upon release, DA enters the post-synaptic cleft where it may interact with DA receptors that are present on a postsynaptic target cell or on the presynaptic membrane. The DA receptor will be further discussed in more detail in section 1.4.3.

The ability to terminate DA neurotransmission is relegated to the high-affinity dopamine transporter (DAT), which is present on the terminals of dopaminergic neurons and is responsible for removing DA from the extracellular environment.[51] The DAT is an 80 kDa protein that has 12 transmembrane segments and is a sodium and calcium dependent transporter.[52] Much interest has been given to the DAT in the past as it is the target for a series of compounds with

pharmacological promise. Certain compounds that resemble DA, such as amphetamine, are readably taken up by the DAT which leads to an increase in DA release and a stimulatory effect.[53,54] The DAT is also an extremely high affinity target for the highly addictive stimulant, cocaine, which effectively inhibits DAT leading to the extraneuronal build-up of DA.[55] The DAT has been given much attention from researchers as alterations in its function prove to have profound neurological consequences. A representative image describing the process od DA neurotransmission can be seen in Figure 7.

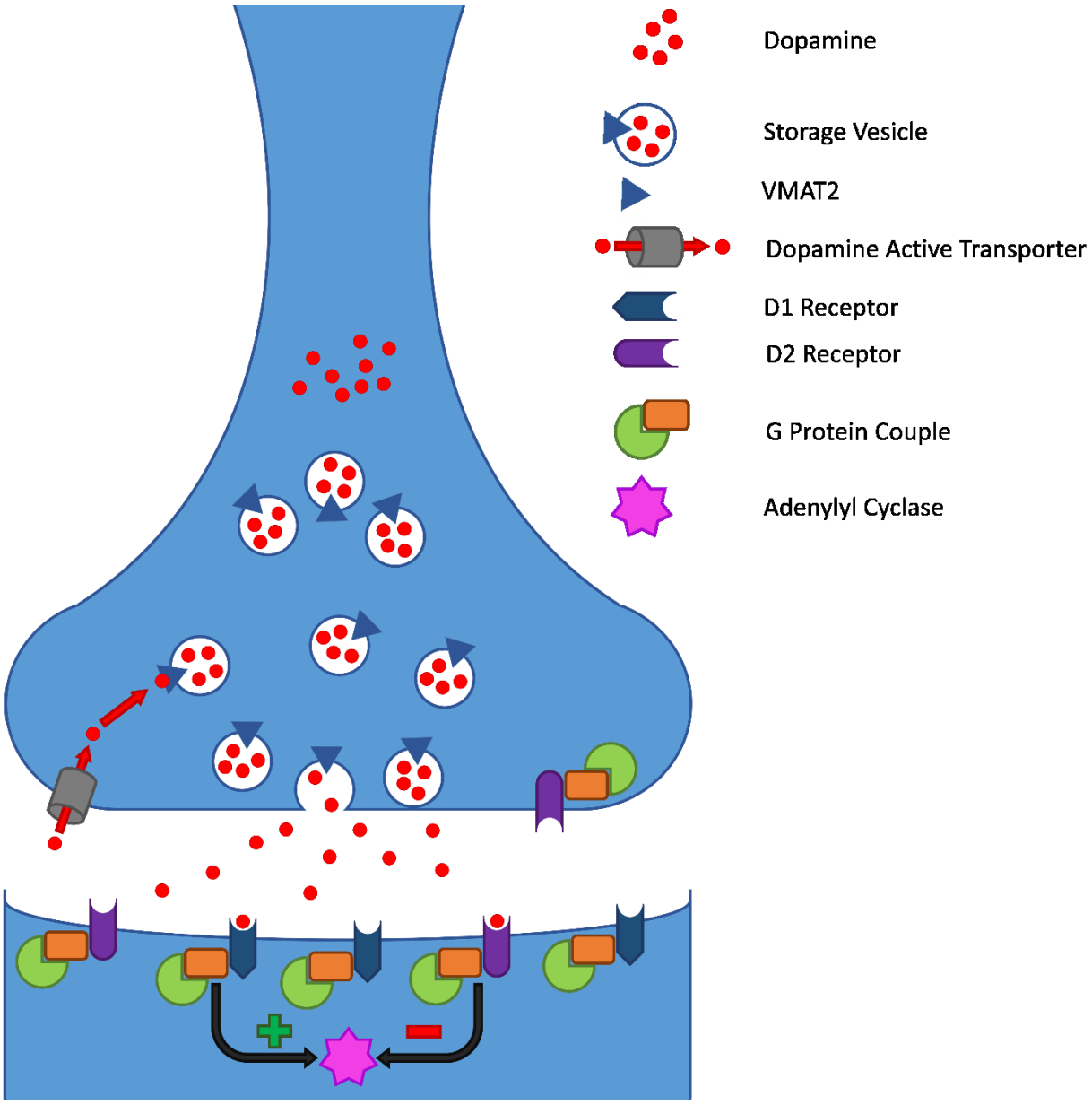

Figure 7. Dopamine release and reuptake.

1.4.3 Dopamine Receptors

Dopamine receptors are made up of two general types, known as D_1 and D_2 . There have been 6 different DA receptors identified within these two classes. The D_1 class includes receptors D_1 and D_5 while the D_2 class includes receptors D_{2short}, D_{2long}, D_3, and D_4. The D_1 and D_2 classes

of DA receptors differ in how they affect adenylyl cyclase (AC) activity. The D_1-like receptors stimulate AC activity whereas D_2-like generally inhibit it.[43] All DA receptors are G protein-coupled receptors (GPCRs) and each subtype contains considerable homology within their primary structure.[56,57] For a more in-depth look into the complex and well-studied intricacies of the DA receptor please see the review by Missale *et al*.[57]

The receptor of interest relevant to the research described in this dissertation is the DA autoreceptor. An autoreceptor is a receptor expressed on a neuron that is sensitive to the neurotransmitter released by that same neuron. DA autoreceptor activation is one of the principal mechanisms of DA regulation. These autoreceptors tend to be expressed both on the axonally and dendritically on dopaminergic neurons and therefore respond to both dendritic and terminal release. It can generally be said that all DA autoreceptors are D_2-like and involve the inhibition of AC. Stimulation of DA autoreceptors therefore tends to inhibit DA release, although their mechanism of doing so varies by location. For instance, dendritic autoreceptor stimulation generally reduces the neuronal firing rate whereas terminal autoreceptor stimulation generally inhibits DA synthesis or release.[43] The DA receptors are represented in Figure 7.

1.4.4 Dopamine Metabolism

Dopamine metabolism occurs through catalysis by some common enzymes found in the neuronal environment. The location and route of DA metabolism varies and is dependent on the cell type and brain region. The key enzymes responsible for the metabolism of DA are monoamine oxidase (MAO), aldehyde dehydrogenase (ALDH), and catechol-O-methyl transferase (COMT). Figure 7 shows the common metabolites generated by the COMT and MAO catalysis of DA. These include dihydroxyphenylacetic acid (DOPAC), homovanillic acid

(HVA), 3.4-dihydroxyphenylethanol (DOPET), and 3-methoxy-4-hydroxyphenylethanol (MOPET). Although there are quite a few metabolites of DA, DOPAC and HVA are the most abundant in the brain.[43]

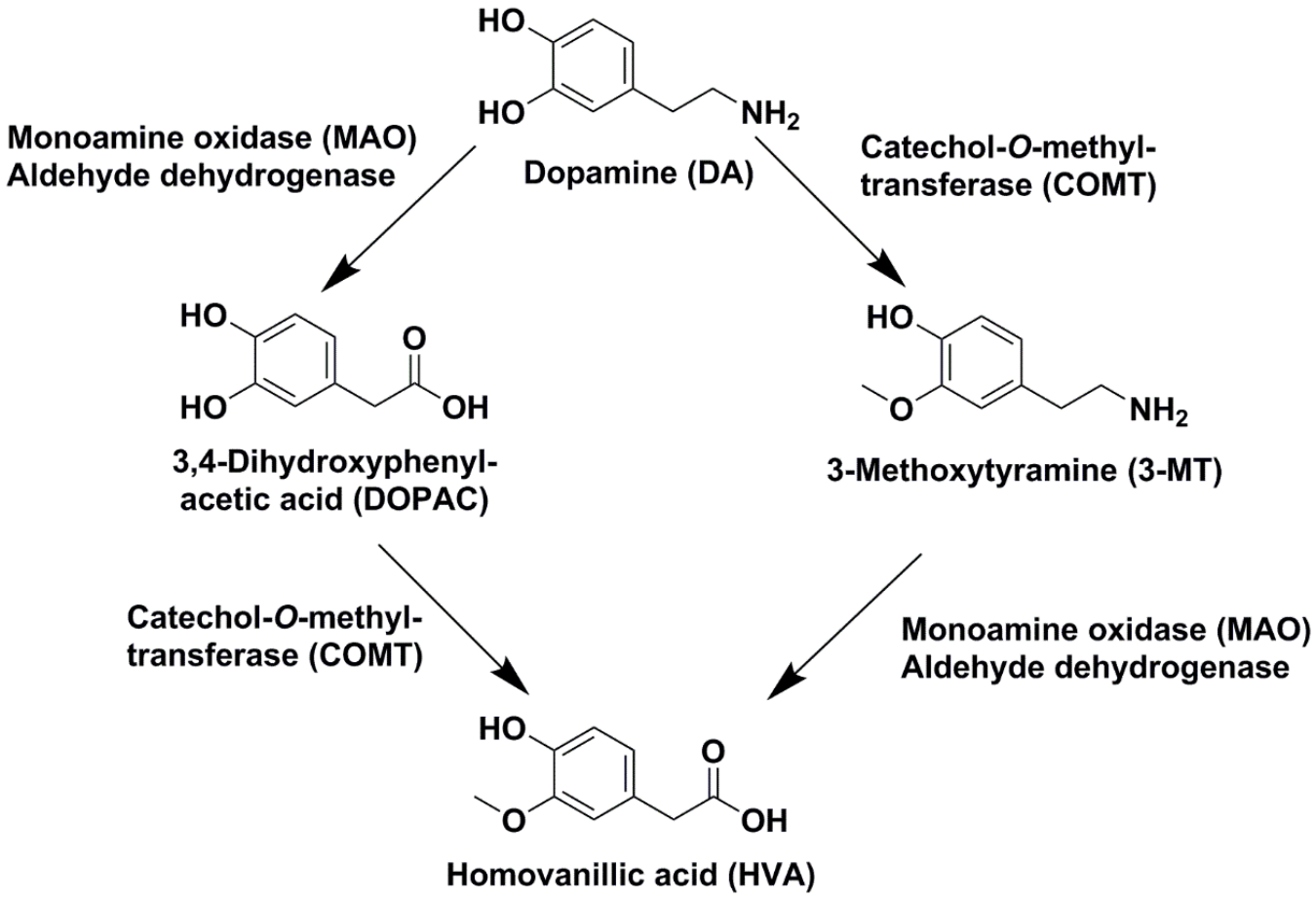

Figure 8. Commonly generated metabolites via enzyme catalysis.

1.4.5 Relevant Anatomy

All of the studies discussed in the subsequent chapters of this dissertation include using FSCV to measure DA release in the striatum of rodents. The striatum is the principal sub-nuclei of the basal ganglia, which contains a group of subcortical nuclei located in the forebrain.[58,59] The components of the dorsal basal ganglia include the striatum, the globus pallidus (GP), the entopeduncular nucleus (EP), the subthalamic nucleus (STN), the substantia nigra pars compacta (SNc), and the substantia nigra pars reticulate (SNr).[58] The ventral components of the basal ganglia include the nucleus accumbans (ventral striatum).[58] The basal ganglia is heavily innervated by dopaminergic terminals. Given the role of dopamine in motor function and cognition,[60] it is not surprising that the basal ganglia has numerous pathologies associated with DA dysregulation, including Parkinson's disease, Huntington's disease, Schizophrenia, and Tourette's syndrome.[37,61–72] The striatum is the principal component of the basal ganglia and is the largest contributor and recipient of the DA system.

The striatum consists of the caudate putamen and the nucleus accumbans (Nac). The striatum is primarily composed of GABAergic medium spiny neurons (90-95%) that are characterized by their dendritic projections covered in "spines".[58,73,74] The dopaminergic terminals within the striatum originate from two main pathways: the mesolimbic pathway from the ventral tegmental area (VTA) and the nigrostriatal pathway from the substantia nigra pars compacta (SNc). The description of DA innervation of the striatum is undoubtedly more complex than described here and for a more in-depth commentary on this subject in both humans and primates, please see Joel and Weiner.[60]

While there exists no clear neurophysiological differences in these regions, studies have identified the role of each region in controlling behavior.[79] Further, there exists an input gradient

throughout the striatum. This gradient is established by two unique dopaminergic inputs to the striatum from the mesolimbic pathway, which projects from the ventral tegmental area via A10 neurons, and nigrostriatal pathway, which projects from the substantia nigra pars compacta via A9 neurons.[80] Differing functionalities have resulted from this gradient. Motor function and execution are associated with the dorsal striatum.[75,76,78,81] The ventral striatum is associated with appetitive motivation and reinforcement learning.[77,78,82,83] In healthy humans and rats, there exists an intrinsic dorsal to ventral gradient for stimulated dopamine release.[78]

1.5 Measuring DA Release in Brain tissue

1.5.1 FSCV to Measure DA in Brain Slices

FSCV has been extensively used to quantify neurotransmitter release in brain slices obtained from rodents.[10,12,14,16,36–38,84,85] Using FSCV in brain slices for the measurement of DA release is one of the principal techniques performed and described in this work. Experimental details regarding the harvesting and maintaining of brain slices can be found in the Materials and Methods sections of the subsequent chapters. However, to briefly explain, mice or rats are deeply anesthetized by a gaseous anesthetic and decapitated. The brain is then immediately removed and placed into ice-cold artificial cerebral spinal fluid (aCSF) which, as the name would imply, is a solution made to mimic cerebral spinal fluid. This solution contains the salt content, glucose necessary to maintain metabolism, and is buffered to a physiological pH. Once the brain is sufficiently chilled, 350μm thick coronal brain slices are obtained containing the striatum. Harvested brain slices are then transferred to a perfusion chamber where oxygenated aCSF is perfused over the brain slice. The slice is warmed to physiological temperature prior to taking electrochemical measurements.

After the brain slice is allowed to equilibrate for an hour in the perfusion chamber, the electrochemical analysis can begin. The procedures for measuring DA release and uptake with background-subtracted FSCV has been described previously,[38, 39,86,87] and will be discussed in more detail in the materials and methods sections of the subsequent chapters. Briefly, a pre-calibrated cylinder carbon-fiber microelectrode is inserted 100μm into the brain slice using micromanipulators and a stereoscope. The electrode is positioned between two stimulating electrodes in the striatum. An image of a coronal brain slice containing the striatum, the stimulating electrodes, and the working electrodes can be seen in Figure 9. In order to evoke DA release, a biphasic current is applied to the stimulating electrode to initiate neuronal firing. When the neurons undergo exocytosis, DA that diffuses out of the synaptic clefts and comes in contact to the working electrode surface is detected.

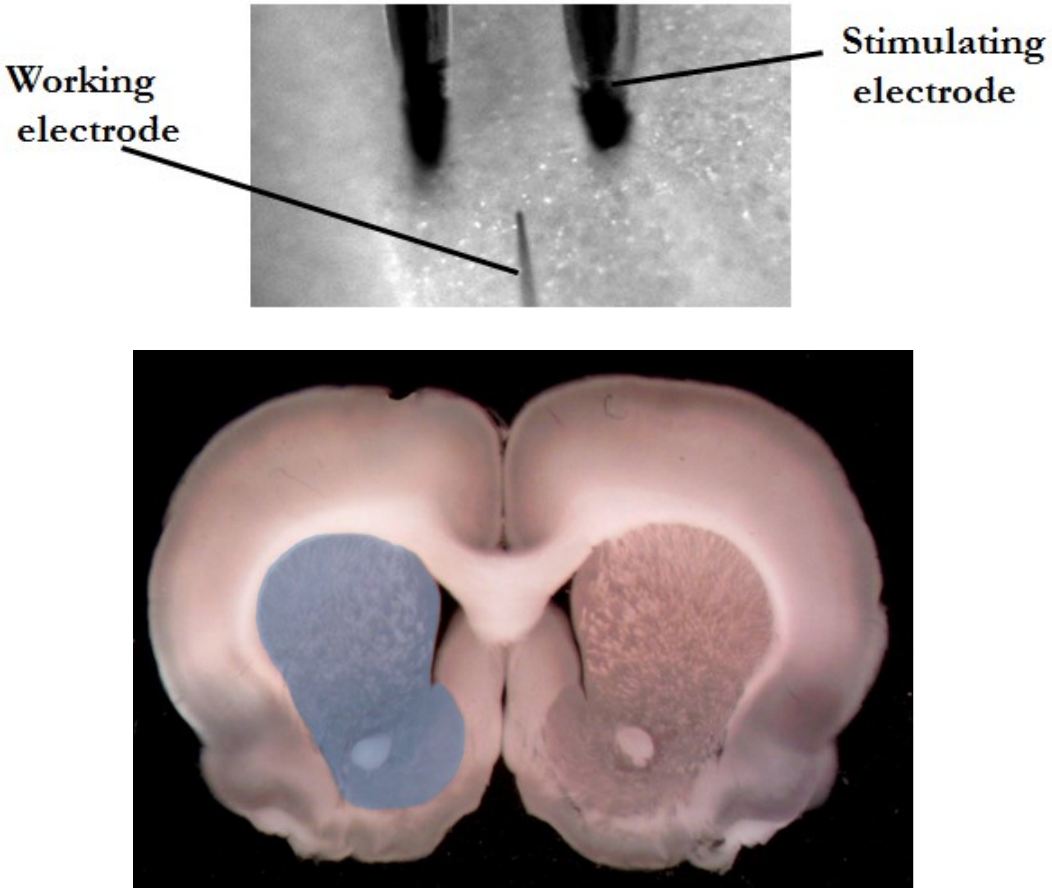

Figure 9. Image of coronal brain slice, stimulating electrodes, and working electrode. The working electrode and stimulating electrodes (top) are inserted 100μm into the striatum (shaded blue) of a coronal brain slice harvested from a male Wistar rat (bottom)

Brain slice experiments are considered to be *ex vivo* experiments, providing some of the benefits of both *in vitro* and *in vivo* experiments. Similar to an *in vitro* experiment, a researcher can easily control the microenvironment of the tissue sample. However using a brain slice allows for this environmental control while maintaining significant tissue architecture and neuronal

connections that are relevant to the brain *in vivo*. This conservation of neuronal connection/tissue architecture has allowed for pharmacological and genetic manipulations used for *in vivo* research to be reproduced in the brain slice.[88–91]

1.5.2 Relevant Pharmacology

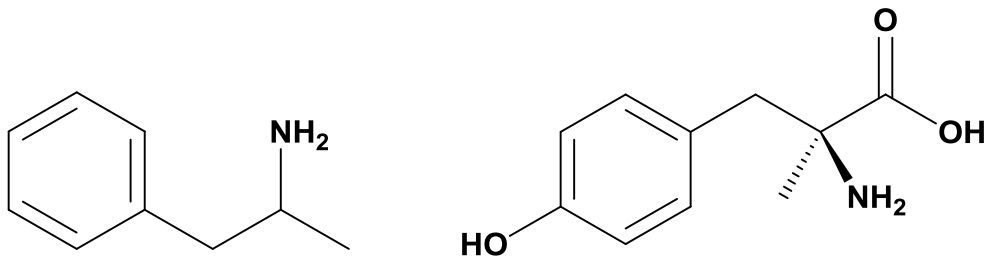

Figure 10. Structures of amphetamine and α-methyl-p-tyrosine.

Pharmacological manipulations can be used to elucidate specific mechanisms of neurotransmission. In this document two principal drugs were used to study how vesicular storage is affected in models of neurotoxicity. The two compounds used for such manipulation in this dissertation are amphetamine (1-methyl-2-phenethylamine, AMPH) and α-methyl-p-tyrosine (AMPT).

Amphetamine (1-methyl-2-phenethylamine, AMPH) is a psychostimulant used to treat attention deficit disorder and narcolepsy. It was first developed and tested on animals in the late 19th and early 20th centuries and was later synthesized in an attempt to develop powerful decongestants.[92] It was the later development in which Alles *et. al.* reported on its affects as a

powerful stimulant. It was not until the 1950s that it was determined that AMPH caused the release catecholamines in the CNS.[92]

AMPH causes DA release by a few potential mechanisms. Firstly, AMPH can be transported from the extracellular space via DAT leading to an AMPH/DA exchange which therefore causes the release of DA.[93,94] However, at high concentrations AMPH, which is extremely lipophilic,[95] readily crosses the plasma membrain of the neuron and releases DA from intraneuronal binding which will then be free to undergo release via DAT.[92] It is this mechanism that makes AMPH capable of pharmacologically liberating reserve pool DA.

AMPT is a compound that effectively blocks catecholamine synthesis by inhibiting the enzyme tyrosine hydroxylase (TH). The conversion of tyrosine to L-DOPA via TH is the first and rate limiting step in the synthesis of catecholamines. AMPT has been used clinically to control hypertension and disorders involving catecholamine excess.[96]

1.6 The Summary of the Subsequent Chapters

It was the goal of this introductory chapter to provide information regarding the background information on the methodologies used, relevant neuroscience, and relevant neuroanatomy that will aid in understanding the recurring themes in the following chapters. The subsequent chapters describe three separate projects that represent the amalgamation of my research completed throughout my career as a graduate student. The focus of Chapter 2 is how DA regulation is altered after chemotherapy treatment. This study was performed to elucidate the physiological mechanism of post-chemotherapy cognitive impairment (PCCI). The focus of Chapter 3 is to describe regional differences in DA dysregulation in the striatum of transgenic

Huntington's disease model mice. Finally, Chapter 4 describes novel methodology employing the use of photoreleasable compounds to aid in neurological research.

1.7 References

(1) Travis, E. R., and Wightman, R. M. (1998) Spatio-temporal resolution of exocytosis from individual cells. *Annu. Rev. Biophys. Biomol. Struct. 27*, 77–103.

(2) Stamford, J. A. (1990) Fast cyclic voltammetry: measuring transmitter release in "real time." *J. Neurosci. Methods 34*, 67–72.

(3) Wilson, G. S., and Johnson, M. A. (2008) In-Vivo Electrochemistry: What Can We Learn about Living Systems? *Chem. Rev. 108*, 2462–2481.

(4) Kissinger, P. T., and Heineman, W. R. (1983) Cyclic voltammetry. *J. Chem. Educ. 60*, 702.

(5) Bard, A. J., and Faulkner, L. R. (1980) Electrochemical methods: fundamentals and applications. Wiley New York.

(6) Kuhr, W. G., and Wightman, R. M. (1986) Real-time measurement of dopamine release in rat brain. *Brain Res. 381*, 168–171.

(7) Baur, J. E., Kristensen, E. W., May, L. J., Wiedemann, D. J., and Wightman, R. M. (1988) Fast-scan voltammetry of biogenic amines. *Anal. Chem. 60*, 1268–1272.

(8) Stamford, J. A., Kruk, Z. L., and Millar, J. (1986) Sub-second striatal dopamine release measured by in vivo voltammetry. *Brain Res. 381*, 351–355.

(9) Armstrong-James, M., Fox, K., Kruk, Z. L., and Millar, J. (1981) Quantitative ionophoresis of catecholamines using multibarrel carbon fibre microelectrodes. *J. Neurosci. Methods 4*, 385–406.

(10) Robinson, D. L., Venton, B. J., Heien, M. L. A. V., and Wightman, R. M. (2003) Detecting subsecond dopamine release with fast-scan cyclic voltammetry in vivo. *Clin. Chem. 49*, 1763–1773.

(11) Pihel, K., Walker, Q. D., and Wightman, R. M. (1996) Overoxidized polypyrrole-coated carbon fiber microelectrodes for dopamine measurements with fast-scan cyclic voltammetry. *Anal. Chem. 68*, 2084–2089.

(12) Heien, M. L. A. V., Johnson, M. A., and Wightman, R. M. (2004) Resolving Neurotransmitters Detected by Fast-Scan Cyclic Voltammetry. *Anal. Chem. 76*, 5697–5704.

(13) Hermans, A., Keithley, R. B., Kita, J. M., Sombers, L. A., and Wightman, R. M. (2008) Dopamine Detection with Fast-Scan Cyclic Voltammetry Used with Analog Background Subtraction. *Anal. Chem. 80*, 4040–4048.

(14) Garris, P. A., and Wightman, R. M. (1995) Regional differences in dopamine release, uptake, and diffusion measured by fast-scan cyclic voltammetry, in *Voltammetric Methods in Brain Systems*, pp 179–220. Springer.

(15) Zachek, M. K., Hermans, A., Wightman, R. M., and McCarty, G. S. (2008) Electrochemical dopamine detection: Comparing gold and carbon fiber microelectrodes using background subtracted fast scan cyclic voltammetry. *J. Electroanal. Chem. 614*, 113–120.

(16) Walker, Q. D., Rooney, M. B., Wightman, R. M., and Kuhn, C. M. (1999) Dopamine release and uptake are greater in female than male rat striatum as measured by fast cyclic voltammetry. *Neuroscience 95*, 1061–1070.

(17) Wightman, R. M. (2006) Probing Cellular Chemistry in Biological Systems with Microelectrodes. *Science 311*, 1570–1574.

(18) Wightman, R. M., Amatore, C., Engstrom, R. C., Hale, P. D., Kristensen, E. W., Kuhr, W. G., and May, L. J. (1988) Real-time characterization of dopamine overflow and uptake in the rat striatum. *Neuroscience 25*, 513–523.

(19) Kraft, J. C., Osterhaus, G. L., Ortiz, A. N., Garris, P. A., and Johnson, M. A. (2009) In vivo dopamine release and uptake impairments in rats treated with 3-nitropropionic acid. *Neuroscience 161*, 940–949.

(20) Boulton, A. A., Baker, G. B., and Adams, R. N. (Eds.). (1995) Fast Cyclic Voltammetry in Brain Slices - Springer. Humana Press.

(21) John, C. E., and Jones, S. R. (2007) Fast Scan Cyclic Voltammetry of Dopamine and Serotonin in Mouse Brain Slices, in *Electrochemical Methods for Neuroscience* (Michael, A. C., and Borland, L. M., Eds.). CRC Press, Boca Raton (FL).

(22) Maina, F. K., Khalid, M., Apawu, A. K., and Mathews, T. A. (2012) Presynaptic dopamine dynamics in striatal brain slices with fast-scan cyclic voltammetry. *J. Vis. Exp. JoVE*.

(23) Sanford, A. L., Morton, S. W., Whitehouse, K. L., Oara, H. M., Lugo-Morales, L. Z., Roberts, J. G., and Sombers, L. A. (2010) Voltammetric Detection of Hydrogen Peroxide at Carbon Fiber Microelectrodes. *Anal. Chem. 82*, 5205–5210.

(24) Cechova, S., and Venton, B. J. (2008) Transient adenosine efflux in the rat caudate–putamen. *J. Neurochem. 105*, 1253–1263.

(25) Kissinger, P., and Heineman, W. R. (1996) Laboratory Techniques in Electroanalytical Chemistry, revised and expanded. CRC press.

(26) Fleischmann, M., and Pons, S. (1987) The behavior of microelectrodes. *Anal. Chem. 59*, 1391A–1399A.

(27) Davies, P. W. (1942) Microelectrodes for Measuring Local Oxygen Tension in Animal Tissues. *Rev. Sci. Instrum. 13*, 524.

(28) Adams, R. N. (1976) Probing brain chemistry with electroanalytical techniques. *Anal. Chem. 48*, 1126A–1138A.

(29) Adams, R. N. (1990) In vivo electrochemical measurements in the CNS. *Prog. Neurobiol. 35*, 297–311.

(30) Chidsey, C. E., Feldman, B. J., Lundgren, C., and Murray, R. W. (1986) Micrometer-spaced platinum interdigitated array electrode: Fabrication, theory, and initial use. *Anal. Chem. 58*, 601–607.

(31) Wehmeyer, K. R., Deakin, M. R., and Wightman, R. M. (1985) Electroanalytical properties of band electrodes of submicrometer width. *Anal. Chem. 57*, 1913–1916.

(32) Bartelt, J. E., Deakin, M. R., Amatore, C., and Wightman, R. M. (1988) Construction and use of paired and triple band microelectrodes in solutions of low ionic strength. *Anal. Chem. 60*, 2167–2169.

(33) Ewing, A. G., Dayton, M. A., and Wightman, R. M. (1981) Pulse voltammetry with microvoltammetric electrodes. *Anal. Chem. 53*, 1842–1847.

(34) Schultz, W. (2002) Getting Formal with Dopamine and Reward. *Neuron 36*, 241–263.

(35) Bäckman, L., Nyberg, L., Lindenberger, U., Li, S.-C., and Farde, L. (2006) The correlative triad among aging, dopamine, and cognition: Current status and future prospects. *Neurosci. Biobehav. Rev. 30*, 791–807.

(36) Ortiz, A. N., Oien, D. B., Moskovitz, J., and Johnson, M. A. (2011) Quantification of reserve pool dopamine in methionine sulfoxide reductase A null mice. *Neuroscience 177*, 223–229.

(37) Johnson, M. A., Rajan, V., Miller, C. E., and Wightman, R. M. (2006) Dopamine release is severely compromised in the R6/2 mouse model of Huntington's disease. *J. Neurochem. 97*, 737–746.

(38) Ortiz, A. N., Kurth, B. J., Osterhaus, G. L., and Johnson, M. A. (2010) Dysregulation of intracellular dopamine stores revealed in the R6/2 mouse striatum. *J. Neurochem. 112*, 755–761.

(39) Ortiz, A. N., Osterhaus, G. L., Lauderdale, K., Mahoney, L., Fowler, S. C., von Hörsten, S., Riess, O., and Johnson, M. A. (2012) Motor function and dopamine release measurements in transgenic Huntington's disease model rats. *Brain Res. 1450*, 148–156.

(40) Liberatore, G. T., Jackson-Lewis, V., Vukosavic, S., Mandir, A. S., Vila, M., McAuliffe, W. G., Dawson, V. L., Dawson, T. M., and Przedborski, S. (1999) Inducible nitric oxide synthase stimulates dopaminergic neurodegeneration in the MPTP model of Parkinson disease. *Nat. Med. 5*, 1403–1409.

(41) Masliah, E. (2000) Dopaminergic Loss and Inclusion Body Formation in -Synuclein Mice: Implications for Neurodegenerative Disorders. *Science 287*, 1265–1269.

(42) Morgan, D. G., May, P. C., and Finch, C. E. (1987) Dopamine and serotonin systems in human and rodent brain: effects of age and neurodegenerative disease. *J. Am. Geriatr. Soc.*

(43) Elsworth, J. D., and Roth, R. H. (1997) Dopamine synthesis, uptake, metabolism, and receptors: relevance to gene therapy of Parkinson's disease. *Exp. Neurol. 144*, 4–9.

(44) Neves, G., and Lagnado, L. (1999) The kinetics of exocytosis and endocytosis in the synaptic terminal of goldfish retinal bipolar cells. *J. Physiol. 515*, 181–202.

(45) Zucker, R. S., and Regehr, W. G. (2002) S HORT -T ERM S YNAPTIC P LASTICITY. *Annu. Rev. Physiol. 64*, 355–405.

(46) Rizzoli, S. O., and Betz, W. J. (2005) Synaptic vesicle pools. *Nat. Rev. Neurosci. 6*, 57–69.

(47) Harata, N., Ryan, T. A., Smith, S. J., Buchanan, J., and Tsien, R. W. (2001) Visualizing recycling synaptic vesicles in hippocampal neurons by FM 1-43 photoconversion. *Proc. Natl. Acad. Sci. 98*, 12748–12753.

(48) Kuromi, H., and Kidokoro, Y. (2003) Two synaptic vesicle pools, vesicle recruitment and replenishment of pools at the Drosophila neuromuscular junction. *J. Neurocytol. 32*, 551–565.

(49) Richards, D. A., Guatimosim, C., Rizzoli, S. O., and Betz, W. J. (2003) Synaptic vesicle pools at the frog neuromuscular junction. *Neuron 39*, 529–541.

(50) Kelly, R. B. (1993) Storage and release of neurotransmitters. *Cell 72*, 43–53.

(51) Garris, P. A., and Wightman, R. M. (1994) Different kinetics govern dopaminergic transmission in the amygdala, prefrontal cortex, and striatum: an in vivo voltammetric study. *J. Neurosci. Off. J. Soc. Neurosci. 14*, 442–450.

(52) Chen, N., and Reith, M. E. (2000) Structure and function of the dopamine transporter. *Eur. J. Pharmacol. 405*, 329–339.

(53) Jones, S. R., Gainetdinov, R. R., Wightman, R. M., and Caron, M. G. (1998) Mechanisms of amphetamine action revealed in mice lacking the dopamine transporter. *J. Neurosci. 18*, 1979–1986.

(54) Miller, G. W., Gainetdinov, R. R., Levey, A. I., and Caron, M. G. (1999) Dopamine transporters and neuronal injury. *Trends Pharmacol. Sci. 20*, 424–429.

(55) Pomara, C., Cassano, T., D'Errico, S., Bello, S., Romano, A. D., Riezzo, I., and Serviddio, G. (2012) Data available on the extent of cocaine use and dependence: biochemistry, pharmacologic effects and global burden of disease of cocaine abusers. *Curr. Med. Chem. 19*, 5647–5657.

(56) Probst, W. C., Snyder, L. A., Schuster, D. I., Brosius, J., and Sealfon, S. C. (1992) Sequence alignment of the G-protein coupled receptor superfamily. *DNA Cell Biol. 11*, 1–20.

(57) Missale, C., Nash, S. R., Robinson, S. W., Jaber, M., and Caron, M. G. (1998) Dopamine receptors: from structure to function. *Physiol. Rev. 78*, 189–225.

(58) Bolam, J. P., Hanley, J. J., Booth, P. A. C., and Bevan, M. D. (2000) Synaptic organisation of the basal ganglia. *J. Anat. 196*, 527–542.

(59) Gerfen, C. R. (1992) The neostriatal mosaic: multiple levels of compartmental organization in the basal ganglia. *Annu. Rev. Neurosci. 15*, 285–320.

(60) Joel, D., and Weiner, I. (2000) The connections of the dopaminergic system with the striatum in rats and primates: an analysis with respect to the functional and compartmental organization of the striatum. *Neuroscience 96*, 451–474.

(61) Albin, R. L., Young, A. B., and Penney, J. B. (1989) The functional anatomy of basal ganglia disorders. *Trends Neurosci. 12*, 366–375.

(62) DeLong, M. R., and Georgopoulos, A. P. (2011) Motor functions of the basal ganglia. *Compr. Physiol.*

(63) DeLong, M. R., and Wichmann, T. (1993) Basal ganglia-thalamocortical circuits in Parkinsonian signs. *Clin. Neurosci. 1*, 18–26.

(64) Goldman-Rakic, P. S., and Selemon, L. D. (1990) New frontiers in basal ganglia research. *Trends Neurosci. 13*, 241–244.

(65) Graybiel, A. M. (1990) Neurotransmitters and neuromodulators in the basal ganglia. *Trends Neurosci. 13*, 244–254.

(66) Marden, C. D. (1982) The mysterious motor functions of the basal ganglia. *Neurology 32*, 514–539.

(67) Paladini, C. A., and Tepper, J. M. (1999) GABAA and GABAB antagonists differentially affect the firing pattern of substantia nigra dopaminergic neurons in vivo. *Synapse 32*, 165–176.

(68) Penney, J. B., and Young, A. B. (1983) Speculations on the functional anatomy of basal ganglia disorders. *Annu. Rev. Neurosci. 6*, 73–94.

(69) Penney, J. B., and Young, A. B. (1986) Striatal inhomogeneities and basal ganglia function. *Mov. Disord. 1*, 3–15.

(70) Robbins, T. W., and Brown, V. J. (1990) The role of the striatum in the mental chronometry of action: a theoretical review. *Rev. Neurosci. 2*, 181–214.

(71) Swerdlow, N. R., and Koob, G. F. (1987) Dopamine, schizophrenia, mania, and depression: toward a unified hypothesis of cortico-striatopallido-thalamic function. *Behav. Brain Sci. 10*, 197–208.

(72) André, V. M., Cepeda, C., and Levine, M. S. (2010) Dopamine and Glutamate in Huntington's Disease: A Balancing Act. *CNS Neurosci. Ther. 16*, 163–178.

(73) Kemp, J. M., and Powell, T. P. S. (1970) The cortico-striate projection in the monkey. *Brain 93*, 525–546.

(74) Wilson, C. J., and Groves, P. M. (1980) Fine structure and synaptic connections of the common spiny neuron of the rat neostriatum: a study employing intracellular injection of horseradish peroxidase. *J. Comp. Neurol. 194*, 599–615.

(75) Volkow, N. D., Wang, G.-J., Fowler, J. S., Gatley, S. J., Logan, J., Ding, Y.-S., Hitzemann, R., and Pappas, N. (1998) Dopamine transporter occupancies in the human brain induced by therapeutic doses of oral methylphenidate. *Am. J. Psychiatry 155*, 1325–1331.

(76) Palmiter, R. D. (2008) *Dopamine Signaling in the Dorsal Striatum Is Essential for Motivated Behaviors*. *Ann. N. Y. Acad. Sci. 1129*, 35–46.

(77) Jocham, G., Klein, T. A., and Ullsperger, M. (2011) Dopamine-Mediated Reinforcement Learning Signals in the Striatum and Ventromedial Prefrontal Cortex Underlie Value-Based Choices. *J. Neurosci. 31*, 1606–1613.

(78) Calipari, E. S., Huggins, K. N., Mathews, T. A., and Jones, S. R. (2012) Conserved dorsal–ventral gradient of dopamine release and uptake rate in mice, rats and rhesus macaques. *Neurochem. Int. 61*, 986–991.

(79) Voorn, P., Vanderschuren, L. J. M. ., Groenewegen, H. J., Robbins, T. W., and Pennartz, C. M. . (2004) Putting a spin on the dorsal–ventral divide of the striatum. *Trends Neurosci. 27*, 468–474.

(80) Zahm, D. S., Cheng, A. Y., Lee, T. J., Ghobadi, C. W., Schwartz, Z. M., Geisler, S., Parsely, K. P., Gruber, C., and Veh, R. W. (2011) Inputs to the midbrain dopaminergic complex in the rat, with emphasis on extended amygdala-recipient sectors. *J. Comp. Neurol. 519*, 3159–3188.

(81) Reep, R. L., Cheatwood, J. L., and Corwin, J. V. (2003) The associative striatum: Organization of cortical projections to the dorsocentral striatum in rats. *J. Comp. Neurol. 467*, 271–292.

(82) Kelley, A. E. (2004) Ventral striatal control of appetitive motivation: role in ingestive behavior and reward-related learning. *Neurosci. Biobehav. Rev. 27*, 765–776.

(83) Lynd-Balta, E., and Haber, S. N. (1994) The organization of midbrain projections to the ventral striatum in the primate. *Neuroscience 59*, 609–623.

(84) Budygin, E. A., Kilpatrick, M. R., Gainetdinov, R. R., and Wightman, R. M. (2000) Correlation between behavior and extracellular dopamine levels in rat striatum: comparison of microdialysis and fast-scan cyclic voltammetry. *Neurosci. Lett. 281*, 9–12.

(85) Kume-Kick, J., and Rice, M. E. (1998) Dependence of dopamine calibration factors on media Ca 2+ and Mg 2+ at carbon-fiber microelectrodes used with fast-scan cyclic voltammetry. *J. Neurosci. Methods 84*, 55–62.

(86) Jackson, B. P., Dietz, S. M., and Wightman, R. M. (1995) Fast-scan cyclic voltammetry of 5-hydroxytryptamine. *Anal. Chem. 67*, 1115–1120.

(87) Hashemi, P., Danoski, E., Petrovic, J., Keithley, R. B., and Wightman, R. M. (2009) Voltammetric Detection of 5-Hydroxytryptamine Release in the Rat Brain. *Anal. Chem. 81*, 9462–9471.

(88) Cho, S. (2004) Spatiotemporal evidence of apoptosis-mediated ischemic injury in organotypic hippocampal slice cultures. *Neurochem. Int. 45*, 117–127.

(89) Pringle, A. K., Sundstrom, L. E., Wilde, G. J. C., and Williams, L. R. (1996) Brain-derived neurotrophic factor, but not neurotrophin-3, prevents ischaemia-induced neuronal cell death in organotypic rat hippocampal slice cultures. *Neurosci. Lett. 211*, 203–206.

(90) Ray, A. M., Owen, D. E., Evans, M. L., Davis, J. B., and Benham, C. D. (2000) Caspase inhibitors are functionally neuroprotective against oxygen glucose deprivation induced CA1 death in rat organotypic hippocampal slices. *Brain Res. 867*, 62–69.

(91) Cho, S., Wood, A., and Bowlby, M. R. (2007) Brain slices as models for neurodegenerative disease and screening platforms to identify novel therapeutics. *Curr. Neuropharmacol. 5*, 19.

(92) Fleckenstein, A. E., Volz, T. J., Riddle, E. L., Gibb, J. W., and Hanson, G. R. (2007) New Insights into the Mechanism of Action of Amphetamines. *Annu. Rev. Pharmacol. Toxicol. 47*, 681–698.

(93) Fischer, J. F., and Cho, A. K. (1979) Chemical release of dopamine from striatal homogenates: evidence for an exchange diffusion model. *J. Pharmacol. Exp. Ther. 208*, 203–209.

(94) Liang, N. Y., and Rutledge, C. O. (1982) Comparison of the release of [3 H] dopamine from isolated corpus striatum by amphetamine, fenfluramine and unlabelled dopamine. *Biochem. Pharmacol. 31*, 983–992.

(95) Mack, F., and Bönisch, H. (1979) Dissociation constants and lipophilicity of catecholamines and related compounds. *Naunyn. Schmiedebergs Arch. Pharmacol. 310*, 1–9.

(96) Brogden, R. N., Heel, R. C., Speight, T. M., and Avery, G. S. (1981) α-Methyl-p-tyrosine: a review of its pharmacology and clinical use. *Drugs 21*, 81–89.

Chapter 2. The role of DA Regulation in Post-Chemotherapy Cognitive Impairment

Alterations in DA release and uptake as a result of chemotherapy treatment in rats is discussed in this chapter. The results presented regarding carboplatin-treated rats were recently accepted for publication in *ACS Chemical Neuroscience*.

2.1 Introduction to PCCI

The use of chemotherapy for the treatment of cancer has proven to be clinically essential. Unfortunately, chemotherapeutic treatment approaches, while effective in killing cancer cells, are also toxic to other cell populations in the body. This toxicity has been addressed to a certain extent and has led to alterations in chemotherapy strageties with the goal of maximizing effective treatment while minimizing side effects. Nevertheless, chemotherapy leads to multiple side effects that decrease a patients' quality of life not only during treatment, but also long after the treatment has concluded. It has been determined that cells in the central nervous system (CNS) are particularly vulnerable to the effects of chemotherapy. This vulnerability applies to both dividing and non-dividing cell populations after both localized and peripheral treatment with chemotherapy.[1–7]

Post-chemotherapy cognitive impairment (PCCI), also known as "chemobrain," is a syndrome caused by CNS toxicity as a result of chemotherapy agents.[8] The term is representative of any alterations in cognition as a direct result of chemotherapy treatment. Improvements in cancer treatment and early detection capabilities have made chemobrain more abundant and of greater relevance to the medical community. Past studies have revealed that 18% of breast cancer patients that receive standard chemotherapy treatment[9] and 30% of all cancer patients that

receive high level chemotherapy treatment experience chemobrain.[10] Additionally, up to one-third of females who have undergone chemotherapy treatment for breast cancer report symptoms of PCCI.[11] Various alterations in neurological function that occur with chemobrain include loss of verbal/visual memory, a decrease in mental flexibility, attention deficits, and a loss of motor function.[12,13]

Although the underlying causes of chemobrain are still unknown, a variety of mechanisms have been proposed. One possibility is that the expression of genes that heighten the probability of getting cancer may also increase the likelihood for vulnerability to the negative side effects of chemotherapy treatment.[14] These genetic factors include blood brain barrier dysfunction, impaired DNA repair mechanisms, and dysregulation of the immune system.[14–18] It has also been proposed that chemotherapy-induced DNA damage can lead to an increase in cytokine production that promotes a chronic state of inflammation leading to cognitive impairments.[19–22] Chemobrain may also be caused, in part, by the disruption of blood flow throughout the vasculature of the brain. This phenomenon could result in ischemia, which may directly affect cognition due to oxidative stress.[23] Moreover, it has been suggested that the inherent toxicity of many chemotherapeutic agents may impair neurotransmitter signaling.[14] Both dividing and non-dividing progenitor cells and oligodendrocytes in the brain have also been shown to be highly sensitive to some chemotherapeutics, even more so than the cancer itself.[24] Exposure to chemotherapeutics resulting in oligodendrocyte dysfunction could lead to downstream effects similar to chemobrain since these cells are responsible for forming myelin sheaths. The destruction or damaging of these cells might slow down the speed of neural impulse propagation, therefore contributing to the cognitive impairments associated with chemobrain.

2.1.1 PCCI and Dopamine

Dopamine (DA) is a CNS neurotransmitter involved in many neurological functions, including reward,[25] cognition,[26] and locomotor control.[26] Alterations in DA system function have been observed in response to chemically induced oxidative insult,[27] genetic modifications that model oxidative stress,[28] and neurodegenerative disease.[27,29–34] We therefore hypothesized that treatment with chemotherapeutic agents would result in alterations in DA release and uptake. The identification of such impairments could have important consequences for the cognitive processes associated with DA signaling and may imply that other neurotransmitter systems could also be affected.

Potential treatment to alleviate or prevent chemobrain has supported DA's potential role in the disorder. Psychostimulants have proven to be somewhat successful in symptomatic treatment. For example, methylphenidate, a DA uptake inhibitor typically used to treat ADHD, has been successfully used to improve cognitive function.[35–37] Another study performed by Kohli *et al.* involved the treatment of breast cancer patients with modafinil, which is a drug used to promote wakefulness and is typically used to treat narcolepsy. This study found that patients who received 200mg of modafinil showed a significant improvement in speed memory and attention skills in comparison to their placebo controls.[38] The fact that DA reuptake inhibitors may alleviate the cognitive impairments associated with chemobrain supported our hypothesis, therefore providing justification to further investigate how DA dysregulation may be implicated in chemobrain.

2.1.2 Animal Models of PCCI

Few studies addressing chemobrain using animal models have been published. The studies that have been done have suggested that the majority of types of chemotherapeutics, including DNA cross-linking agents, mitotic inhibitors, antimetabolites, and antihormonal agents can lead to a range of cognitive impairments.[39] There have been animal studies performed whose results suggest that cognitive impairments analogous to those found in humans afflicted by PCCI occur in animals treated with a variety of chemotherapeutic agents.[40–45] Some of the cognitive tests used in these studies include the Morris water maze, novel location recognition, and non-matching to sample learning.[43,46]

The majority of animal studies investigating chemobrain have been done using rats. A study by Mustafa *et al.* found that 5-fluorouracil (5FU) negatively impacted spatial working memory and neuronal proliferation in male Lister-hooded rats.[47] This study showed that there was a decrease in exploratory time after rats were placed in a novel location after a cycle of 5FU treatment. Although it was determined that there was no significant difference in proliferating cell counts, it was determined that brain-derived neurotrophic factor (BDNF) levels were significantly diminished in 5-FU treated rats in comparison to their vehicle-treated controls.[47]

Mice have also been used to model chemobrain. A study by Joshi *et al*. looked into how adriamycin (ADR) treatment, a commonly used chemotherapeutic agent, could possibly affect the brain through oxidative stress. This was accomplished by measuring glutathione (GSH) levels, which is an antioxidant found in the CNS. The study determined that there was significantly less GSH in mice treated with ADR in comparison to saline-treated controls.[48] This finding corresponds to an increase in oxidative stress which may contribute to the symptoms associated with chemobrain. Further work in mice by Dietrich *et al.* found that clinically relevant

treatment with carmustine (BCNU), cisplatin, and arabinoside led to enhanced neuronal cell death both *in vitro* and *in vivo* in treated mice.[24] This study began the process of identifying certain cell populations that are specifically vulnerable to chemotherapy-related toxicity. Although there are limited animal studies regarding PCCI, the previous work involving cognitive testing in chemotherapy-treated rodents and the early physiological studies performed have proven that animal models of PCCI are clinically relevant models applicable to the human condition.

2.1.3 Chemotherapy Agents Associated with PCCI

2.1.3.1 Carboplatin

Carboplatin (cis-Diammine(1,1-cyclobutanedicarboxylato)platinum(II)), depicted in figure 1, is a chemotherapeutic agent commonly employed in the treatment of various cancers, including cancers of the head and neck, breast, ovaries, bladder, and colon.[49–51] It effectively treats cancer by forming interstrand and intrastrand DNA crosslinks that lead to apoptosis and cell growth inhibition. Carboplatin has become popular as an alternative to cisplatin, which had caused severe side effects during and after treatment.[52] Despite its advantages over cisplatin, carboplatin has been implicated in PCCI and readily crosses the blood brain barrier.[8,53,54]

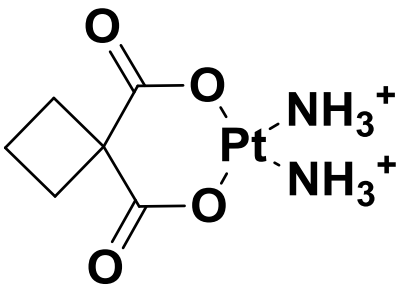

Figure 1. Carboplatin structure

2.1.3.2 CMF Chemotherapeutic Cocktail

The cocktail containing cyclophosphamide, methotrexate, and 5-fluorouracil (CMF) is typically used as a frontline treatment of breast cancer.[55–60] The modes of action for these drugs are a DNA alkylating agent, an anti-folate agent, and a thymidylate synthase inhibitor, respectively. CMF is known to disrupt the blood brain barrier and potentially cause encephalopathy. The three components of this cocktail can be seen in Figure 2.

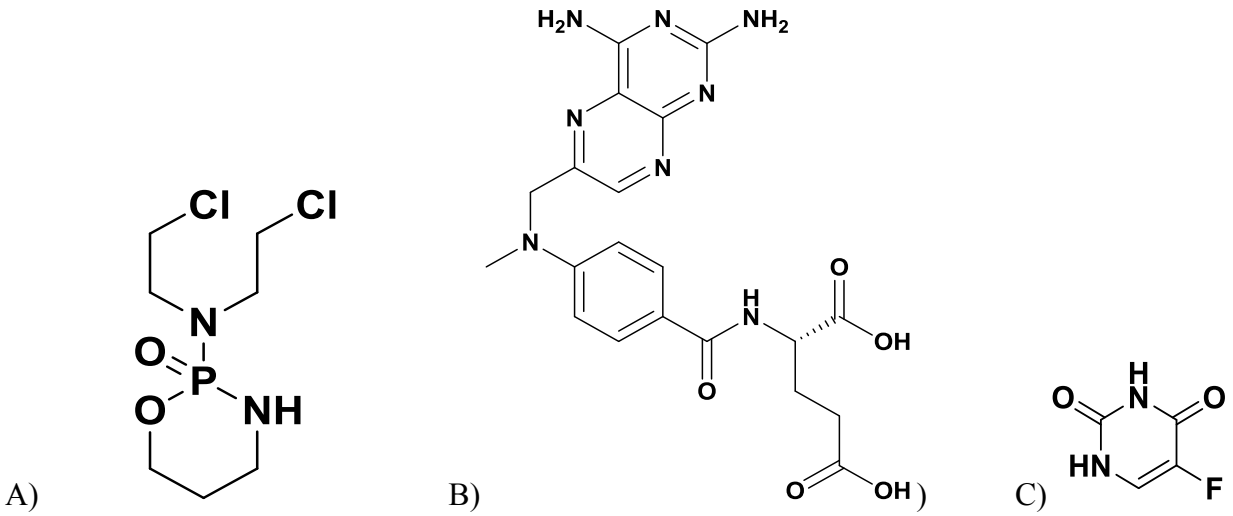

Figure 2. CMF component structures. A) Cyclophosphamide B) Methotrexate C) 5-Fluorouracil

2.2 Summary of the Studies Described in this Chapter

The following sections describe the studies performed on DA dysregulation involved in chemobrain. These studies involve measuring DA release and uptake with FSCV, HPLC analysis of DA metabolites, and behavior measurements. These studies were performed with carboplatin-treated rats and rats treated with the CMF cocktail.

2.3 Materials and Methods

2.3.1 Animals

2.3.1.1 Carboplatin Studies

All experiments were carried out in accordance with the National Institutes of Health *Guide for the Care and Use of Laboratory Animals.* All procedures were approved by the University of Kansas Institutional Animal Care and Use Committee. Male Wistar rats (Charles River Laboratories, Inc., Wilmington, MA, USA) were housed 3 per cage in the University of Kansas Animal Care Unit. Food and water was available *ad libitum*. Rats were maintained on a 12 hour light/dark cycle with lights on at 6:00 AM and lights out at 6:00 PM. A temperature of 70 ± 2 °C and humidity level of 50 ± 20% was maintained. Rats were approximately 9 weeks old upon arrival, 10 weeks old at time of first treatment with carboplatin or saline, and 14 weeks old at the time of neurochemical analysis by FSCV.

2.3.1.1 CMF Studies

Female Wistar rats (Charles River Laboratories, Inc., Wilmington, MA, USA) were housed three per cage with food and water *ad libitum* in a temperature/humidity-controlled environment. Rats were maintained on a 12 hour light/dark cycle with lights on at 6:00 AM and lights out at 6:00 PM. A temperature of 70 ± 2 °C and humidity level of 50 ± 20% was maintained. All experiments were carried out in accordance with the National Institutes of *Health Guide for the Care and Use of Laboratory Animals.* All procedures were approved by the University of Kansas Institutional Animal Care and Use Committee.

2.3.2 Drugs

Carboplatin (lot number C2538), d-amphetamine sulfate (lot number 065K1894), and α-Methyl-DL-tyrosine methyl ester hydrochloride (lot number 037K1402) were purchased from Sigma-Aldrich (St. Louis, MO, USA). AMPH was dissolved in biological saline (0.9% NaCl, 2.5 mg/mL) prior to use. For all 5-HT and reserve pool DA experiments, pharmaceutical grade carboplatin (lot number 61703-339-50) was purchased from Hospira (Lake Forest, IL, USA). Cyclophosphamide, methotrexate, and 5-fluorouracil were purchased from Sigma-Aldrich (St. Louis, MO, USA).

2.3.3 Electrode fabrication

Carbon-fiber cylindrical microelectrodes were fabricated as previously described.[27,61] Briefly, 7µm carbon-fiber purchased from Goodfellow Cambridge Ltd. (Huntingdon, England) was loaded into glass capillaries (4in, 1.2mm OD; A-M Systems, Inc. Carlsborg, WA, USA) and pulled using a heated coil puller (Narishige International USA, East Meadow, NY, USA). Carbon-fiber tips were then cut with a scalpel 25µm from the end of the glass seal. Electrodes were then sealed by dipping into a well-mixed epoxy mixture of 0.24g EPI-CURE 3234 Curing Agent (lot FCXC4114/0886GG) and 2.00g EPON Resin 815C (lot HADN0003/1307GG). Excess resin was removed by dipping several times in toluene and electrodes were then baked for 1 hour at 100°C. The electrodes were back-filled with 0.5 M potassium acetate in order to establish an electrical connection between the carbon-fiber and the inserted silver wire.

2.3.4 Chemotherapy Treatment

2.3.4.1 Carboplatin Studies

Male Wistar rats received an injection (iv, tail vein) of carboplatin once a week for four consecutive weeks. All carboplatin solutions were made up in biological saline (2.5mg/mL, 15mg/mL, and 26.6mg/mL) prior to injection. There were 3 experimental groups that included treatments with 0.9% biological saline, 5.0mg/kg carboplatin, and 20mg/kg carboplatin. Both dosage and treatment regimen were chosen to mimic a reasonable clinical dosing regimens and to allow for the drug effects to stabilize.

To further examine the effect of carboplatin treatment on DA reserve pool, Male Wistar rats received one injection (iv. tail vein) of carboplatin once a week for four consecutive weeks. For this round of treatment, there were two experimental groups consisting of treatment with 0.9% biological saline or a 20mg/kg dose of pharmaceutical grade carboplatin (10mg/mL, Hospira, Inc).

2.3.4.2 CMF studies

Female Wistar rats received weekly intraperitoneal injections of 0.9% biological saline vehicle or a CMF drug mixture of 40mg/kg cyclophosphamide, 37.5mg/kg methotrexate, 75mg/kg 5-fluorouracil for four weeks. There were two experimental groups that included treatments of 0.9% biological saline (n=6) and CMF-treated (n=4). Cyclophosphamide, methotrexate, and 5-fluorouracil were purchased from Sigma-Aldrich (St. Louis, MO, USA). The chemotherapeutic rat dosages for the CMF injections were based on previous studies by Briones and Woods.[64]

2.3.5 Behavioral Methods

Throughout carboplatin (or saline control) treatment, locomotor activity was monitored as a function of total distance traveled using a force-plate actometer. The force-plate actometer was constructed by Professor S. C. Fowler at the University of Kansas and is described elsewhere.[65] The actometer was located in a sound-attenuated cubicle. The door of the cubicle was closed and the room was evacuated when taking measurements to ensure that the animal was not disturbed during recording. Each animal was placed in the force plate actometer for behavioral analysis for 30 minutes once a week for four consecutive weeks prior to chemotherapy administration. Ambient temperature was held at 70°C during the collection of all behavioral recordings. All behavioral measurements were taken during the rodent light cycle between 11:00 AM and 2:00 PM

2.3.6 Brain Slices

Brain slices were harvested as previously described.[31] In summary, rats were deeply anesthetized by isoflurane inhalation and decapitated. The brain was then immediately removed and placed into ice-cold artificial cerebral spinal fluid (aCSF). The aCSF solution contained the following concentrations: 2.5 mM KCl, 126 mM NaCl, 1.2 mM NaH_2PO_4, 25 mM $NaHCO_3$, 2.4 mM $CaCl_2$, 1.2 mM $MgCl_2$, 20 mM HEPES, 11 mM D-glucose. The pH was adjusted to 7.4 with NaOH. To ensure the tissue received ample oxygen, the aCSF was continuously bubbled with 95% O_2/5% CO_2 throughout the experiment. After chilling for one minute, the cerebellum was removed and the brain was bisected longitudinally using a sterile razor blade. The sample was then stored at -80°C and saved for HPLC analysis. The other hemisphere of the brain was then glued to a plate against a cube of agar for support. Several 300 μm coronal brain slices were then

obtained using a vibratome (*Leica Microsystems, Bannockburn, IL, USA*). In a typical recording session, a single striatal brain slice was transferred to a perfusion chamber where oxygenated aCSF, maintained at 34 ºC using a thermostatted perfusion chamber and in-line heater, flowed over the slice at 2 mL/min. Slices were equilibrated for at least one hour before collecting measurements.

2.3.7 Striatal Area Measurements in Carboplatin Treated Rats.

After tissue harvesting, coronal slices containing the striatum was transferred to a petri dish containing aCSF. A glass slide was immediately placed on top of the slide to prevent the tissue from curling. The slice was then placed under a stereomicroscope (Nikon SMZ745, Japan). Brain slices were imaged by an eyepiece camera (AmScope MU300, Irvine, CA) mounted on the stereomicroscope. The striatum was selected and outlined (Figure 7) using Photoshop CS6 (Adobe, San Jose, CA). The area of the striatum in pixels was determined and converted to cm^2 via calibration (See Figure 7).

2.3.8 Electrochemical Measurements

2.3.8.1 Single Pulse Measurements

Procedures for measuring DA release and uptake with background-subtracted FSCV have been described in detail previously.[30, 31,63,66] Briefly, a pre-calibrated cylinder carbon-fiber microelectrode was inserted 100µm into the brain slice using micromanipulators and a stereoscope. The electrode was positioned between two biphasic stimulating electrodes (A-M Systems Inc, Carlsborg, WA, USA) in the striatum. For DA detection, a triangular waveform

starting at -0.4V, scanning up to 1.0V, and back to -0.4V vs an Ag/AgCl reference electrode, was applied to the carbon-fiber microelectrode at a scan rate of 300V/s and an update rate of 10 Hz. Dopamine release was evoked by applying a single, biphasic current pulse (current of 350 μA, 4 ms total duration) to the stimulating electrode. The peak current after stimulation was used for all release measurements. The current measured from DA oxidation was plotted versus potential and the successive voltammograms were plotted versus time. To account for the natural heterogeneity of DA release in the striatum, measurements were taken in four different regions of the striatum four times.

2.3.8.2 Reserve pool DA Measurements in Carboplatin-Treated Rats

In order to monitor reserve pool DA efflux, single pulse measurements were taken every five minutes while treating the brain slice with alpha methyl p tyrosine (αMPT). These measurements were taken until stimulated DA release was completely diminished. At this point the brain slice was perfused with 20μM amphetamine (AMPH) and 50μM αMPT. DA release was then continuously measured for 25 minutes without electrical stimulation.

2.3.8.3 Multiple Pulse Measurements in CMF-Treated Rats

After measuring the four quadrants of the caudate-putamen four times, DA efflux was evaluated under electrical stimulated DA efflux. To evaluate DA efflux, electrical stimulation pulses of either 1, 2, 4, 6, 8, or 10 times within the 15 second file durations were done within the caudatelateral quadrant of the caudate-putamen region. Slices were allowed to equilibrate for 5 minutes between sample recordings.

2.3.9 Modeling Stimulated Release

Dopamine release and uptake kinetics were analyzed using modeling software written by the R.M. Wightman group (University of North Carolina, Chapel Hill, NC, USA). This modeling software was used to measure dopamine per pulse ($[DA]_p$), which is dopamine release per electrical stimulus corrected for electrode performance and uptake, and V_{max}, which is the maximum rate of dopamine uptake. The time of stimulation is loaded into the software; however, the actual rise in the DA oxidation current typically does not occur immediately after stimulation. This delay, which may be on the order of 100 ms, is influenced by several factors, including the time it takes for DA to diffuse to the electroactive surface and adsorption of DA to the electrode surface. The mechanism of DA reuptake has been well-defined previously.[29] Briefly, DA uptake obeys Michaelis-Menten kinetics[67–69]under the following reaction paradigm:

$$(DA)_o + T \leftrightarrow (DA)T \rightarrow (DA)_i + T$$

where extracellular dopamine, $(DA)_o$, is converted to intracellular dopamine, $(DA)_i$. T represents the dopamine transporter. The curves were fitted to the equation that describes the rate of DA uptake:

$$\frac{d[DA]}{dt} = [DA]_p - \frac{V_{max}}{\frac{K_M}{[DA]} + 1}$$

where [DA] represents the extracellular concentration of DA in the brain, $[DA]_p$ is the change in [DA] at the electrode surface in response to each electrical stimulus pulse, and V_{max} and K_M are constants in the Michaelis-Menten equation that described how the transporter functions.[70] A K_M value of 0.2 μM was used during the modeling operation. The parameters V_{max} and $[DA]_p$ were then adjusted to fit the traces, as shown in Fig. 5A.

2.3.10 Striatal Dopamine Content

Striatal tissue samples were stored at -80 °C until use. Samples were homogenized in 0.1 M perchloric acid and centrifuged at 7200g for 10 minutes. Same day dopamine tissue content was determined using HPLC coupled with electrochemical detection. The supernatant was manually injected onto a Phenomenex Luna 2.5u C18(2)-HST column (100 x 3.00 mm) for separation followed by detection using an ESA 5014B microdialysis cell (E1 = -150 mV; E2 = +230 mV). A guard cell (ESA 5020) was used in-line before injection loop and was set at +350 mV. The mobile phase was delivered at a flow rate of 0.38 mL/min by a Shimadzu LC-20AD HPLC pump (Shimadzu Scientific Instruments, Columbia, MD). Mobile phase composition: 75.18 mM sodium phosphate (monobasic, monohydrate), 1.387 mM 1-octanesulfonic acid (sodium salt, anhydrous), 0.125 mM ethylene diamine tetraacetic acid, 0.0025 % triethylamine, and 10 % acetonitrile; pH 3.0 adjusted with 85% phosphoric acid. Dopamine peak area was integrated and quantified against known standards using LC Solutions Shimadzu Software. Dopamine concentrations were normalized to total protein levels as determined (in duplicate) by the commercially available BCA™ protein assay kit from Thermo Scientific (Thermo Fisher Scientific Inc., Waltham, MA). Final values were reported as μg dopamine/mg protein.

2.3.11 Statistics

Statistical analyses were conducted using GraphPad Prism software (GraphPad Software Inc., San Diego, CA, USA). For statistical analyses, n = the number of rats. Data are given as mean ± SEM.

2.4 Carboplatin Results and Discussion

Impairments in the release of DA, 5-HT, Glutamate, GABA and other neurotransmitters could be detrimental to many neurological functions, including cognition, mood, and the control of movement. Clinical studies have suggested that DA may play a role in chemobrain.[71,72] Additionally, non-clinical research implies the involvement of DA impairment in chemobrain.[14,43,72–75] It has been well-established that dopaminergic function in the basal ganglia is important in cognition.[26,76–81] Therefore, we investigated the release and uptake properties of DA, which is readily measured electrochemically with FSCV.

Electrically-stimulated DA release and uptake was quantified in the four quadrants of the striatum of rat brain slices. The dorsal striatum is associated with motivation and reward and motor function,[82,83] whereas the ventral striatum is associated with reinforcement learning.[84] Measurements were taken in the four quadrants to account for potential regional differences of release, which are known to have a dorsal to ventral gradient in multiple rodent species and non-human primates.[85] It was determined that DA release was diminished among all quadrants, and also that uptake is decreased. DA content, measured by HPLC, and the DA reserve pool, assayed by electrochemical measurement of AMPH-induced efflux, were unaffected by carboplatin

treatment. These results suggest that this treatment impairs the ability of terminals to function properly.

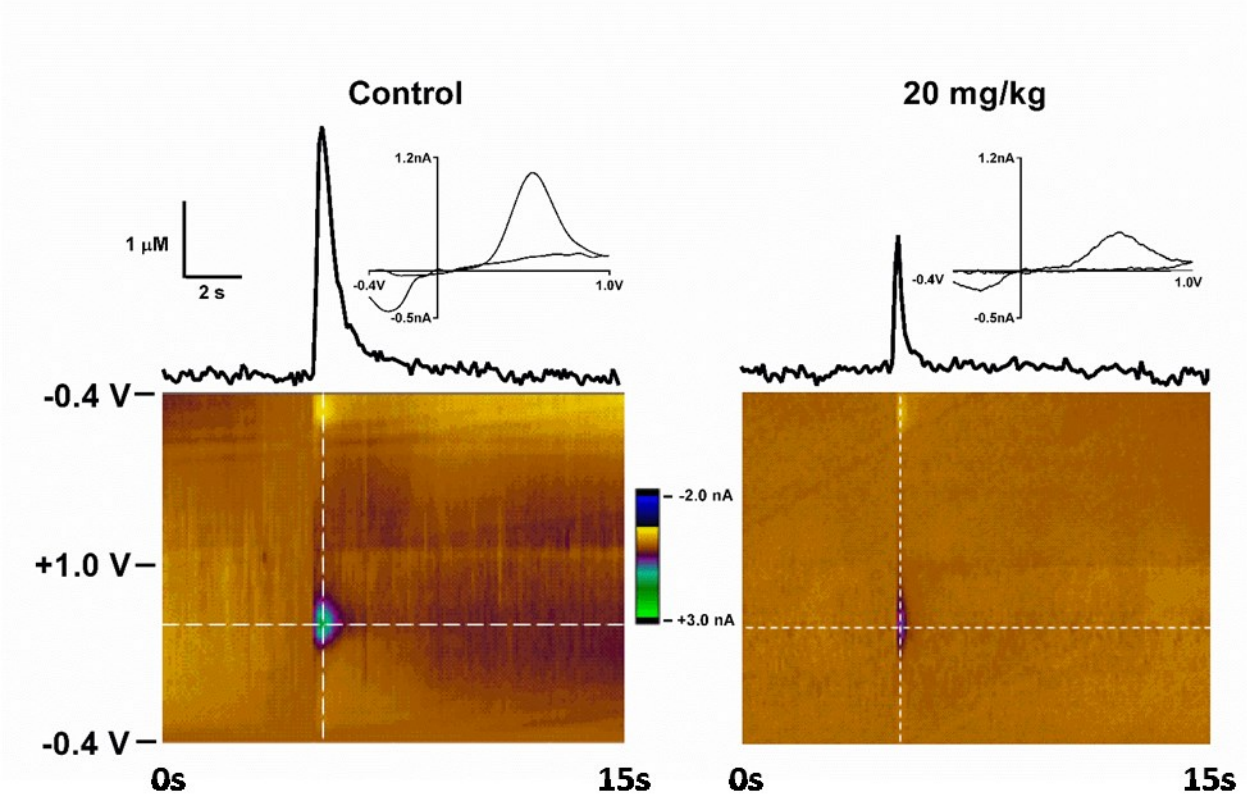

Figure 3. Dopamine release comparison of a saline-injected control rat and a highest dose carboplatin-injected rat. Representative color plots and stimulated DA release plots, sampled along the horizontal dashed lines on the color plots, are shown. Cyclic voltammograms, sampled along the vertical dashed lines on the color plots, are shown directly above the stimulated release plots to confirm the presence of DA. Carboplatin dose was 20 mg/kg.

2.4.1 Striatal Dopamine Release

Electrically stimulated DA release in the dorsal lateral (DL), dorsal medial (DM), ventral medial (VM), and ventral lateral (VL) quadrants of the striatum was measured with FSCV in coronal brain slices. Four measurements were taken at random locations within each quadrant and averaged. Representative data for 0 mg/kg and 20 mg/kg carboplatin treatment groups are shown in Fig. 3. The representative cyclic voltammograms confirm that the analyte measured is DA. Each color plot consists of a series of unfolded, stacked cyclic voltammograms. The current response is color-coded. The absence of faradaic currents, other than those due to DA oxidation and reduction, suggest that no electroactive species are released in response to electrical stimulation in either the carboplatin-naïve slices or the 20 mg/kg carboplatin slices.

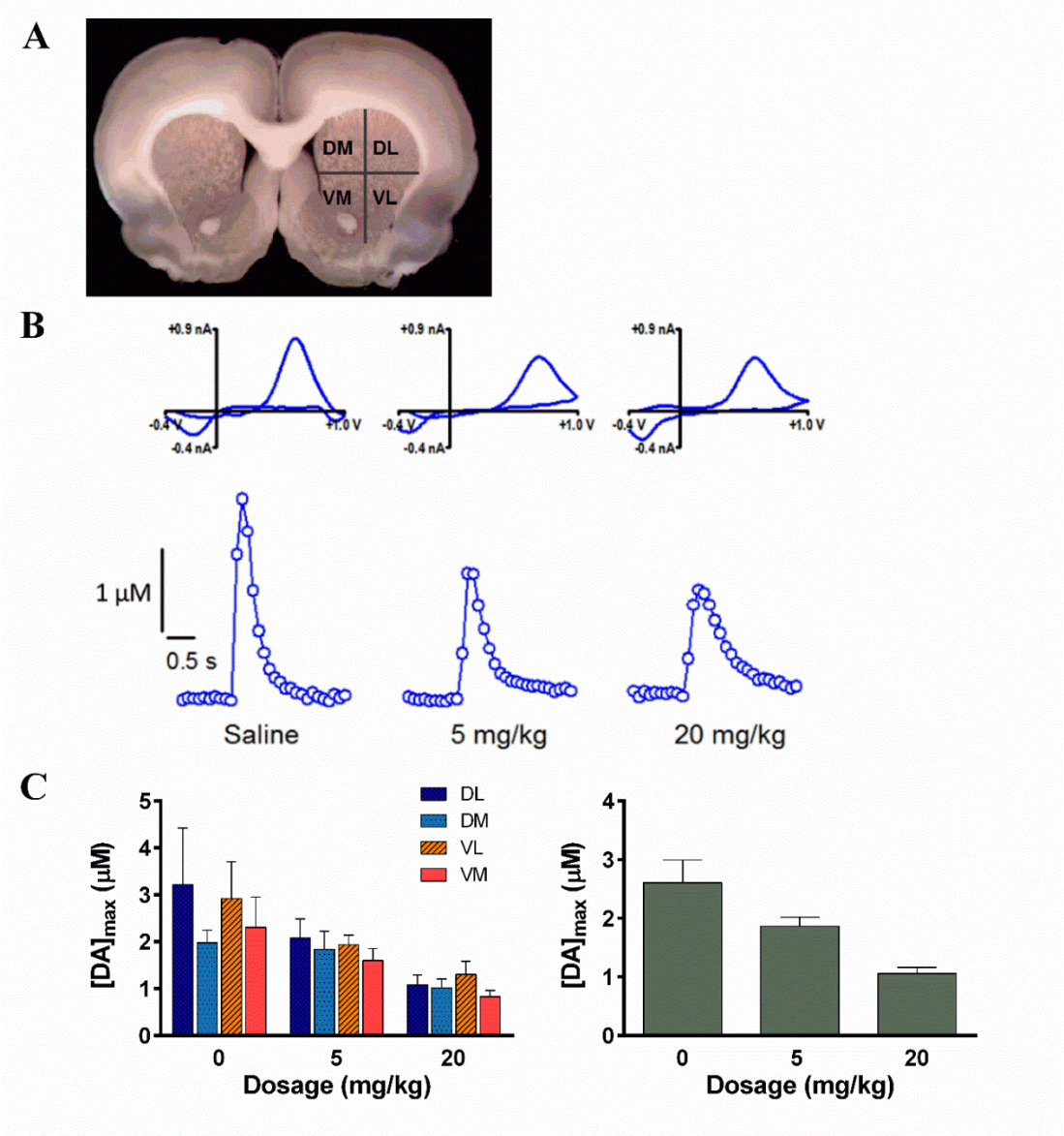

Figure 4. A) Image of a coronal brain slice with labeled quadrants of the striatum. **B)** Representative stimulated DA release plots for each dose taken from the DL quadrant of the striatum. The cyclic voltammograms acquired at the point of maximum DA oxidation are located above the corresponding release plots. **C)** $[DA]_{max}$ at each dose shown in each of the four regions of the striatum (two-way ANOVA: main region effect, $p = 0.5288$; main dose effect, $p < 0.001$; 0, 5, 20 mg/kg, n = 5).). **D)** $[DA]_{max}$ averaged across all brain regions at each dose (one-way ANOVA: main dose effect, $p < 0.001$; 0, 5, 20 mg/kg, n = 5).

Representative stimulated release plots (current versus time) for each treatment group, collected from striata, are shown in Fig. 4B. The presence of DA was confirmed by the cyclic voltammograms sampled at the point of peak release on each plot. The data reveal a statistically significant carboplatin treatment effect on DA release in the striatum: 71.5% of vehicle control at 5 mg/kg and 40.6% at 20 mg/kg. (Fig. 4C; two-way ANOVA main dose effect, $p < 0.001$; Fig 4D; one-way ANOVA: main dose effect, $p < 0.001$; 0, 5, 20 mg/kg, n = 5). However, there was no significant effect of region on stimulated DA release (Fig. 4C; two-way ANOVA, $p = 0.5288$, $F_{3,52} = 0.7474$, number of rats: 0, 5, 20 mg/kg, n = 5). The attenuation of DA release was, therefore, found to be generalized throughout the entire striatum. A bar graph of $[DA]_{max}$ values averaged across the four quadrants (Fig 4A) is shown in Fig. 4D. Since DA is involved in motor function and cognition,[25] it is possible that the symptoms of chemobrain—such as short term memory loss and fatigue—could be influenced by a generalized depression of the release of dopamine into the striatal synapses for chemotherapy treated patients.[26,86,87] However, the suppression of other neuronal populations, including GABAergic neurons and glutamatergic neurons, cannot be ruled out.

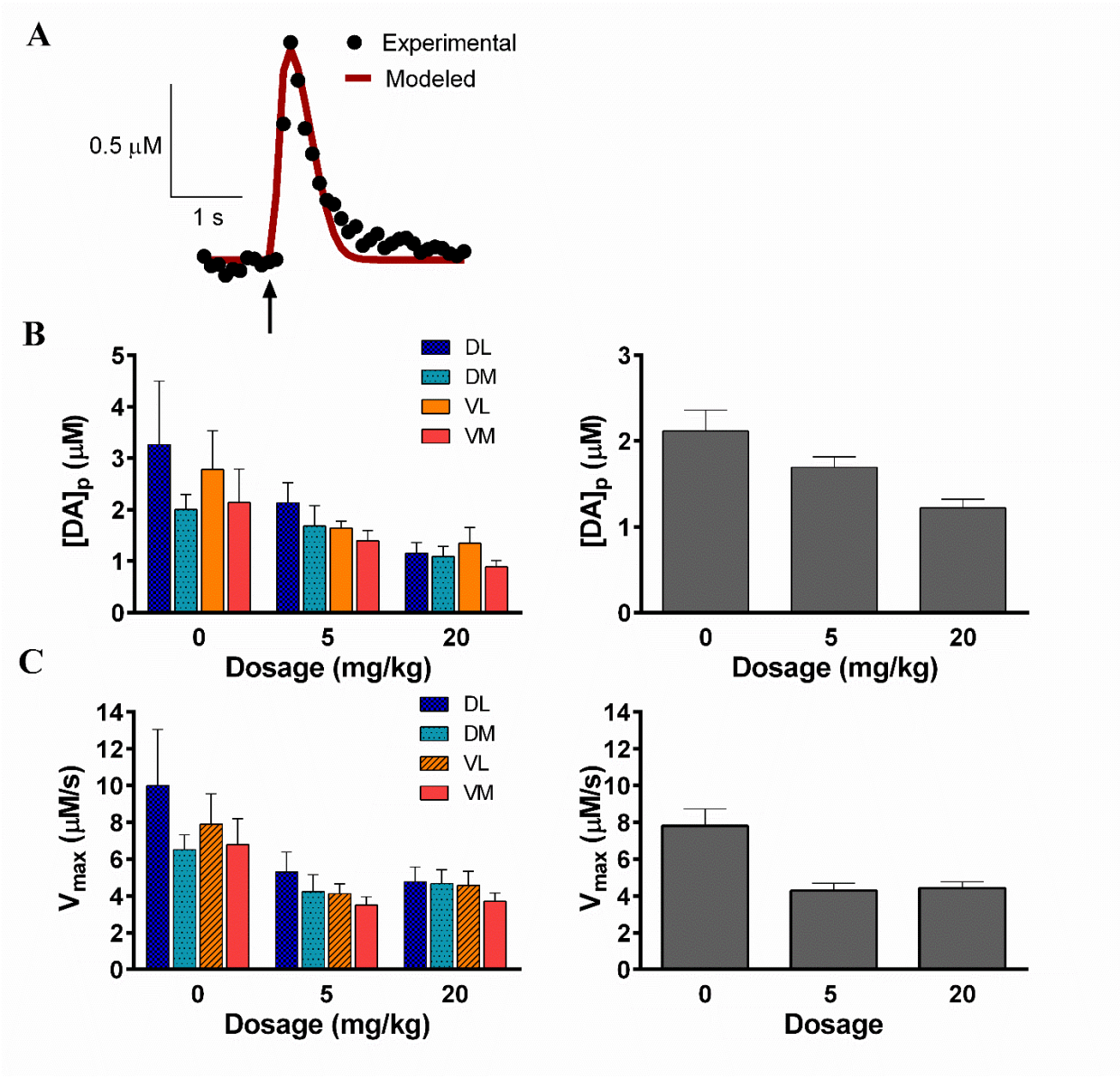

Figure 5. Dopamine release and uptake is attenuated in carboplatin treated rats compared to saline controls. A) Representative example of a fitting curve used for modeling. The arrow indicates the point of stimulation. B) $[DA]_p$ measured from each dosing group in each region. No regional differences in the striatum were found, but generalized release was sharply attenuated (two-way ANOVA: main region effect, $p = 0.4430$, 0, 5, 20 mg/kg, n = 5; main dose effect, $p < 0.001$; 0, 5, 20 mg/kg, n = 5). C) $[DA]_p$ averaged across all brain regions at each dose

(one-way ANOVA: main dose effect, $p = 0.0011$; 0, 5, 20 mg/kg, n = 5) D) V_{max} measured from each dosing group in each region. No significant difference of V_{max} was found between regions (two-way ANOVA: main region effect, $p = 0.3836$, 0, 5, 20 mg/kg, n = 5; main dose effect, $p < 0.001$; 0, 5, 20 mg/kg, n = 5). E) V_{max} averaged across all brain regions at each dose (one-way ANOVA: main dose effect, $p < 0.001$; 0, 5, 20 mg/kg, n = 5)

2.4.2 Determination of $[DA]_p$ and V_{max}

In order to quantify DA uptake in carboplatin-treated rats, the stimulated release plots were modeled. This modeling process allowed the determination of V_{max}, the maximum rate of DA uptake, and $[DA]_p$, DA release per electrical stimulus pulse. The determination of $[DA]_p$ corrects for electrode performance and DA uptake by the dopamine transporter. This modeling process is described in Materials and Methods, and a representative modeled stimulated release plot is shown in Fig. 5A. A statistically significant attenuation in $[DA]_p$ was found across all regions of the striatum after four weeks of carboplatin treatment: 80.0% of saline control at 5 mg/kg and 57.7% at 20 mg/kg (Fig. 5B; two-way ANOVA main dose effect; $p < 0.001$; Fig 3C; one-way ANOVA: main dose effect, $p = 0.0011$; 0, 5, 20 mg/kg, n = 5). Similar to the uncorrected release data in which $[DA]_{max}$ was determined, no significant effect was found between the four regions of the striatum probed (two-way ANOVA main region effect, $p = 0.4430$; 0, 5, 20 mg/kg, n = 5). Additionally, a substantial effect of carboplatin dose on V_{max} (Fig. 3D and 3E), the maximum rate of DA uptake by the membrane-bound dopamine transporter protein molecules, was found: 54.9% of saline control at 5 mg/kg and 56.8% at 20 mg/kg (two-way ANOVA main dose effect, $p < 0.001$; Fig 5E; one-way ANOVA: main dose effect, $p < 0.001$; 0, 5, 20 mg/kg, n = 5). However, similar to the $[DA]_p$ data, there was also no statistical

difference in V_{max} between the regions of the striatum sampled (two-way ANOVA main region effect, $p = 0.3836$, 5, 20 mg/kg, n = 5). To illustrate the overall effect of carboplatin treatment on striatal DA release within the striatum, graphical representations of $[DA]_p$ and V_{max} are shown in Figs 5C and 5E, respectively, with these values averaged across the four quadrants.

These data show that DA per pulse, as well as DA uptake, is diminished in carboplatin-treated rats. This finding suggests that the decrease in stimulated DA release that occurred in response to electrical stimulation did not arise from enhanced DA clearance, given the competitive relationship between DA release and uptake, by the dopamine transport system. According to Michaelis-Menten enzyme kinetics, V_{max} is directly proportional to the total number of functioning dopamine transporter protein molecules.[70] Therefore, it is possible that the total number of functioning dopaminergic terminals decreases with carboplatin treatment—a finding that is not surprising given the inherent toxicity of carboplatin. It is important, however, to obtain measures of how much DA is present within the terminals since this parameter would be a direct measure of how much DA is available for release.

2.4.3 Dopamine Reserve Pool Content

The generalized three-pool model of neurotransmitter-containing vesicles within neurons consists of a readily releasable pool, a recycling pool, and a reserve pool.[88–90] The readily releasable pool contains only 1-2% of vesicles within a neuron.[90] In the context of our voltammetric recordings, DA from the readily releasable pool in striatal slices would be released and detected by FSCV upon application of a single electrical stimulus pulse. After depleting the readily releasable pool vesicles, they are replenished by the recycling pool, which accounts for 5-

20% of the total number of vesicles within the neuron.[91–93] The reserve pool contains 80-90% of the total number of vesicles within a neuron and is thought to be mobilized in response to increased levels of synaptic activity.[88–90]

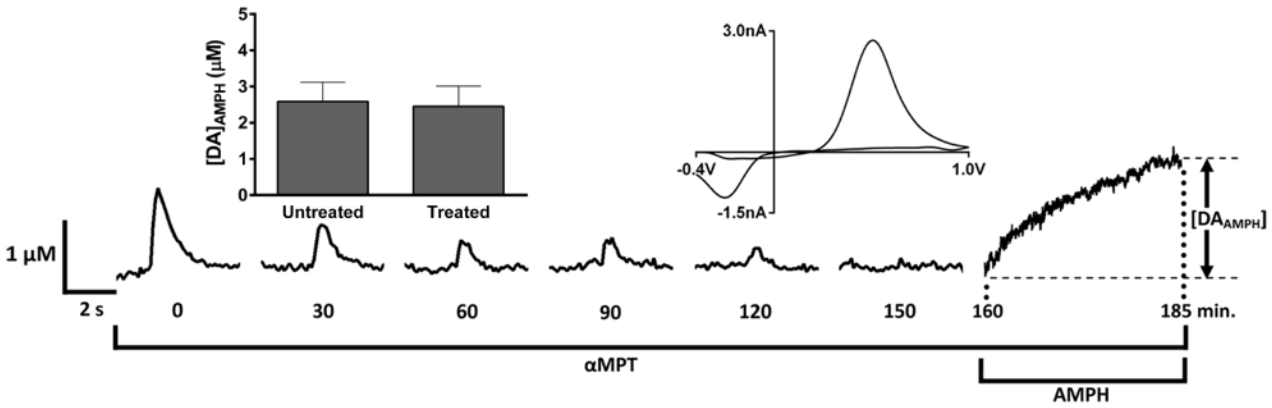

Figure 6. Quantitation of reserve pool DA. The brain slice was continuously exposed αMPT, a tyrosine hydroxylase inhibitor, in order to block DA synthesis. Electrically evoked DA release was measured every five minutes until the signal diminished (occurring at 150 minutes in the data shown). Traces are shown here every 30 minutes for clarity. The addition of AMPH then caused the efflux of reserve pool DA. The cyclic voltammogram confirms the presence of DA at the peak of the AMPH-induced efflux.

Experimentally, reserve pool DA can be mobilized by intense electrical stimulation[28,30,93–95] or pharmacological manipulation.[30,95] Here, we isolated reserve pool DA in striatal brain slices by blocking DA synthesis with αMPT while applying single-pulse electrical stimulations every five minutes (Fig. 6).[30] The compound αMPT inhibits DA production by blocking tyrosine hydroxylase, the rate-limiting enzyme in DA synthesis.[96] When αMPT was present in the perfusion buffer, the DA signal dissipated in response to stimulation, leaving only reserve pool DA within the terminals. Subsequent application of AMPH and αMPT together resulted in the spontaneous, quantifiable efflux of this reserve pool DA. The concentration of DA measured as a result of this treatment was 2.59 ± 0.53 μM in slices from control rats and 2.45 ± 0.63 μM in slices from 20 mg/kg carboplatin-treated rats. There was no significant difference in DA efflux (unpaired t-test, $p > 0.05$, n = 6 control rats and 5 rats treated with 20 mg/kg carboplatin), suggesting that the mechanism leading to stimulated DA attenuation in the striatum is not based on storage impairment.

2.4.4 Striatal Dopamine Content

Homogenized striatal tissue samples were analyzed by high performance liquid chromatography (HPLC) with electrochemical detection in order to measure the total content of DA and DOPAC (Table 1). Although there appears to be a trend, we found no significant dose effect on DA content (one-way ANOVA, $p = 0.81$; 0, 5, and 20 mg/kg, n = 5), DOPAC content (one-way ANOVA, $p = 0.87$; 0, 5, and 20, n = 5), or DA/DOPAC (one-way ANOVA, $p = 0.39$; 0, 5, and 20mg/kg, n = 5) in homogenized striatal samples from vehicle- and carboplatin-treated rats. Several conclusions can be drawn from these data. First, since DOPAC levels, as well as the DA/DOPAC ratio, did not change with carboplatin treatment, it is unlikely that the

metabolism of DA to DOPAC is altered by this treatment. Second, these results agree with the reserve pool efflux results; thus, DA is present in proper amounts in carboplatin treated rats, but it is not released efficiently.

Table 1: Total DA and DOPAC content and DA/DOPAC ratio from homogenized striatal lysates. The number of rats analyzed (n) is indicated in parentheses.

	DA	**DOPAC**	**DA/DOPAC**
	µg DA / mg protein	µg DOPAC / mg protein	
0 mg/kg (n=5)	1.15 ± 0.29	0.31 ± 0.09	4.12 ± 0.53
5 mg/kg (n=5)	1.10 ± 0.27	0.30 ± 0.09	3.59 ± 0.63
20 mg/kg (n=5)	0.88 ± 0.33	0.25 ± 0.08	2.90 ± 0.65

2.4.5 Striatal area measurements in carboplatin treated rats

Visible neurodegeneration of the striatum is hallmark to certain neurodegenerative diseases and toxic events.[97–100] In order to see if carboplatin treatment lead to visible striatal degeneration, striatal area measurements were made. A representative image of a coronal brain slice with the striatum shaded in can be seen in Fig 7. After analyzing the striatal areas of carboplatin-treated rats (n = 5) and saline-treated controls (n = 6) it was determined that there is no significant visible striatal loss after carboplatin treatment (unpaired t-test, $p > 0.05$, n = 6 control rats and n = 5 rats treated with 20 mg/kg carboplatin). Along with the content data and since the striatal area was not altered by carboplatin treatment, it is not likely that the striatum has undergone a significant amount of atrophy; thus, the decrease in release is likely not due to extensive damage of the neurons themselves.

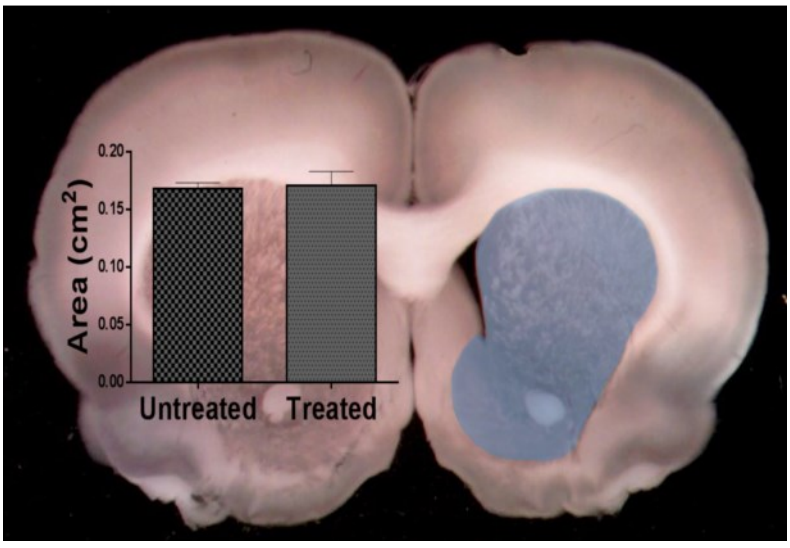

Figure 7. Striatal area was unaffected in rats treated with carboplatin. (unpaired t-test, $p > 0.05$, n = 6 control rats and n = 5 rats treated with 20 mg/kg carboplatin)

2.4.6 Behavioral Measurements.

Throughout their four weeks of carboplatin treatment, rats were subjected to behavioral analysis. To study the effects of carboplatin treatment on locomotion, animals were placed in a force-plate actometer to determine if carboplatin treatment decreased the natural tendency to explore when placed in the new environment of the force-plate recording chamber. Throughout carboplatin treatment, the subjects expressed a significant decline in locomotion as measured by total distance traveled (Fig. 8). Additionally, the magnitude of decline correlated with the number of doses administered (two-way ANOVA: time effect, $p = 0.0001$; n = 3 per week per dose).

Although there was a significant time affect, there was not a significant treatment effect throughout the 4 week treatment period (two-way ANOVA: treatment effect, $p = 0.36$, n = 3 per week per dose). Because the distance traveled of the vehicle-treated control rats did not decrease with increasing time of treatment, while the distance traveled of rats treated with 5 and 20 mg/kg carboplatin did decrease, the time effect is not likely caused by habituation (for example, 0 mg/kg, $p > 0.05$, n=5; 5 mg/kg $p < 0.05$, n=5; 20 mg/kg, $p < 0.001$, Bonferroni post-hoc test, Week 1 versus Week 4, statistical tests for other pairings provided in Table 6, *Supplementary Information*). Upon analyzing each treatment group separately, it was found that there was a significant decline in locomotor activity for the 20mg/kg dosage group over the 4 week treatment period (one-way repeated measures ANOVA, $p < 0.01$; n=3). It is possible that other physiological factors associated with carboplatin treatment could impede locomotor activity; nevertheless, since DA plays a significant role in motor function,[26] it is likely that inhibition of DA release would contribute to a decrease in locomotion. In fact, previous studies have supported the association of decreased DA levels in the dorsal striatum with suppressed

locomotor activity.[83] Therefore, our results collectively suggest that the decreased ability of carboplatin-treated rats to release striatal DA contributes to this behavioral suppression.

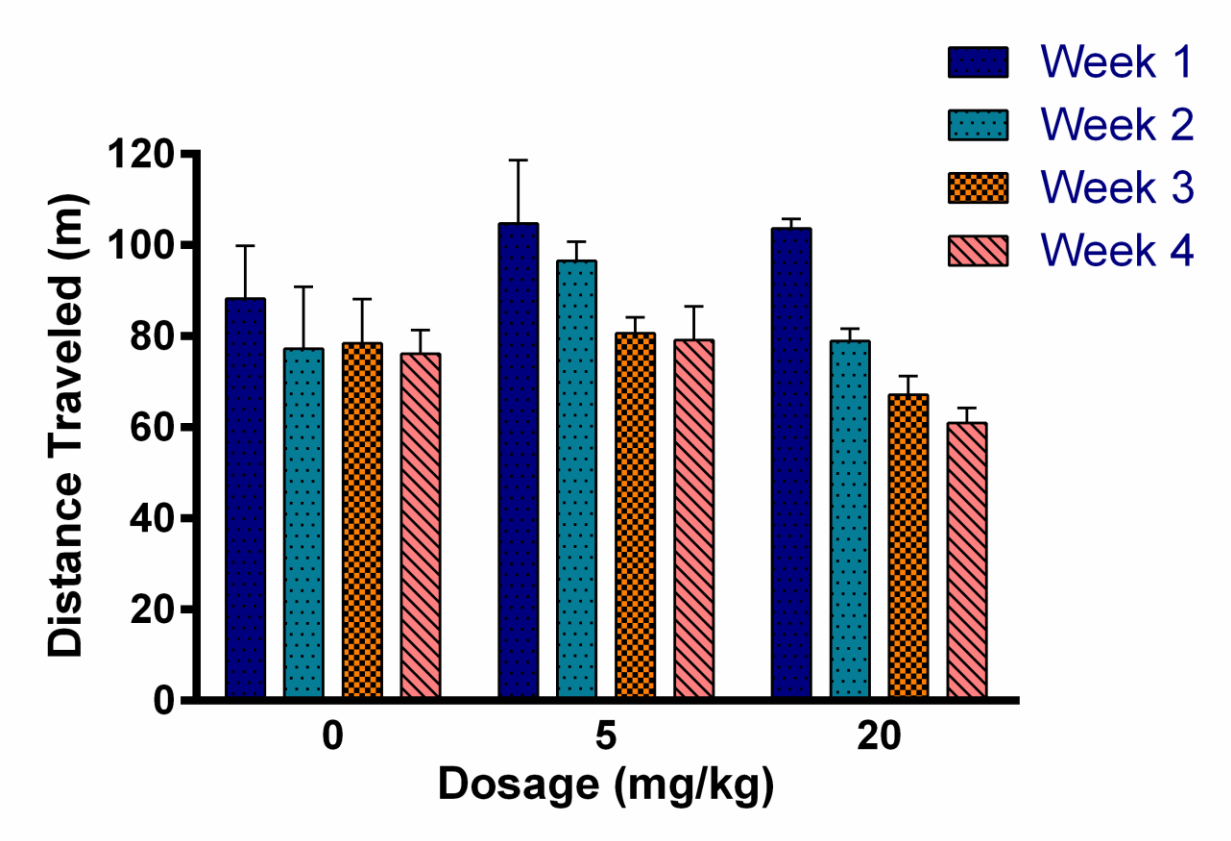

Figure 8. Locomotor activity was measured using a force-plate actometer. Total distance traveled was attenuated and a significant time effect was found (two-way ANOVA: time effect, $p < 0.0001$; n = 3 per week per dosage, dose effect, $p = 0.3490$). There was a significant decline in locomotor activity for the 20mg/kg treatment group over the 4 week treatment period (one-way repeated measures ANOVA, $p < 0.01$; n=3).

2.5 CMF Results and Discussion

2.5.1 CMF Peak Stimulated DA Release in the Striatum

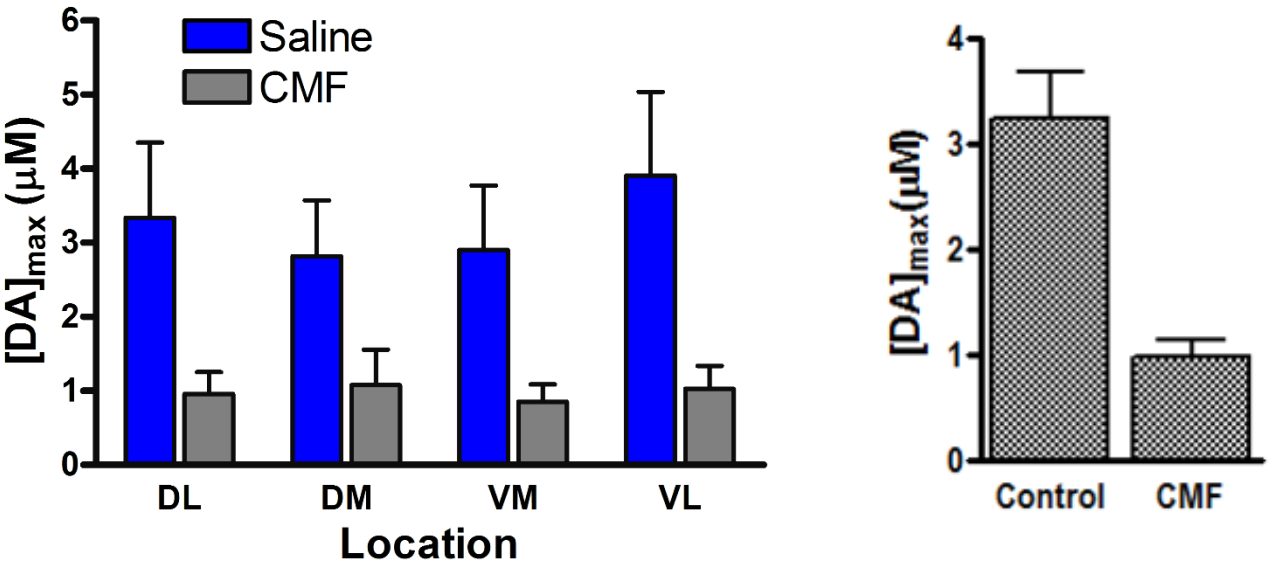

Figure 9. Maximum electrically-evoked DA release separated by striatal region (left) and with all regions combined (right). Striatal DA release is attenuated across all regions ($p=0.0001$, 2-way ANOVA, $n = 4$).

DA release measurements were also taken in rats treated with the clinically relevant chemotherapeutic cocktail, CMF. Electrically-evoked DA release in the dorsal lateral (DL), dorsal medial (DM), ventral medial (VM), and ventral lateral (VL) quadrants of the striatum was measured with FSCV in coronal brain slices. Four single pulse measurements were taken in each quadrant and averaged. DA release in the CMF-treated rats revealed a significant dose affect attenuation in all regions of the striatum: 31% of vehicle control (Fig 9; 2-way ANOVA,

p=0.0001, n = 4). Concurrent with the results obtained in carboplatin-treated rats there were no regional differences in DA release attenuation (Fig. 9; 2-way ANOVA, $p > 0.05$, n = 4). The attenuation of DA release was, therefore, found to be generalized throughout the entire striatum.

2.5.2 Multiple pulse study

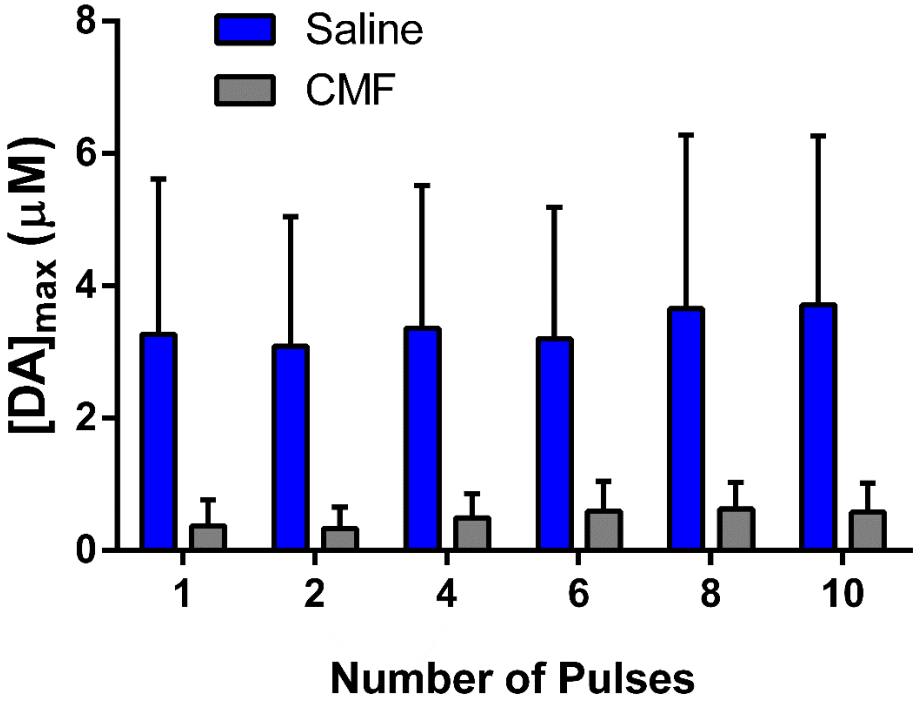

Figure 10. Maximum DA release vs number of stimulus pulses applied. Although DA release is attenuated in CMF-treated rats ($p < 0.01$, 2-way ANOVA, n = 4), there were no statistically significant differences in DA release at different numbers of pulses ($p > 0.05$, 1-way ANOVA).

To further elucidate the impact of CMF treatment on regional DA release in the striatum, we chose to measure DA release under prolonged electrical stimulation, which can lead to reserve pool mobilization.[28,30,93–95] Neurons were increasingly stressed by increasing the number

of pulses applied. Measurements were taken in the DL striatum and the number of pulses were applied from lowest to highest. Varying the number of pulses can shed light on any differences in neuronal sensitivity to prolonged stimulation. As seen in Figure 9, there is significant decline in DA release post-CMF treatment ($p < 0.01$, 2-way ANOVA, $n = 4$) and this attenuation is independent of the number of stimulus pulses applied (Fig. 10; $p > 0.05$, 1-way ANOVA).

Similar to the carboplatin study, CMF treatment severely attenuates striatal DA release. This attenuation is also generalized across all regions of the striatum, suggesting that the CMF treatments affected the striatum in a similar manner as carboplatin. These data suggest that DA dysregulation is not a carboplatin-specific phenomenon and has implications to other chemotherapy treatment regimes.

2.6 Conclusions

The neurochemical analyses of rats treated with the carboplatin and CMF were performed to possibly uncover the underlying mechanisms of PCCI. In both studies, it was found that chemotherapy treatment led to an attenuation in DA release in the striatum of treated rats. This attenuation was generalized throughout the striatum. Although DA release was attenuated, DA content and striatal area remain unaffected after chemotherapy treatment. Reserve pool DA was measured in carboplatin-treated rats to determine if chemotherapy treatment altered vesicular storage, and it was determined that reserve pool DA storage and mobilization is unaffected after treatment. This suggests that DA release attenuation is not simply the result of massive neurodegeneration but is actually an impairment in the mechanism of release. Since DA is involved in motor function and cognition,[25] it is possible that the symptoms of chemobrain, such

as short term memory loss and fatigue, could be influenced by a generalized depression of the release of dopamine into the striatal synapses for chemotherapy treated patients. However, the suppression of other neuronal populations, including those containing GABA, glutamate, and serotonin, cannot be ruled out. The data presented here may therefore provide insight, and possible points of intervention leading to possible therapeutics alleviating or eliminating the cognitive impairments caused by chemotherapy treatment.

2.7 References

(1) Shapiro, W. R., and Young, D. F. (1983) Neurological complications of antineoplastic therapy. *Acta Neurol. Scand. Suppl. 100*, 125–132.

(2) Keime-Guibert, F., Napolitano, M., and Delattre, J.-Y. (1998) Neurological complications of radiotherapy and chemotherapy. *J. Neurol. 245*, 695–708.

(3) Verstappen, C. C., Heimans, J. J., Hoekman, K., and Postma, T. J. (2003) Neurotoxic complications of chemotherapy in patients with cancer. *Drugs 63*, 1549–1563.

(4) Minisini, A., Atalay, G., Bottomley, A., Puglisi, F., Piccart, M., and Biganzoli, L. (2004) What is the effect of systemic anticancer treatment on cognitive function? *Lancet Oncol. 5*, 273–282.

(5) Poppelreuter, M., Weis, J., Külz, A. ., Tucha, O., Lange, K. ., and Bartsch, H. . (2004) Cognitive dysfunction and subjective complaints of cancer patients. *Eur. J. Cancer 40*, 43–49.

(6) Wefel, J. S., Kayl, A. E., and Meyers, C. A. (2004) Neuropsychological dysfunction associated with cancer and cancer therapies: a conceptual review of an emerging target. *Br. J. Cancer*.

(7) Dietrich, J., Han, R., Yang, Y., Mayer-Pröschel, M., and Noble, M. (2006) of Biology. *J. Biol. 5*, 22.

(8) Argyriou, A. A., Assimakopoulos, K., Iconomou, G., Giannakopoulou, F., and Kalofonos, H. P. (2011) Either Called "Chemobrain" or "Chemofog," the Long-Term Chemotherapy-Induced Cognitive Decline in Cancer Survivors Is Real. *J. Pain Symptom Manage. 41*, 126–139.

(9) Meyers, C. A., and Abbruzzese, J. L. (1992) Cognitive functioning in cancer patients Effect of previous treatment. *Neurology 42*, 434–434.

(10) Schagen, S. B., van Dam, F. S., Muller, M. J., Boogerd, W., Lindeboom, J., and Bruning, P. F. (1999) Cognitive deficits after postoperative adjuvant chemotherapy for breast carcinoma. *Cancer 85*, 640–650.

(11) Reid-Arndt, S. A. (2009) Breast cancer and "chemobrain": the consequences of cognitive difficulties following chemotherapy and the potential for recovery. *Mo. Med. 106*, 127–131.

(12) Nelson, C. J., Nandy, N., and Roth, A. J. (2007) Chemotherapy and cognitive deficits: mechanisms, findings, and potential interventions. *Palliat. Support. Care 5*, 273–280.

(13) Boykoff, N., Moieni, M., and Subramanian, S. K. (2009) Confronting chemobrain: an in-depth look at survivors' reports of impact on work, social networks, and health care response. *J. Cancer Surviv. 3*, 223–232.

(14) Ahles, T. A., and Saykin, A. J. (2007) Candidate mechanisms for chemotherapy-induced cognitive changes. *Nat. Rev. Cancer 7*, 192–201.

(15) Dietrich, J., Han, R., and Yang, Y. Mayer-Prö fischel, M., and Noble, M.(2006). CNS progenitor cells and oligodendrocytes are targets of chemotherapeutic agents in vitro and in vivo. *J Biol 5*, 22.

(16) Jamroziak, K., and Robak, T. (2004) Pharmacogenomics of MDR1/ABCB1 gene: the influence on risk and clinical outcome of haematological malignancies. *Hematology 9*, 91–105.

(17) Hoffmeyer, S., Burk, O., Von Richter, O., Arnold, H. P., Brockmöller, J., Johne, A., Cascorbi, I., Gerloff, T., Roots, I., and Eichelbaum, M. (2000) Functional polymorphisms of the human multidrug-resistance gene: multiple sequence variations and correlation of one allele with P-glycoprotein expression and activity in vivo. *Proc. Natl. Acad. Sci. 97*, 3473–3478.

(18) Von Zglinicki, T. (2002) Oxidative stress shortens telomeres. *Trends Biochem. Sci. 27*, 339–344.

(19) Meyers, C. A., Albitar, M., and Estey, E. (2005) Cognitive impairment, fatigue, and cytokine levels in patients with acute myelogenous leukemia or myelodysplastic syndrome. *Cancer 104*, 788–793.

(20) Kelley, K. W., Bluthé, R.-M., Dantzer, R., Zhou, J.-H., Shen, W.-H., Johnson, R. W., and Broussard, S. R. (2003) Cytokine-induced sickness behavior. *Brain. Behav. Immun. 17*, 112–118.

(21) Scheibel, R. S., Valentine, A. D., O'Brien, S., and Meyers, C. A. (2004) Cognitive dysfunction and depression during treatment with interferon-alpha and chemotherapy. *J. Neuropsychiatry Clin. Neurosci. 16*, 185–191.

(22) De Visser, K. E., Eichten, A., and Coussens, L. M. (2006) Paradoxical roles of the immune system during cancer development. *Nat. Rev. Cancer 6*, 24–37.

(23) Ramassamy, C., Averill, D., Beffert, U., Bastianetto, S., Theroux, L., Lussier-Cacan, S., Cohn, J. S., Christen, Y., Davignon, J., and Quirion, R. (1999) Oxidative damage and protection by antioxidants in the frontal cortex of Alzheimer's disease is related to the apolipoprotein E genotype. *Free Radic. Biol. Med. 27*, 544–553.

(24) Dietrich, J., Han, R., Yang, Y., Mayer-Proschel, M., and Noble, M. (2006) CNS progenitor cells and oligodendrocytes are targets of chemotherapeutic agents in vitro and in vivo. *J. Biol. 5*, 22.

(25) Schultz, W. (2002) Getting Formal with Dopamine and Reward. *Neuron 36*, 241–263.

(26) Bäckman, L., Nyberg, L., Lindenberger, U., Li, S.-C., and Farde, L. (2006) The correlative triad among aging, dopamine, and cognition: Current status and future prospects. *Neurosci. Biobehav. Rev. 30*, 791–807.

(27) Kraft, J. C., Osterhaus, G. L., Ortiz, A. N., Garris, P. A., and Johnson, M. A. (2009) In vivo dopamine release and uptake impairments in rats treated with 3-nitropropionic acid. *Neuroscience 161*, 940–949.

(28) Ortiz, A. N., Oien, D. B., Moskovitz, J., and Johnson, M. A. (2011) Quantification of reserve pool dopamine in methionine sulfoxide reductase A null mice. *Neuroscience 177*, 223–229.

(29) Johnson, M. A., Rajan, V., Miller, C. E., and Wightman, R. M. (2006) Dopamine release is severely compromised in the R6/2 mouse model of Huntington's disease. *J. Neurochem. 97*, 737–746.

(30) Ortiz, A. N., Kurth, B. J., Osterhaus, G. L., and Johnson, M. A. (2010) Dysregulation of intracellular dopamine stores revealed in the R6/2 mouse striatum. *J. Neurochem. 112*, 755–761.

(31) Ortiz, A. N., Osterhaus, G. L., Lauderdale, K., Mahoney, L., Fowler, S. C., von Hörsten, S., Riess, O., and Johnson, M. A. (2012) Motor function and dopamine release measurements in transgenic Huntington's disease model rats. *Brain Res. 1450*, 148–156.

(32) Liberatore, G. T., Jackson-Lewis, V., Vukosavic, S., Mandir, A. S., Vila, M., McAuliffe, W. G., Dawson, V. L., Dawson, T. M., and Przedborski, S. (1999) Inducible nitric oxide synthase stimulates dopaminergic neurodegeneration in the MPTP model of Parkinson disease. *Nat. Med. 5*, 1403–1409.

(33) Masliah, E. (2000) Dopaminergic Loss and Inclusion Body Formation in -Synuclein Mice: Implications for Neurodegenerative Disorders. *Science 287*, 1265–1269.

(34) Morgan, D. G., May, P. C., and Finch, C. E. (1987) Dopamine and serotonin systems in human and rodent brain: effects of age and neurodegenerative disease. *J. Am. Geriatr. Soc.*

(35) Rozans, M., Dreisbach, A., Lertora, J. J., and Kahn, M. J. (2002) Palliative uses of methylphenidate in patients with cancer: a review. *J. Clin. Oncol. 20*, 335–339.

(36) Sood, A., Barton, D. L., and Loprinzi, C. L. (2006) Use of methylphenidate in patients with cancer. *Am. J. Hosp. Palliat. Med. 23*, 35–40.

(37) Meyers, C. A., Weitzner, M. A., Valentine, A. D., and Levin, V. A. (1998) Methylphenidate therapy improves cognition, mood, and function of brain tumor patients. *J. Clin. Oncol. 16*, 2522–2527.

(38) Kohli, S., Fisher, S. G., Tra, Y., Adams, M. J., Mapstone, M. E., Wesnes, K. A., Roscoe, J. A., and Morrow, G. R. (2009) The effect of modafinil on cognitive function in breast cancer survivors. *Cancer 115*, 2605–2616.

(39) Seigers, R., Schagen, S. B., Van Tellingen, O., and Dietrich, J. (2013) Chemotherapy-related cognitive dysfunction: current animal studies and future directions. *Brain Imaging Behav. 7*, 453–459.

(40) Liedke, P. E. R., Reolon, G. K., Kilpp, B., Brunetto, A. L., Roesler, R., and Schwartsmann, G. (2009) Systemic administration of doxorubicin impairs aversively motivated memory in rats. *Pharmacol. Biochem. Behav. 94*, 239–243.

(41) Long, J. M., Lee, G. D., Kelley-Bell, B., Spangler, E. L., Perez, E. J., Longo, D. L., de Cabo, R., Zou, S., and Rapp, P. R. (2011) Preserved learning and memory following 5-fluorouracil and cyclophosphamide treatment in rats. *Pharmacol. Biochem. Behav. 100*, 205–211.

(42) Seigers, R., Schagen, S. B., Coppens, C. M., van der Most, P. J., van Dam, F. S. A. M., Koolhaas, J. M., and Buwalda, B. (2009) Methotrexate decreases hippocampal cell proliferation and induces memory deficits in rats. *Behav. Brain Res. 201*, 279–284.

(43) Seigers, R., and Fardell, J. E. (2011) Neurobiological basis of chemotherapy-induced cognitive impairment: A review of rodent research. *Neurosci. Biobehav. Rev. 35*, 729–741.

(44) Meyers, C. A., and Wefel, J. S. (2010) Cognitive dysfunction: is chemobrain real? *Cancer Symptom Sci. Meas. Mech. Manag.* 51.

(45) Winocur, G., Vardy, J., Binns, M., Kerr, L., and Tannock, I. (2006) The effects of the anti-cancer drugs, methotrexate and 5-fluorouracil, on cognitive function in mice. *Pharmacol. Biochem. Behav. 85*, 66–75.

(46) Fardell, J. E., Vardy, J., Shah, J. D., and Johnston, I. N. (2012) Cognitive impairments caused by oxaliplatin and 5-fluorouracil chemotherapy are ameliorated by physical activity. *Psychopharmacology (Berl.) 220*, 183–193.

(47) Mustafa, S., Walker, A., Bennett, G., and Wigmore, P. M. (2008) 5-Fluorouracil chemotherapy affects spatial working memory and newborn neurons in the adult rat hippocampus. *Eur. J. Neurosci. 28*, 323–330.

(48) Joshi, G., Aluise, C. D., Cole, M. P., Sultana, R., Pierce, W. M., Vore, M., St Clair, D. K., and Butterfield, D. A. (2010) Alterations in brain antioxidant enzymes and redox proteomic identification of oxidized brain proteins induced by the anti-cancer drug adriamycin: implications for oxidative stress-mediated chemobrain. *Neuroscience 166*, 796–807.

(49) Eisenberger, M., Hornedo, J., Silva, H., Donehower, R., Spaulding, M., and Van Echo, D. (1986) Carboplatin (NSC-241-240): an active platinum analog for the treatment of squamous-cell carcinoma of the head and neck. *J. Clin. Oncol. 4*, 1506–1509.

(50) Kavanagh, J. J., and Nicaise, C. (1989) Carboplatin in refractory epithelial ovarian cancer., in *Seminars in oncology*, p 45.

(51) Wagstaff, A. J., Ward, A., Benfield, P., and Heel, R. C. (1989) Carboplatin. *Drugs 37*, 162–190.

(52) Smith, I. E., Harland, S. J., Robinson, B. A., Evans, B. D., Goodhart, L. C., Calvert, A. H., Yarnold, J., Glees, J. P., Baker, J., and Ford, H. T. (1985) Carboplatin: a very active new cisplatin analog in the treatment of small cell lung cancer. *Cancer Treat. Rep. 69*, 43–46.

(53) Schagen, S. B., Muller, M. J., Boogerd, W., Mellenbergh, G. J., and van Dam, F. S. A. M. (2006) Change in Cognitive Function After Chemotherapy: a Prospective Longitudinal Study in Breast Cancer Patients. *JNCI J. Natl. Cancer Inst. 98*, 1742–1745.

(54) D Craig, C. (2013) Cognitive Impairment in Gynecologic Cancers: A Systematic Review of Current Approaches to Diagnosis and Treatment. *J. Palliat. Care Med. 03*.

(55) Bonadonna, G., Rossi, A., Valagussa, P., Banfi, A., and Veronesi, U. (1977) The CMF program for operable breast cancer with positive axillary nodes: Updated analysis on the disease-free interval, site of relapse and drug tolerance. *Cancer 39*, 2904–2915.

(56) Bonadonna, G., Valagussa, P., Rossi, A., Tancini, G., Brambilla, C., Zambetti, M., and Veronesi, U. (1985) Ten-year experience with CMF-based adjuvant chemotherapy in resectable breast cancer. *Breast Cancer Res. Treat. 5*, 95–115.

(57) Bonadonna, G., Moliterni, A., Zambetti, M., Daidone, M. G., Pilotti, S., Gianni, L., and Valagussa, P. (2005) 30 years' follow up of randomised studies of adjuvant CMF in operable breast cancer: cohort study. *bmj 330*, 217.

(58) Engelsman, E., Klijn, J. C. M., Rubens, R. D., Wildiers, J., Beex, L., Nooij, M. A., Rotmensz, N., and Sylvester, R. (1991) "Classical" CMF versus a 3-weekly intravenous CMF schedule in postmenopausal patients with advanced breast cancer: An EORTC Breast Cancer Co-operative Group Phase III Trial (10808). *Eur. J. Cancer Clin. Oncol. 27*, 966–970.

(59) O'shaughnessy, J. A., Blum, J., Moiseyenko, V., Jones, S. E., Miles, D., Bell, D., Rosso, R., Mauriac, L., Osterwalder, B., and Burger, H.-U. (2001) Randomized, open-label, phase II trial of oral capecitabine (Xeloda®) vs. a reference arm of intravenous CMF (cyclophosphamide, methotrexate and 5-fluorouracil) as first-line therapy for advanced/metastatic breast cancer. *Ann. Oncol. 12*, 1247–1254.

(60) Thomson, C. S., Twelves, C. J., Mallon, E. A., Leake, R. E., Group, S. C. T. B., and Network, S. C. T. (2002) Adjuvant ovarian ablation vs CMF chemotherapy in premenopausal breast cancer patients: Trial update and impact of immunohistochemical assessment of ER status. *The Breast 11*, 419–429.

(61) Kawagoe, K. T., Jankowski, J. A., and Wightman, R. M. (1991) Etched carbon-fiber electrodes as amperometric detectors of catecholamine secretion from isolated biological cells. *Anal. Chem. 63*, 1589–1594.

(62) Rice, M. E., and Nicholson, C. (1989) Measurement of nanomolar dopamine diffusion using low-noise perfluorinated ionomer-coated carbon fiber microelectrodes and high-speed cyclic voltammetry. *Anal. Chem. 61*, 1805–1810.

(63) Hashemi, P., Danoski, E., Petrovic, J., Keithley, R. B., and Wightman, R. M. (2009) Voltammetric Detection of 5-Hydroxytryptamine Release in the Rat Brain. *Anal. Chem. 81*, 9462–9471.

(64) Briones, T. L., and Woods, J. (2011) Chemotherapy-induced cognitive impairment is associated with decreases in cell proliferation and histone modifications. *BMC Neurosci. 12*, 124.

(65) Fowler, S. C., Birkestrand, B. R., Chen, R., Moss, S. J., Vorontsova, E., Wang, G., and Zarcone, T. J. (2001) A force-plate actometer for quantitating rodent behaviors: illustrative data

on locomotion, rotation, spatial patterning, stereotypies, and tremor. *J. Neurosci. Methods 107*, 107–124.

(66) Jackson, B. P., Dietz, S. M., and Wightman, R. M. (1995) Fast-scan cyclic voltammetry of 5-hydroxytryptamine. *Anal. Chem. 67*, 1115–1120.

(67) Wightman, R. M., Amatore, C., Engstrom, R. C., Hale, P. D., Kristensen, E. W., Kuhr, W. G., and May, L. J. (1988) Real-time characterization of dopamine overflow and uptake in the rat striatum. *Neuroscience 25*, 513–523.

(68) Jones, S. R., Garris, P. A., Kilts, C. D., and Wightman, R. M. (1995) Comparison of dopamine uptake in the basolateral amygdaloid nucleus, caudate-putamen, and nucleus accumbens of the rat. *J. Neurochem. 64*, 2581–2589.

(69) Kawagoe, K. T., Garris, P. A., Wiedemann, D. J., and Wightman, R. M. (1992) Regulation of transient dopamine concentration gradients in the microenvironment surrounding nerve terminals in the rat striatum. *Neuroscience 51*, 55–64.

(70) Mathews, C., and Van Holde, K. (1996) Biochemistry, 1996. *Benj AminCummings*.

(71) Staat, K., and Segatore, M. (2005) The Phenomenon of Chemo Brain. *Clin. J. Oncol. Nurs. 9*, 713–721.

(72) Merriman, J. D., Von Ah, D., Miaskowski, C., and Aouizerat, B. E. (2013) Proposed Mechanisms for Cancer- and Treatment-Related Cognitive Changes. *Semin. Oncol. Nurs. 29*, 260–269.

(73) Wefel, J. S., Kesler, S. R., Noll, K. R., and Schagen, S. B. (2014) Clinical characteristics, pathophysiology, and management of noncentral nervous system cancer-related cognitive impairment in adults. *CA. Cancer J. Clin.*

(74) Madhyastha, S., Somayaji, S. N., Rao, M. S., Nalini, K., and Bairy, K. L. (2002) Hippocampal brain amines in methotrexate-induced learning and memory deficit. *Can. J. Physiol. Pharmacol. 80*, 1076–1084.

(75) Evenden, J. (2013) Cognitive impairments and cancer chemotherapy: Translational research at a crossroads. *Life Sci. 93*, 589–595.

(76) Gerfen, C. R. (1992) The neostriatal mosaic: multiple levels of compartmental organization in the basal ganglia. *Annu. Rev. Neurosci. 15*, 285–320.

(77) Ferguson, S. M., Eskenazi, D., Ishikawa, M., Wanat, M. J., Phillips, P. E. M., Dong, Y., Roth, B. L., and Neumaier, J. F. (2011) Transient neuronal inhibition reveals opposing roles of indirect and direct pathways in sensitization. *Nat. Neurosci. 14*, 22–24.

(78) Cazorla, M., de Carvalho, F. D., Chohan, M. O., Shegda, M., Chuhma, N., Rayport, S., Ahmari, S. E., Moore, H., and Kellendonk, C. (2014) Dopamine D2 Receptors Regulate the Anatomical and Functional Balance of Basal Ganglia Circuitry. *Neuron 81*, 153–164.

(79) Hikida, T., Kimura, K., Wada, N., Funabiki, K., and Nakanishi, S. (2010) Distinct Roles of Synaptic Transmission in Direct and Indirect Striatal Pathways to Reward and Aversive Behavior. *Neuron 66*, 896–907.

(80) Hikosaka, O., Takikawa, Y., and Kawagoe, R. (2000) Role of the basal ganglia in the control of purposive saccadic eye movements. *Physiol. Rev. 80*, 953–978.

(81) Kravitz, A. V., Tye, L. D., and Kreitzer, A. C. (2012) Distinct roles for direct and indirect pathway striatal neurons in reinforcement. *Nat. Neurosci. 15*, 816–818.

(82) Volkow, N. D., Wang, G.-J., Fowler, J. S., Gatley, S. J., Logan, J., Ding, Y.-S., Hitzemann, R., and Pappas, N. (1998) Dopamine transporter occupancies in the human brain induced by therapeutic doses of oral methylphenidate. *Am. J. Psychiatry 155*, 1325–1331.

(83) Palmiter, R. D. (2008) *Dopamine Signaling in the Dorsal Striatum Is Essential for Motivated Behaviors*. *Ann. N. Y. Acad. Sci. 1129*, 35–46.

(84) Jocham, G., Klein, T. A., and Ullsperger, M. (2011) Dopamine-Mediated Reinforcement Learning Signals in the Striatum and Ventromedial Prefrontal Cortex Underlie Value-Based Choices. *J. Neurosci. 31*, 1606–1613.

(85) Calipari, E. S., Huggins, K. N., Mathews, T. A., and Jones, S. R. (2012) Conserved dorsal–ventral gradient of dopamine release and uptake rate in mice, rats and rhesus macaques. *Neurochem. Int. 61*, 986–991.

(86) Bã¢«man, L., Ginovart, N., Dixon, R. A., Wahlin, T.-B. R., Wahlin, Ä«., Halldin, C., and Farde, L. (2000) Age-Related Cognitive Deficits Mediated by Changes in the Striatal Dopamine System. *Am. J. Psychiatry 157*, 635–637.

(87) Brozoski, T. J., Brown, R. M., E, H., and Goldman, P. S. (1979) Cognitive deficit caused by regional depletion of dopamine in prefrontal cortex of rhesus monkey. *Science 205*, 929–931.

(88) Neves, G., and Lagnado, L. (1999) The kinetics of exocytosis and endocytosis in the synaptic terminal of goldfish retinal bipolar cells. *J. Physiol. 515*, 181–202.

(89) Zucker, R. S., and Regehr, W. G. (2002) Short-Term Synaptic Plasticity. *Annu. Rev. Physiol. 64*, 355–405.

(90) Rizzoli, S. O., and Betz, W. J. (2005) Synaptic vesicle pools. *Nat. Rev. Neurosci. 6*, 57–69.

(91) Harata, N., Ryan, T. A., Smith, S. J., Buchanan, J., and Tsien, R. W. (2001) Visualizing recycling synaptic vesicles in hippocampal neurons by FM 1-43 photoconversion. *Proc. Natl. Acad. Sci. 98*, 12748–12753.

(92) Kuromi, H., and Kidokoro, Y. (2003) Two synaptic vesicle pools, vesicle recruitment and replenishment of pools at the Drosophila neuromuscular junction. *J. Neurocytol. 32*, 551–565.

(93) Richards, D. A., Guatimosim, C., Rizzoli, S. O., and Betz, W. J. (2003) Synaptic vesicle pools at the frog neuromuscular junction. *Neuron 39*, 529–541.

(94) Heien, M., and Wightman, R. M. (2006) Phasic dopamine signaling during behavior, reward, and disease states. *Curr. Drug Targets-CNS Neurol. Disord. 5*, 99–108.

(95) Venton, B. J. (2006) Cocaine Increases Dopamine Release by Mobilization of a Synapsin-Dependent Reserve Pool. *J. Neurosci. 26*, 3206–3209.

(96) Spector, S., Sjoerdsma, A., and Udenfriend, S. (1965) Blockade of endogenous norepinephrine synthesis by α-methyl-tyrosine, an inhibitor of tyrosine hydroxylase. *J. Pharmacol. Exp. Ther. 147*, 86–95.

(97) (2002) Huntington's disease 3rd ed. Oxford University Press, Oxford ; New York.

(98) Kish, S. J., Shannak, K., and Hornykiewicz, O. (1988) Uneven pattern of dopamine loss in the striatum of patients with idiopathic Parkinson's disease. *N. Engl. J. Med. 318*, 876–880.

(99) Alston, T. A., Mela, L., and Bright, H. J. (1977) 3-Nitropropionate, the toxic substance of Indigofera, is a suicide inactivator of succinate dehydrogenase. *Proc. Natl. Acad. Sci. 74*, 3767–3771.

(100) Piallat, B., Benazzouz, A., and Benabid, A. L. (1996) Subthalamic nucleus lesion in rats prevents dopaminergic nigral neuron degeneration after striatal 6-OHDA injection: behavioural and immunohistochemical studies. *Eur. J. Neurosci. 8*, 1408–1414.

Chapter 3. Electrochemical measurements in R6/2 Huntington's Disease Model Mice

3.1 Introduction

Huntington's disease (HD) is a fatal, autosomal dominant neurodegenerative disorder that is characterized by motor dysfunction, altered behavior, and cognitive impairment. HD is caused by a CAG repeat expansion on chromosome 4 of the IT15 gene, which encodes the huntingtin protein (htt).[1] An average person normally has 16 to 20 CAG repeats on the huntingtin gene while a person with HD will have 40 or more.[2] This protein is ubiquitously expressed and is highly concentrated in the central nervous system (CNS).[3] The mutation results in a polyglutamine (polyQ) expansion near the N-terminus of htt. HD affects 4 to 10 out of 100,000 people of western European descent and 0.4 out of 100,000 people of Asian descent [4]. Symptom onset for HD typically occurs between 35 and 50 years of age and the age of onset is directly correlated to the length of the expanded CAG repeat.[2,5–7] With an extremely long CAG repeat typically of 52 or more, symptomatic onset may begin in juveniles.[5,6,8] This early onset most often also includes a more rapid progression of the disease and increased severity.[2]

Documentation of the existence of HD can be found as early as the mid-14th century. Although little was known about the cause of the disease, it was described as an epidemic of what was called "a dancing mania".[9] It was not until later that the term "chorea" was used by the famed student of all sciences, Paracelsus (more specifically, Philippus Aureolus Theophrastus Bombastus von Hohenheim) in the late 15th and early 16th centuries.[9] This term, which is derived from the Greek word for "dance," was used to describe the involuntary muscle movements that result from the disorder. HD eventually spread to the new world in the early 17th century. In the American colonies, HD was coined as "San Vitus" or "That disorder".[9] Due to the

uncontrollable, unusually rhythmic movements associated with HD, people with the disorder were often observed by the top physicians and were misdiagnosed with demonic possession. This diagnosis was tragic as the appropriate cure at the time was public execution. It is assumed that at least one of the victims of the Salem witch trials was burned at the stake because she suffered from HD.[9] Despite a few previous attempts, an accurate medical description of HD was unavailable until 1872 when Dr. George Huntington published his findings in the *Medical and Surgical Reporter of Philadelphia.*[10] Hence, the disease was named after the young doctor. It is interesting to note that this was one of only two publications he would ever write.

The progression of HD typically occurs over the course of 15 to 20 years from the time of initial clinical diagnosis to death.[1] During the early stages, a slow deterioration in intellectual capabilities and minor emotional changes occur.[11] Other symptoms may include weight loss, interruptions in the patient's sleep cycle, or changes in sexual behavior, and may be caused by hypothalamic dysfunction.[12] Furthermore, patients may begin to exhibit minor motor abnormalities such as restlessness, abnormal eye movements, and unusual hand movements.[13] As the syndrome associated with HD progresses, motor function deficits gradually worsen. The clinical diagnosis of HD is most commonly based on the development of chorea, which is exhibited by 90% of patients, and is characterized by excessive, non-rhythmic, abrupt, unintentional movements.[1,14]

The severity of this phenotypical response to HD ranges from excessive fidgeting and exaggerated gesture to severely violent, disabling movements.[11,14] In the later stages of HD, chorea is often replaced with other, more severe movement abnormalities such as bradykinesia, dystonia, rigidity, and complete loss of coordination.[13,15] Eventually, patients with HD lose their ability to support themselves. Reasons for this loss of independence include the complete loss of

mobility and ability to communicate. Due to its progressive nature, the effects of late stage HD are ultimately fatal. Death can be caused by physical injuries (falling), malnutrition, choking, and most commonly, pneumonia.[16] Along with the physical abnormalities and cognitive impairments discussed, HD is also characterized by psychiatric manifestations that may include aggression, anxiety, depression, and the initiation or progression of addictive behaviors. The progression of such psychiatric changes can often lead to necessary institutionalization and/or an increase in suicidal thoughts and action.[11,17] The observance of motor function impairments in conjunction with these psychiatric and behavior abnormalities can be used to diagnose HD. Additionally, due to its autosomal dominant pattern of inheritance, information regarding familial history has also been used to diagnose HD. Nevertheless, definitive HD diagnosis can only be confirmed by genetic testing. The development of DNA diagnostics has made it possible to properly diagnose HD without obtaining standard clinical information.[11] Despite the available information regarding pathology, the underlying mechanism leading to neuronal degeneration is not well understood. HD, therefore, remains incurable and much effort has been and is currently focused on understanding the mechanisms of neuronal degradation.

3.1.2 Mechanism of HD

The striatum, a brain region richly innervated with dopamine-releasing terminals, undergoes extensive atrophy throughout the course of HD. About 90 to 95% of the neuronal cell bodies in the striatum are GABAergic medium spiny neurons, which receive input from dopaminergic neurons that project from the substantia nigra pars compacta (SN_c). These GABAergic neurons project to the pallidum through two distinct pathways: the *direct* pathway, which provides inhibitory tone to the globus pallidus internal segment (GPi), and the *indirect*

pathway, which provides inhibitory tone to the globus pallidus external segment (GPe). Activation of the direct pathway facilitates movement, while activation of the indirect pathway inhibits movement. Previous evidence has indicated that the indirect pathway neurons are most vulnerable to degeneration as HD progresses; thus, the loss of this pathway results in the expression of excess movement in the form of chorea, the hallmark motor feature of HD.[18]

The mechanisms that underlie the degeneration of these striatal medium spiny neurons have been extensively investigated. It has been shown that mutant htt forms insoluble aggregates and nuclear inclusions in medium spiny neurons of patients with HD.[19–21] The role of aggregates in the pathology of HD is considered to be of key importance as their presence suggests that mutant htt is processed differently in those afflicted with HD. Additionally, mutant htt acts to impede the function of normal huntingtin protein, which is essential to the viability to the neuronal populations that degenerate in HD.[22] However, it is thought that the toxicity of mutant htt itself, a direct result of the polyQ extension, contributes to the majority of the disease pathogenesis.[23,24] This toxicity appears to be enhanced by a mechanism that involves the activation of D2 family DA receptors and the presence of reactive oxygen species.[25]

3.1.3 HD Model Rodents

Since the discovery of the causative mutation of HD, numerous genetically-engineered animal models of HD have been developed. The R6 line of HD model mice were created using a 1.9 kb gene fragment containing promoter sequences and exon 1 of the mutant human HD gene. [24] Among the most commonly used models are R6/1 and R6/2 mice, which possess CAG repeat lengths of about 115 and 144, respectively. Both models only express exon 1 of the 67 exon gene. This exon encodes only 3% of the N-terminal region of the protein, suggesting that the

expanded polyQ tract responsible for the disease.[26] As would be expected, the longer repeat length is associated with the expression of a more quickly progressing motor phenotype in mice: R6/1 mice express overt motor symptoms at 15-21 weeks of age while R6/2 mice express symptoms at 9-11 weeks.

There have since been other genetic HD mouse lines that include larger portions of the gene. For example, yeast artificial chromosome (YAC) lines contain between 18 to 128 CAG repeats on the whole gene have been reported.[27] Of these lines, YAC 128 mice have used most extensively because they experience progressive neurodegeneration and motor impairments.[9,28,29] Unlike the R6 mice, YAC mice tend to live normal lifespans. For a good review on the development of genetic HD model mice, see Levine et al.[30]

In an attempt to accommodate the need for more complex experiments and to recapitulate the neurological HD syndrome more faithfully, von Hörsten et al. (2003) developed a transgenic HD model rat (HDtg). Like the R6/2 mouse, the HDtg rat possesses a truncated portion of the gene encoding huntingtin, except that the CAG repeat length is significantly shorter: 51 in the rat versus 144 in the R6/2 mouse. Therefore, it is not surprising that the overt motor behavioral phenotype is expressed more gradually by HDtg rats compared to R6/2 mice. In HDtg rats there are no detectable behavioral abnormalities at 5 months of age. Spatial and working memory abnormalities appear at 10 months and coordination loss becomes relevant between 10-15 months of age. Noticeable striatal atrophy occurs at 12 months of age.

The studies involved in this chapter were performed using R6/2 HD model mice. The R6/2 model is considered to be the gold standard for researchers studying HD since they have rapid phenotypical expression in comparison to other mouse models.

3.1.4 Past Microdialysis studies

Microdialysis studies aimed at understanding neurotransmitter alterations in HD model mice have been conducted by other groups. Several features make microdialysis an attractive method for measuring neurotransmitter levels in the brain. First, it allows the sampling of virtually any chemical species, including small molecule neurotransmitters and neuropeptides, that will diffuse into the probe. Furthermore, microdialysis allows the real time, continuous sampling of endogenous biological compounds *in vivo*. Moreover, the concentrations of a specific analyte or set of analytes can be measured over long periods of time. Sampling times can range from minutes to days and perhaps even weeks depending on the probe and its surrounding environment. This ability is quite attractive for studying analyte concentration changes that may occur over long periods of time. However, most commercially available microdialysis probes are large (about 200μm) compared to carbon-fiber microelectrodes used in our work (7μm), resulting in the potential for additional tissue damage upon implantation [31]. This damage may influence detected neurotransmitter release.[32] Moreover, sampling intervals for many molecules tend to be on the order of minutes or hours,[33,34] limiting temporal resolution. In one of the first studies aimed at quantifying DA levels in transgenic HD model mice, Petersén et al.[35] found that extracellular DA levels were diminished in 16-week-old R6/1 mice in comparison to age-matched WT control mice.[35] Moreover, even though these extracellular DA levels were decreased, post mortem tissue content studies showed no significant difference in total DA levels between R6/1 and wild type controls.[35] Further studies, in which malonate was locally applied *in vivo* by infusion through microdialysis probes, were then conducted. Malonate is a mitochondrial complex II inhibitor that induces DA release and ultimately neuronal cell death.[35,36] Malonate-induced increases of extracellular DA levels were significantly less in R6/1

mice compared to WT control mice. Conversely, increases in extracellular glutamate, aspartate, and GABA were not substantially different.

More recent *in vivo* microdialysis studies carried out in R6/2 and YAC128 mice have reaffirmed and expanded on the results obtained by Petersén *et al*. in R6/1 mice, demonstrating that extracellular DA concentrations were diminished in R6/2 mice and YAC128 mice.[37] Taken together, these microdialysis studies revealed that decreases of extracellular DA are not simply due to the loss of neuronal populations or the inability to synthesize DA, but rather that the ability of neurons to release DA is impaired.[35,38] In order to probe the underlying mechanisms responsible for decreased striatal DA release, we applied fast-scan cyclic voltammetry at carbon-fiber microelectrodes to measure sub-second DA release events both *in vivo* and in brain slices, described in subsequent sections of this chapter.

3.1.5 Voltammetric measurements of dopamine release and uptake in R6/2 and R6/1 mice

Previous behavioral studies have demonstrated that, compared to WT controls, R6/2 mice have a blunted locomotor response to cocaine (COC) and methamphetamine (METH), inhibitors of DA uptake, suggesting an impairment of DA release.[8,38] These behavioral studies, taken with the microdialysis results of Petersen et al. (2002), prompted us to investigate how mechanisms of DA release and uptake are impacted in HD model rodents. Initially, DA release and uptake was measured using FSCV in striatal slices acutely harvested from R6/2 mice and age-matched wild type (WT) control mice. Exocytotic release was induced by the application of a single, biphasic electrical stimulus pulse (350μA current, 4ms duration).[8] Upon analyzing brain slices from subjects at ages ranging from 6 to 14 weeks, a dramatic attenuation of DA release was found in R6/2 mice compared to WT mice. This attenuation progressively worsened with age, in

agreement with diminished locomotor activity.[8] Experiments in which exogenous DA was iontophoretically injected revealed no difference in the extracellular space due to neuronal atrophy in R6/2 mice in comparison to WT controls.[39] Thus, the attenuation in DA release is not simply a result of neurotransmitter dilution, but rather that DA neurons in the striatum have a diminished capacity for DA release.

The plots of stimulated release were also modeled using simplex modeling software developed by Prof. Paul Garris (Illinois State University, Normal, IL). Values of V_{max}, the maximum rate of uptake by the DA transporter, were extracted from these modeled curves. Importantly, V_{max} was unchanged between genotype and age group, indicating that uptake was not impaired in R6/2 mice. Moreover, the uptake inhibition constants (K_i) for COC and METH, which indicate how strongly the drugs bind to the DA transporter protein molecules, did not significantly differ between R6/2 and WT control mice. Collectively, these results suggest that impairments in DA release, rather than uptake, are responsible for locomotor abnormalities observed in R6/2 mice, either in the presence or absence of psycho-stimulants.[8] Similar FSCV experiments have revealed that DA release is also attenuated in R6/1 HD model mice.[40] These findings are consistent with those found in R6/2 mice in that DA release attenuation progressed with age and the onset of the overt phenotype. Interestingly, DA uptake, again measured as V_{max}, was impaired in R6/1 HD model mice. Although the specific mechanisms underlying this impairment are not clear, the ages of the mice may also play a role, given that R6/1 mice develop significant deficits in rotorod performance at 13 to 20 weeks of age, while R6/2 mice become severely impaired at 8 to 12 weeks of age.[41,42]

3.1.6 Regional differences in DA release attenuation in R6/2 Mice

Previous work in our group has determined sub-second alterations in dopaminergic neurotransmission in R6/2 HD model mice utilizing fast-scan cyclic voltammetry (FSCV). FSCV at the surface of carbon-fiber microelectrodes offers high spatial and temporal resolution, which facilitates the investigation of electroactive biomolecules, such as neurotransmitters, at physiologically relevant timescales.[43,44] In previous work, it was established that electrically evoked DA release is severely attenuated in the dorsolateral striatum of brain slices taken from R6/2 mice.[8,39,45] Here, we have determined stimulated dopamine release is altered in the subdivisions of the striatum, including the dorsal lateral (DL), dorsal medial (DM), ventral lateral (VL), and ventral medial (VM) regions.

While there exists no clear neurophysiological differences in these regions, studies have identified the role of each region in controlling behavior.[46] Furthermore, as mentioned in Chapter 1 of this document, there exists an input gradient throughout the striatum. This gradient is established by two unique dopaminergic inputs to the striatum from the mesolimbic pathway, that project from the ventral tegmental area via A10 neurons, and nigrostriatal pathway, which projects from the substantia nigra pars compacta via A9 neurons.[47] The A9 neurons project to the dorsal striatum from the VTA and the A10 neurons project to the ventral striatum from substantia nigra pars compacta.[48] Differing functionalities have resulted from this gradient. Motor function and execution are associated with the dorsal striatum.[48–51] The ventral striatum is associated with appetitive motivation and reinforcement learning.[48,52–54] In healthy humans and rats, there exists an intrinsic dorsal to ventral gradient for stimulated dopamine release.[48] Previous studies have shown DA dysregulation in HD model mice.[8,39,45,55,56] To date, differences in striatal regional release and their implications in the mechanism of HD pathogenesis have yet

to be addressed. Here, we have uncovered statistically significant regional differences in DA release, in addition to investigating alterations in dopamine transporter (DAT) function and DA release in response to stress from a high pulse stimulation train using FSCV.

The primary mode of dopamine clearance from the synaptic cleft is reuptake by dopamine transporter channel proteins back into the neuron.[57] These integral proteins control the time by which DA may reside in the synaptic cleft and mediate DA diffusion.[58] Modeling of FSCV traces taken from HD and WT mice have been used to deduce the DAT reuptake rate is unaltered in HD mice. Furthermore, the uptake inhibition constants were unchanged between experimental groups for cocaine and methamphetamine binding, which suggests that drugs bind to the dopamine transporter proteins at normal rates.[8] Unlike the modeled data, our autoradiography results indicate that HD plays an important role in affecting the DAT population in the striatum. The rate of DA reuptake can have profound implications in behavior and cognition.[59,60]

The purpose of this work was to determine if DA dysregulation is regionally dependent within the striatum. Here, three important facets of HD pathogenesis are explored in R6/2 model mice. First, we investigated the effect of R6/2 mouse age on dopaminergic neuronal release in all four quadrants of the striatum. This was done using FSCV in R6/2 and wild type (WT) mice at 7-9, 10-12, and 12-14 weeks of age with the goal of determining if the extent of overt motor phenotypic symptoms corresponds to further alterations of the dopaminergic system, according to region in the striatum. Statistically significant regional release differences were seen. Second, the effect of stimulation frequency during high pulse stimulations on regional release was analyzed. This was done to determine if dopamine reserve pool release was altered by the HD phenotype, again according to location in the striatum. It was found that under intense

stimulation, there is a difference in DA release in the dorsal striatum, but not in the ventral striatum. Third, autoradiograpy of the dopamine transporter was conducted to investigate the findings of others from computational modeling studies that the rate of dopamine uptake is unaltered by HD according to age and striatal region. Our results indicate generalized DAT depletions by genotype.

3.2 Experimental Procedures

3.2.1 Animals

All experiments were carried out in accordance with the National Institutes of Health *Guide for the Care and Use of Laboratory Animals.* All procedures were approved by the University of Kansas Institutional Animal Care and Use Committee. Male R6/2 [B6CBA-Tg(HDexon1)62Gpb] and WT mice (Jackson Laboratories; Bar Harbor, ME, USA) were housed 5 per cage in the University of Kansas Animal Care Unit. Food and water was available *ad libitum*. Mice were maintained on a 12 hour light/dark cycle with lights on at 6:00 AM and lights out at 6:00 PM. A temperature of 70 ± 2 °C and humidity level of 50 ± 20% was maintained.

3.2.2 Electrode fabrication

Carbon-fiber cylindrical microelectrodes were fabricated as previously described.[61,62] Briefly, 7µm carbon-fiber purchased from Goodfellow Cambridge Ltd. (Huntingdon, England) was loaded into glass capillaries (4in, 1.2mm OD; A-M Systems, Inc. Carlsborg, WA, USA) and pulled using a heated coil puller (Narishige International USA, East Meadow, NY, USA). Carbon-fiber tips were then cut with a scalpel 25 µm from the end of the glass seal. Electrodes

were then sealed by dipping into a well-mixed epoxy mixture of 0.24g EPI-CURE 3234 Curing Agent (lot FCXC4114/0886GG) and 2.00g EPON Resin 815C (lot HADN0003/1307GG). Excess resin was removed by dipping several times in toluene and electrodes were then baked for 1 hour at 100°C. The electrodes were back-filled with 0.5 M potassium acetate in order to establish an electrical connection between the carbon-fiber and the inserted silver wire.

3.2.3 Brain slices

Brain slices were harvested as previously described.[56] In summary, rats were deeply anesthetized by isoflurane inhalation and decapitated. The brain was then immediately removed and placed into ice-cold artificial cerebral spinal fluid (aCSF). The aCSF solution contained the following concentrations: 2.5 mM KCl, 126 mM NaCl, 1.2 mM NaH_2PO_4, 25 mM $NaHCO_3$, 2.4 mM $CaCl_2$, 1.2 mM $MgCl_2$, 20 mM HEPES, 11 mM D-glucose. The pH was adjusted to 7.4 with NaOH. To ensure the tissue received ample oxygen, the aCSF was continuously bubbled with 95% O_2/5% CO_2 throughout the experiment. After chilling for one minute, the cerebellum was removed and the brain was bisected longitudinally using a sterile razor blade. The sample was then stored at -80°C and saved for HPLC analysis. The other hemisphere of the brain was then glued to a plate against a cube of agar for support. Several 300μm coronal brain slices were then obtained using a vibratome (*Leica Microsystems, Bannockburn, IL, USA*). In a typical recording session, a single striatal brain slice was transferred to a perfusion chamber where oxygenated aCSF, maintained at 34ºC using a thermostatted perfusion chamber and in-line heater, flowed over the slice at 2 mL/min. Slices were equilibrated for at least one hour before collecting measurements.

3.2.4 Electrochemical measurements using FSCV

Procedures for measuring DA release and uptake with background-subtracted FSCV have been described in detail previously.[55, 56,64,65] Briefly, a pre-calibrated cylinder carbon-fiber microelectrode was inserted 100μm into the brain slice using micromanipulators and a stereoscope. The electrode was positioned between two biphasic stimulating electrodes (A-M Systems Inc, Carlsborg, WA, USA) in the striatum. For DA detection, a triangular waveform starting at -0.4V, scanning up to 1.0V, and back to -0.4V, was applied to the carbon-fiber microelectrode at a scan rate of 300V/s and an update rate of 10 Hz. Dopamine release was evoked both by applying a single, biphasic pulse (350 μA, 4 ms total duration) and by applying 120 pulse stimulations. For the 120-pulse stimulations, DA release was measured using stimulation frequencies of 20, 30, 40,50, and 60 Hz at each of the four quadrants of the striatum (DL, DM, VM, and VL). At each location, DA release was measured starting with the lowest stimulation frequency to the highest. The peak current after stimulation was used for all release measurements and there was a 5 minute recovery period between each measurement. The current measured from DA oxidation was plotted versus potential and the successive voltammograms were plotted versus time.

3.2.5 Autoradiography of Dopamine Transporter

Regional densities of DAT were determined by [^{3}H]WIN 35,428 autoradiography according to a modification of the methods of Coulter et al.[66] Briefly, brains were collected, frozen in isopentane, and stored at -70º C until sectioning. Coronal sections (20 μm) were cut on a cryostat. Duplicate sections were incubated with 4 nM [^{3}H]WIN 35,428 (Perkin-Elmer, SA = 84 Ci/mmol) in buffer (50 mM $NaHPO_4$, 50 mM NaCl, pH 7.4) for one hour on ice. Non-

specific binding was defined in the presence of 50 μM cocaine. After incubation, slides were dipped in ice-cold buffer, washed for two consecutive two minute periods in ice-cold buffer, dipped in ice-cold deionized water, and dried. Radiolabeled sections were then opposed to ^{3}H-Hyperfilm (Amersham, Arlington Heights, IL) with [^{3}H]methylmethacrylate autoradiography standards for 19 days. ^{3}H-Hyperfilm was developed according to the manufacturer's instructions. Brain sections were then stained with cresyl violet. Autoradiographic images were digitized and quantified using ImageJ. A Rodbard plot was used to describe the relationship between optical density and radioactivity. Measurements represent average pixel optical density by volume analysis. Brain regions were identified according to the atlas of Paxinos and Watson.[67] The caudate nucleus was divided into quadrants and sampled bilaterally at five levels. Values were averaged to yield a binding density for each animal. Data are reported as specific binding (fmol/mg tissue equivalent) and analyzed for effect of treatment and quadrant by two-way ANOVA (SigmaPlot 12.5).

3.2.5 Statistics

Statistical analyses were conducted using GraphPad Prism software (GraphPad Software Inc., San Diego, CA, USA). For statistical analyses, n = the number of rats. Data are given as mean ± SEM.

3.3 Results and Discussion

It has been previously been shown that single pulse electrically evoked DA release is severely attenuated in the striatum of R6/2 transgenic mice.[8,39] The electrochemical

measurements performed in these studies were taken from the dorsolateral caudate. Experimenters have chosen to take measurements in this brain region as it is known to be exclusively innervated from the nigrostriatal pathway[8,68] which is known to degenerate in HD.[69–72] The vast majority of FSCV research performed has been done on the dorsolateral caudate, but little has been done to determine if DA release is affected in other striatal regions. Regional differences in DA release in the striatum may account for or provide insight into how HD progresses. Here, we have quantified electrically evoked DA release with FSCV in the four quadrants of R6/2 HD model mice and their WT counterparts to probe for possible regional differences on the impact HD has on striatal DA release.

3.3.1 Striatal Dopamine Release

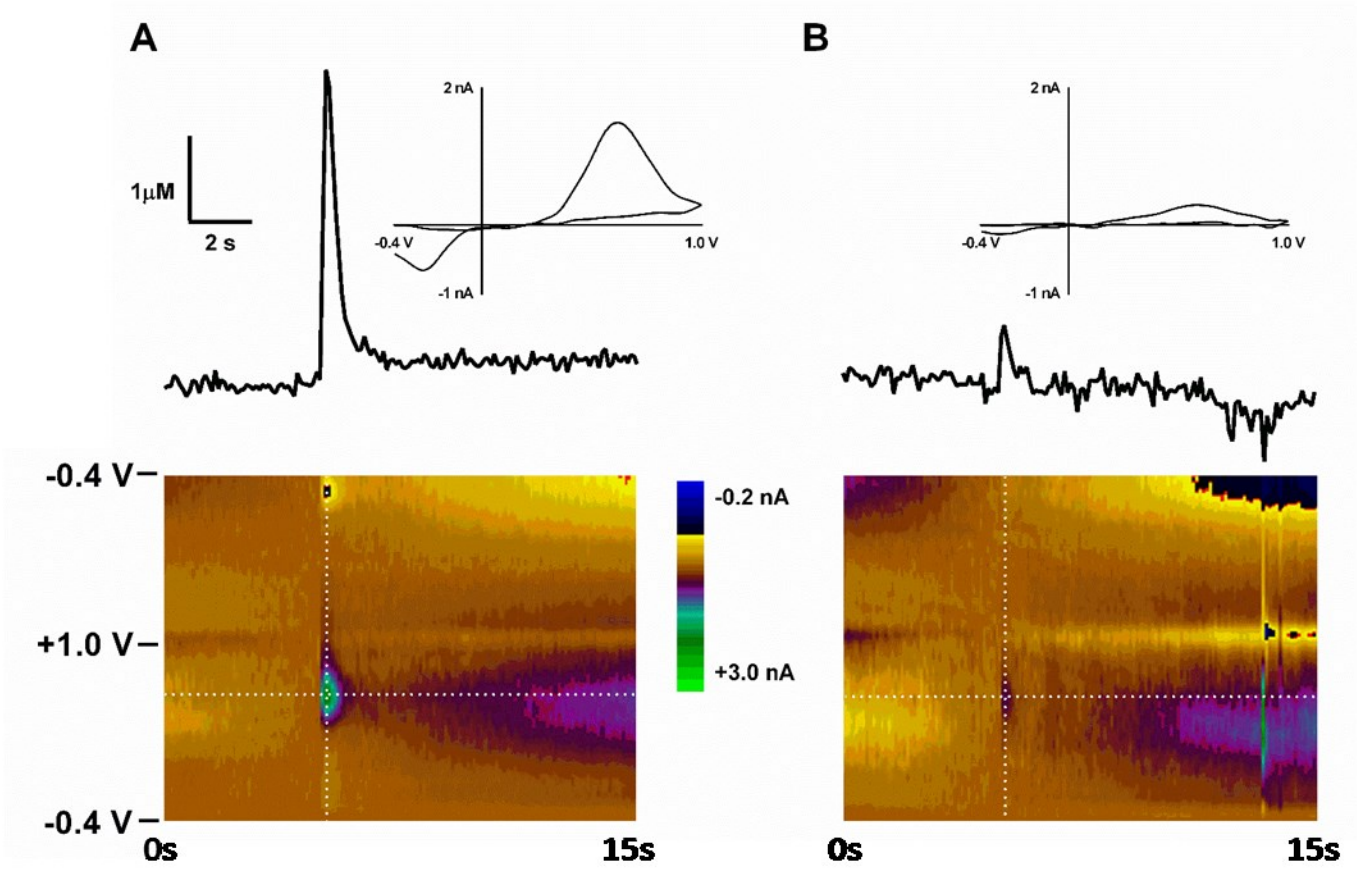

Figure 1. Dopamine release comparison of a wild-type control (A) and an R6/2 mouse (B). Representative color plots and stimulated DA release plots, sampled along the horizontal dashed lines on the color plots, are shown. Cyclic voltammograms, sampled along the vertical dashed lines on the color plots, are shown directly above the stimulated release plots to confirm the presence of DA.

Electrically-evoked DA release was measured by FSCV in the dorsolateral dorsal lateral (DL), dorsal medial (DM), ventral medial (VM), and ventral lateral (VL) quadrants of the striatum in coronal brain slices. Four measurements were taken in each quadrant and averaged to account for possible heterogeneity between single measurements. Representative raw data for a 12 week-old R6/2 and WT mouse can be seen in Fig. 1. The cyclic voltammograms in Fig. 1 confirm that DA is the analyte being measured. The color plots show a series of unfolded and stacked CVs with a color-coded current response. The representative current responses taken from the DL striatum in Figure 1B suggest, as expected, that DA release is attenuated in R6/2 mice.

It was further determined that single-pulse electrically-evoked DA release is attenuated in all quadrants of the striatum when compared to WT controls: 18% of WT averaged across all brain regions $[DA]_{max}$ (Fig. 2; two-way ANOVA , $p < 0.01$, $n = 5$). Our initial studies suggested that DA release attenuation was more severe in the dorsal striatum. To gain further insight as to how regional differences in stimulated DA release progresses over time, measurements were taken from 7-9, 10-11, and 12-14 week old R6/2 and WT mice.

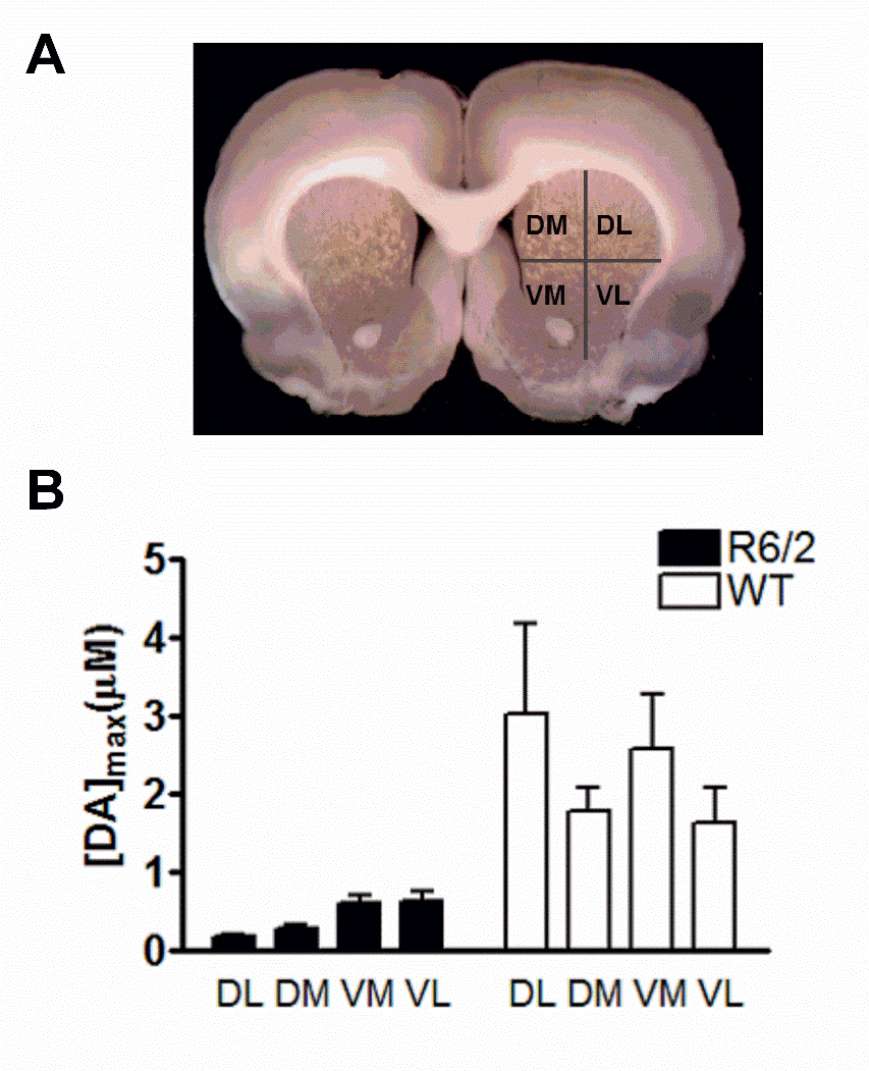

Figure 2. Comparative DA release concentrations by striatal region for R6/2 and WT mice. (A) Image of coronal brain slice containing the striatum. The four quadrants sampled from within the striatum are outlined. (B) $[DA]_{max}$ for R6/2 mice in comparison to WT controls shown per region of the striatum (two-way ANOVA , $p < 0.01$, $n = 5$).

3.3.2 Regional differences in dopamine release attenuation

The progression of DA release attenuation by region can be seen in Fig. 3. At 7-9 weeks of age, there was no significant regional differences in electrically stimulated DA release for both R6/2 and WT mice (Fig. 3A; separate one-way ANOVA for R6/2 and WT; R6/2 $p > 0.05$, $n = 6$; WT $p > 0.05$, $n = 5$). At 10-11 weeks, there is a significant regional difference in stimulated DA release for R6/2 mice (Fig. 3B; one-way ANOVA, $p < 0.05$, $n = 6$). There was no significant regional difference in release for WT mice (Fig. 3B; one-way ANOVA, $p > 0.05$, $n = 6$) at this age group. At 12-14 weeks of age, which is the age at which the HD phenotype is most severe, stimulated DA release in the dorsal striatum is 42% percent of release in the ventral striatum (Fig. 3C; one-way ANOVA, $p < 0.005$, $n = 5$). There was no significant regional difference in stimulated DA release for WT mice for this age group (Fig. 3C; one-way ANOVA, $p > 0.05$, $n = 5$). There is therefore a gradient in the attenuation of DA release caused by the HD mutation in R6/2 transgenic mice. Thus, changes in DA release are not a consequence of regional alterations in DAT function.

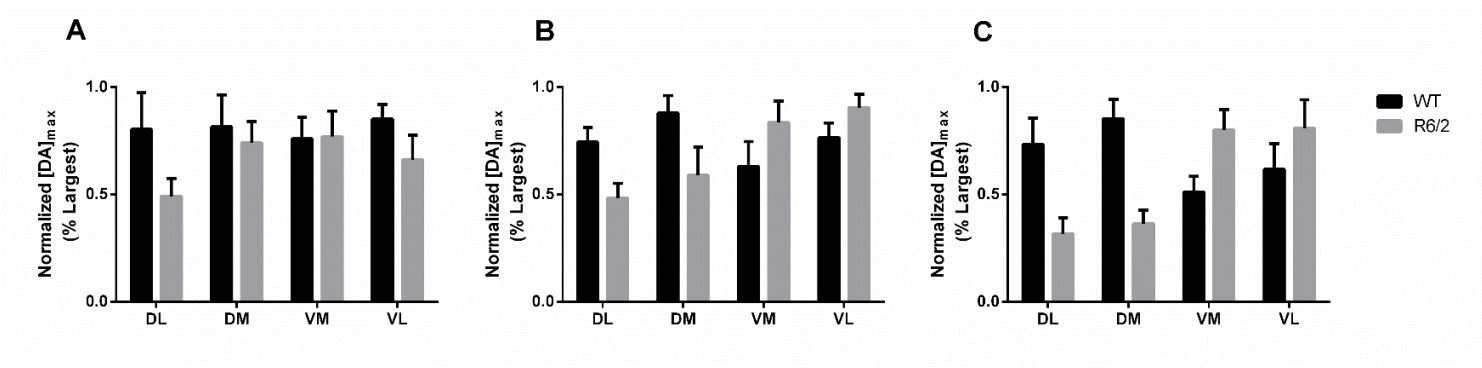

Figure 3. Comparative DA release by region in R/62 and WT mice. A) Normalized $[DA]_{max}$ by striatal region for 7-9 week-old R6/2 and WT mice (two-way ANOVA, $p > 0.05$, n = 5 WT and n = 6 R6/2). B) Normalized $[DA]_{max}$ by striatal region for 10-11 week-old R6/2 and WT mice (two-way ANOVA, $p < 0.05$, n = 6). C) Normalized $[DA]_{max}$ by striatal region for 12-14 week-old R6/2 and WT mice (two-way ANOVA, $p < 0.001$, n = 5).

3.3.3 Regional differences in DA release with 120 stimulus pulses

According to the generalized three-pool model of vesicular neurotransmitter storage within a neuron, there are three distinct neurotransmitter pools. These include the readily releasable, recycling, and reserve pools.[73–75] The readily releasable pool contains 1-2 % of stored vesicles and undergoes release upon mild stimulation. The recycling pool accounts for 5-20 % of vesicles and replenishes the readily releasable pool after its depletion.[76–78] The reserve pool contains the majority of stored vesicles (80-90%) and is mobilized under prolonged neuronal stimulation. Electrical stimulation in conjunction with FSCV has been previously used to obtain information regarding vesicular storage in R6/2 mice.[8,39,55] Specifically, it has previously been

shown there is a significant difference in DA release at high stimulation frequencies (50 and 60Hz) in the dorsolateral striatum when applying 120 stimulation pulse trains.[55] This multiple stimulation pulse study, along with a separate pharmacological manipulation, lead to the conclusion that proper reserve pool DA storage is negatively impacted by HD in the dorsal lateral striatum.

To further elucidate the impact of HD on regional DA release in the striatum, we chose to measure DA release under prolonged electrical stimulation, which can lead to reserve pool mobilization.[45,55,78–80] To accomplish this, 120 stimulation pulses were separately applied to the DL, DM, VM, and VL striatum of brain slices harvested from 12 week-old R6/2 and WT mice. The stimulated DA release was measured via FSCV at carbon-fiber microelectrodes. One measurement was taken at each frequency in each of the four quadrants of the striatum and DA release was measured as the highest point of stimulated release $[DA]_{stim}$. These measurements were all taken in order from lowest to highest stimulation frequency. Representative raw data for a 12 week-old R6/2 and WT brain slice subjected to 120 stimulation pulses at 60Hz can be seen in Fig. 4.

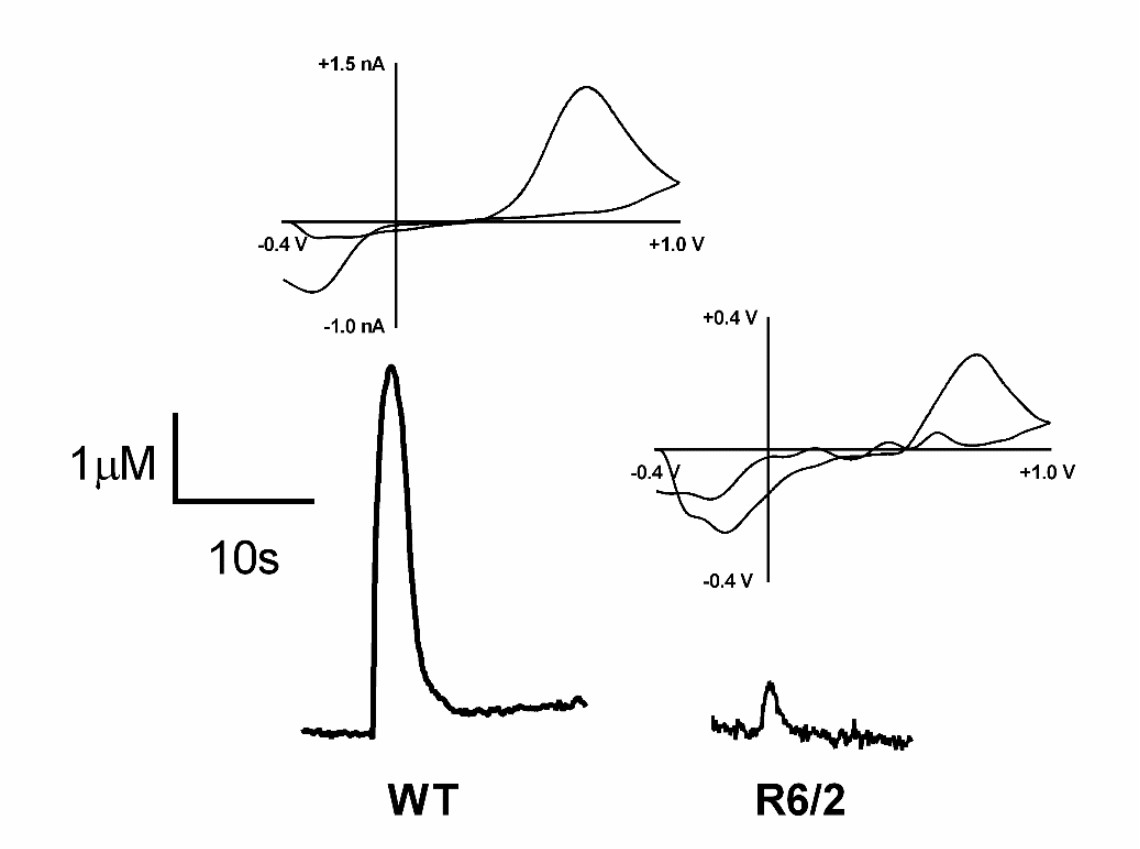

Figure 4. Representative raw data for a 12 week-old R6/2 and WT brain slice subjected to 120 stimulation pulses at 60Hz from the dorsolateral caudate. Representative concentration response to electrical stimulus are shown along with their cyclic voltammograms, confirming the presence of DA.

As is expected, stimulated release response (current vs time) appears to be diminished in the DL striatum of the R6/2 mouse in comparison to the WT trace. All values of $[DA]_{stim}$ for brain slices subjected to 120 stimulation pulses at varying frequencies for each quadrant of the striatum can be seen in Fig. 5. Similar to the results found by Ortiz et al., there appears to be a frequency dependent increase in $[DA]_{stim}$ for WT mice in the DL striatum, however, this is not supported statistically (Fig 5a, one-way ANOVA, $p > 0.05$, $n = 5$). This is also true for measurements taken from WT slices for all other regions of the striatum (Fig 5B-D, one-way ANOVA, $p > 0.05$ $n = 5$). There was no frequency dependent change in $[DA]_{stim}$ in any region of slices obtained from R6/2 brain slices (Fig 5A-D, one-way ANOVA, $p > 0.05$, $n = 4$). Out of the four regions sampled, $[DA]_{stim}$ is only significantly attenuated in the dorsal striatum (DL Fig. 5A, two-way ANOVA, $p < 0.005$; DM Fig. 5B, two-way ANOVA, $p < 0.05$; $n = 5$ WT, $n = 4$ R6/2).

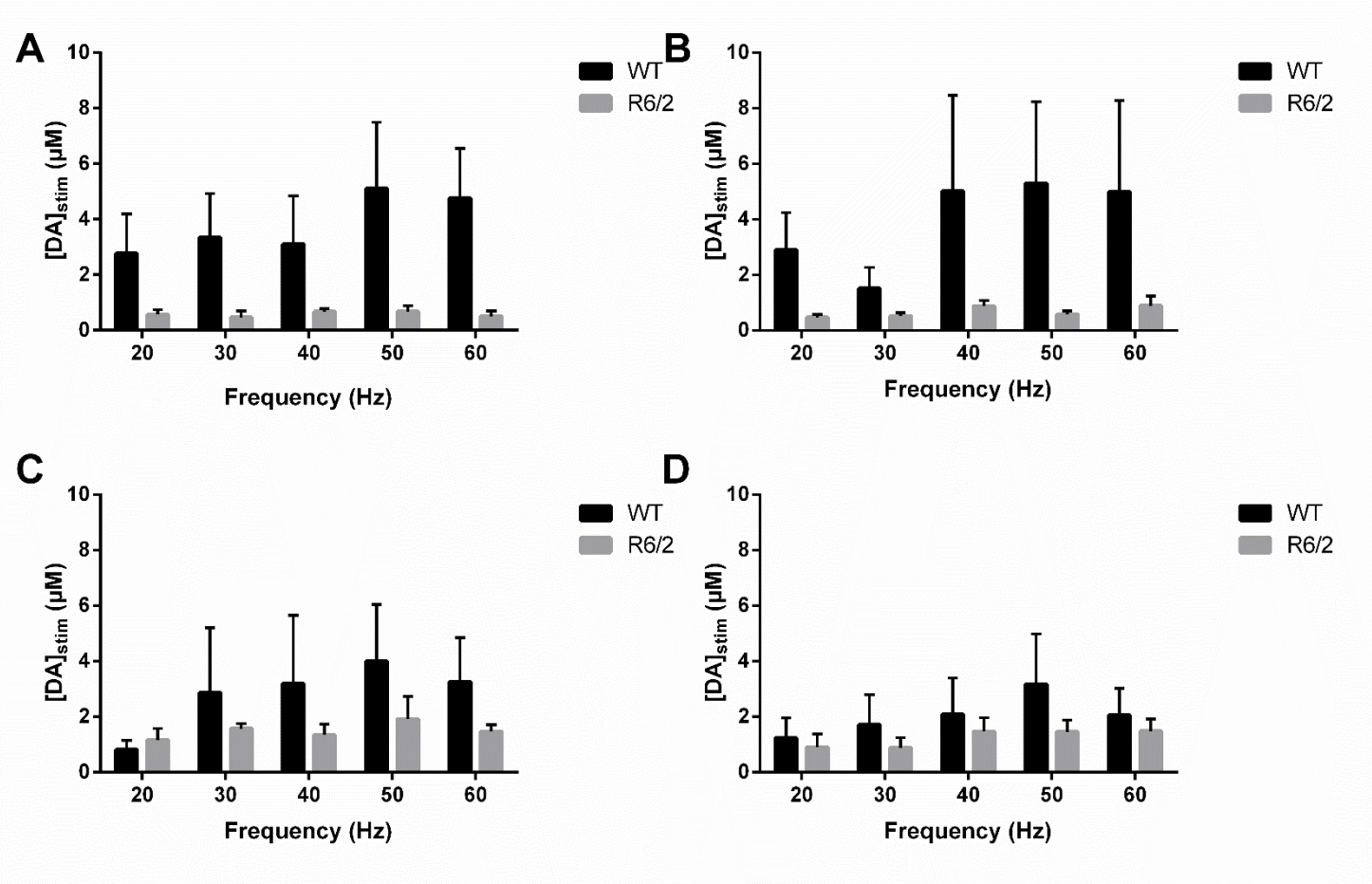

Figure 5. 120 pulse stimulation with altering frequency per region. A) $[DA]_{stim}$ in the dorsal lateral striatum. B) $[DA]_{stim}$ in the dorsal medial striatum. C) $[DA]_{stim}$ in the ventral medial striatum D) $[DA]_{stim}$ in the ventral lateral striatum. There was no significant difference in frequency dependent release in WT or R6/2 mice in any striatum region (Fig 5A-D, one-way ANOVA, $p > 0.05$ $n = 5$). Out of the four regions sampled from, $[DA]_{stim}$ is only significantly attenuated in the dorsal striatum (DL Fig. 5A, two-way ANOVA, $p < 0.005$; DM Fig. 5B, two-way ANOVA, $p < 0.05$; $n = 5$ WT, $n = 4$ R6/2).

3.3.4 Regional distribution of the dopamine transporter

It is clear that that there is a dorsal-to-ventral gradient of attenuation in electrically evoked dopamine release that is caused by the HD mutation in R6/2 mice. These data suggest that the dorsal striatum is more vulnerable to neurological malfunction in HD. These data are consistent with the clinically-determined dorsal-to-ventral gradient of neurodegeneration in humans. This gradient may therefore be at least partially responsible for the observed gradient of impaired DA release. To further investigate the cause of this release gradient, we chose to investigate how the dopamine transporter (DAT) distribution may be affected in the R6/2 striatum. DAT function is the primary route by which DA released into the synaptic cleft may be cleared. These integral protein channels also mediate DA diffusion in the synaptic cleft.[58] The ability of the transporter to efficiently clear DA is critical for ceasing postsynaptic signaling. Aberrations in the DA transporter can have deleterious consequences, including neurodegeneration[81,82] and dyskinesia.[81] Given that overt phenotype of HD includes chorea in 90% of patients,[7] we hypothesized dysfunctions in cellular signaling caused by attenuated clearance of DA may contribute to the onset of these symptoms.

The density of DAT was found through autoradiography of the transporter using [^{3}H]WIN 35,428. Representative striatal slices after [^{3}H]WIN 35,428 binding are shown in Figure 6 alongside cresyl violet only staining. [^{3}H]WIN 35,428 staining proportional to DAT levels is markedly decreased in HD R6/2 mice. The bilateral distribution of DAT in the striatum was 43.9% in HD mice at 12 weeks age in comparison to WT controls (two-way ANOVA, $p<0.0001$). Consistent with these results are DAT levels in the nucleus accumbens, which for HD mice had DAT levels that were 43.1% of WT controls. Although there is a significant difference in the amount of DAT present in the striatum of R6/2 mice in comparison to their WT controls,

there was no regional difference in DAT distribution in R6/2 mice (one-way ANOVA $p > 0.05$) (Fig. 6B). This lack of differential distribution of DAT suggests that the regional difference in stimulated DA release is not attributed solely to a simple dorsal-to-ventral gradient of neurodegeneration.

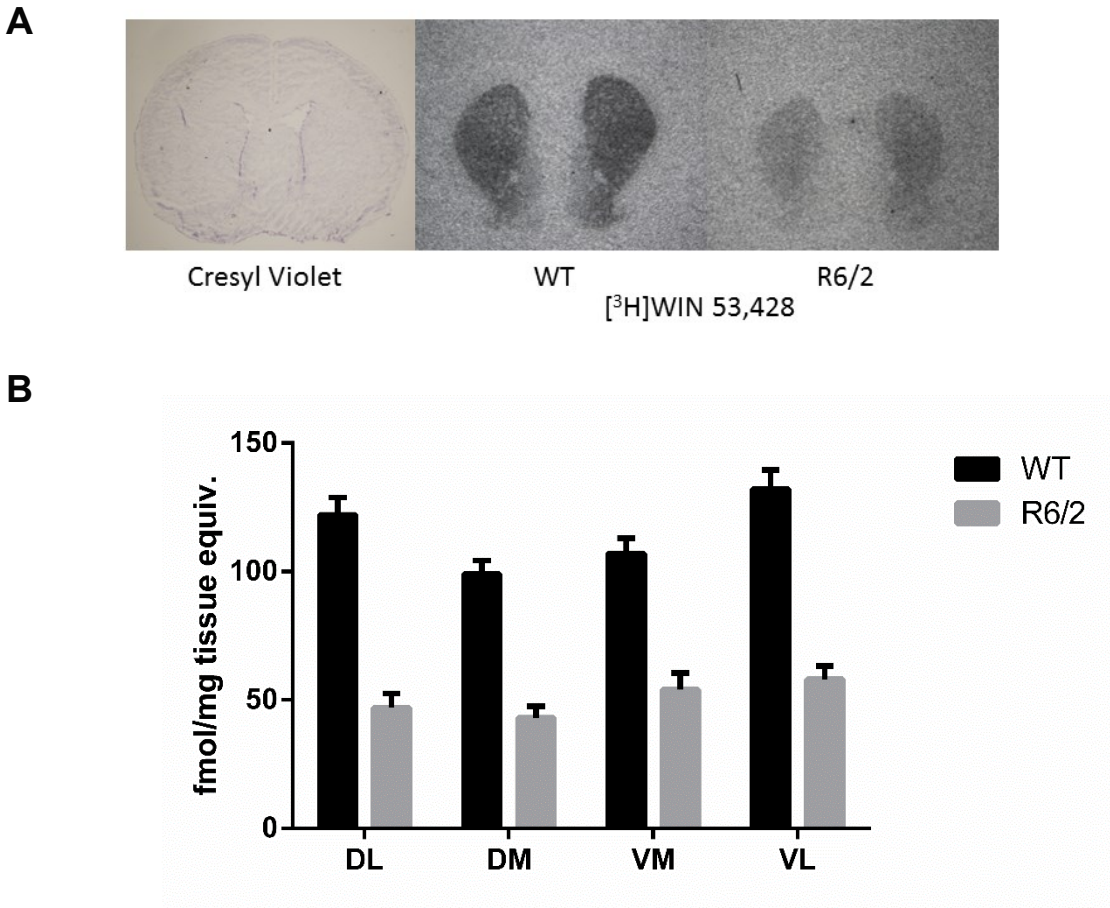

Figure 6. Autoradiographic localization of [^{3}H]WIN 35,428-labeled sites in control and Huntington's mice. Data shown represent total binding. Autoradiograms shown are representative of 8 wild-type and 6 R6/2 mice.

Others have reported through modeling of FSCV traces that the uptake is unchanged by the HD phenotype in R6/2 mice.[8] The maximum rate of DA uptake (V_{max}) is proportional to the number of active DAT channel protein molecules. However, these findings strongly suggest that DA clearance from the synaptic cleft should be impaired since more than half of the channels are not present in R6/2 mice. The motor dysfunctions seen in R6/2 mice and HD patients may well be contributed to by the inability of DAT channels to effectively clear DA from the synapse. Studies in DAT knockout mice have also shown that DA synthesis rates are doubled concurrent with a 90% decrease in tyrosine hydroxylase concentration and enhanced neuronal degeneration.[83] Given that DAT also plays a key role in modulating presynaptic dopamine homeostasis,[83] suppression of the number of DAT channels may culminate in enhanced DA synthesis and elevated degeneration in HD mice, as was seen in genetically engineered DAT-KO mice. Elevated DA levels have been shown to cause the degeneration of neurons when DA is overabundant both in the extracellular matrix[81] and cytoplasm.[84] Given extracellular DA release was sharply attenuated by genotype, it is possible that the loss of DAT channels induced elevated intracellular DA synthesis. This alteration may lead to the degeneration and changes in the dopaminergic system that are seen here in R6/2 mice. Total DA content in the striatal neuron cell bodies would need to be assayed to test this hypothesis.

3.4 Conclusion

In conclusion, it was determined that electrically-evoked DA release is progressively attenuated in the striatum of R6/2 mice and that this attenuation is more severe in the dorsal striatum. Moreover, when applying a 120 stimulation pulse-train, it was found that DA release

was only significantly attenuated in the dorsal striatum, suggesting that the ventral striatum is less vulnerable to the mechanism of impairment caused by the HD mutation. In order to see if regional differences involved the density distribution of the dopamine transporter (DAT), autoradiography using [^{3}H]WIN 35,428 was performed. It was found that the density distribution of DAT is significantly less in R6/2 mice in comparison to their WT controls; however, there were no significant regional differences, suggesting that the regional differences found in DA release attenuation is not simply a result of differential neurodegeneration. These data collectively suggest that the genetic mutation involved in HD leads to the increased vulnerability of the dorsal striatum in comparison to the ventral striatum, therefore providing insight to the disease mechanism.

3.5 References

(1) Martin, J. B., and Gusella, J. F. (1986) Huntington's disease. *N Engl J Med 315*, 1267–1276.

(2) Snell, R. G., MacMillan, J. C., Cheadle, J. P., Fenton, I., Lazarou, L. P., Davies, P., MacDonald, M. E., Gusella, J. F., Harper, P. S., and Shaw, D. J. (1993) Relationship between trinucleotide repeat expansion and phenotypic variation in Huntington's disease. *Nat. Genet. 4*, 393–397.

(3) The Huntington's Disease Collaborative Research Group, MacDonald, M. E., Ambrose, C. M., Duyao, M. P., Myers, R. H., Lin, C., Srinidhi, L., Barnes, G., Taylor, S. A., James, M., and Groot, N. (1993) A novel gene containing a trinucleotide repeat that is expanded and unstable on Huntington's disease chromosomes. *Cell 72*, 971–983.

(4) Pringsheim, T., Wiltshire, K., Day, L., Dykeman, J., Steeves, T., and Jette, N. (2012) The incidence and prevalence of Huntington's disease: A systematic review and meta-analysis. *Mov. Disord. 27*, 1083–1091.

(5) Andrew, S. E., Goldberg, Y. P., Kremer, B., Telenius, H., Theilmann, J., Adam, S., Starr, E., Squitieri, F., Lin, B., and Kalchman, M. A. (1993) The relationship between trinucleotide (CAG) repeat length and clinical features of Huntington's disease. *Nat. Genet. 4*, 398–403.

(6) Duyao, M., Ambrose, C., Myers, R., Novelletto, A., Persichetti, F., Frontali, M., Folstein, S., Ross, C., Franz, M., and Abbott, M. (1993) Trinucleotide repeat length instability and age of onset in Huntington's disease. *Nat. Genet. 4*, 387–392.

(7) MacMillan, J. C., Snell, R. G., Tyler, A., Houlihan, G. D., Fenton, I., Cheadle, J. P., Lazarou, L. P., Shaw, J. D., and Harper, P. S. (1993) Molecular analysis and clinical correlations of the Huntington's disease mutation. *The Lancet 342*, 954–958.

(8) Johnson, M. A., Rajan, V., Miller, C. E., and Wightman, R. M. (2006) Dopamine release is severely compromised in the R6/2 mouse model of Huntington's disease. *J. Neurochem. 97*, 737–746.

(9) Zuccato, C., Valenza, M., and Cattaneo, E. (2010) Molecular Mechanisms and Potential Therapeutical Targets in Huntington's Disease. *Physiol. Rev. 90*, 905–981.

(10) Huntington, G. (2004) On chorea. *Landmarks Med. Genet. Class. Pap. Comment. 51*, 4.

(11) Kremer, B. (2002), in *Huntington's disease* 3rd ed., pp 28–61. Oxford University Press, Oxford ; New York.

(12) Politis, M., Pavese, N., Tai, Y. F., Tabrizi, S. J., Barker, R. A., and Piccini, P. (2008) Hypothalamic involvement in Huntington's disease: an in vivo PET study. *Brain 131*, 2860–2869.

(13) Penney, J. B., Young, A. B., Shoulson, I., Starosta-Rubenstein, S., Snodgrass, S. R., Sanchez-Ramos, J., Ramos-Arroyo, M., Gomez, F., Penchaszadeh, G., and Alvir, J. (1990) Huntington's disease in venezuela: 7 years of follow-up on symptomatic and asymptomatic individuals. *Mov. Disord. 5*, 93–99.

(14) Barbeau, A., Duvoisin, R. C., Gerstenbrand, F., Lakke, J. P., Marsden, C. D., and Stern, G. (1981) Classification of extrapyramidal disorders. Proposal for an international classification and glossary of terms. *J. Neurol. Sci. 51*, 311.

(15) Hayden, M. R. (1981) Huntington's chorea. Springer-Verlag Berlin.

(16) Lanska, D. J., Lanska, M. J., Lavine, L., and Schoenberg, B. S. (1988) Conditions associated with Huntington's disease at death: a case-control study. *Arch. Neurol. 45*, 878.

(17) Lanska, D. J., Lavine, L., Lanska, M. J., and Schoenberg, B. S. (1988) Huntington's disease mortality in the United States. *Neurology 38*, 769–769.

(18) Kandel, E. R., Schwartz, J. H., and Jessell, T. M. (2000) Principles of neural science. McGraw-Hill New York.

(19) DiFiglia, M., Sapp, E., Chase, K., Schwarz, C., Meloni, A., Young, C., Martin, E., Vonsattel, J.-P., Carraway, R., and Reeves, S. A. (1995) Huntingtin is a cytoplasmic protein associated with vesicles in human and rat brain neurons. *Neuron 14*, 1075–1081.

(20) Davies, S. W., Turmaine, M., Cozens, B. A., DiFiglia, M., Sharp, A. H., Ross, C. A., Scherzinger, E., Wanker, E. E., Mangiarini, L., and Bates, G. P. (1997) Formation of neuronal intranuclear inclusions underlies the neurological dysfunction in mice transgenic for the HD mutation. *Cell 90*, 537–548.

(21) Scherzinger, E., Lurz, R., Turmaine, M., Mangiarini, L., Hollenbach, B., Hasenbank, R., Bates, G. P., Davies, S. W., Lehrach, H., and Wanker, E. E. (1997) Huntingtin-encoded polyglutamine expansions form amyloid-like protein aggregates in vitro and in vivo. *Cell 90*, 549–558.

(22) Cattaneo, E., Zuccato, C., and Tartari, M. (2005) Normal huntingtin function: an alternative approach to Huntington's disease. *Nat. Rev. Neurosci. 6*, 919–930.

(23) Ikeda, H., Yamaguchi, M., Sugai, S., Aze, Y., Narumiya, S., and Kakizuka, A. (1996) Expanded polyglutamine in the Machado–Joseph disease protein induces cell death in vitro and in vivo. *Nat. Genet. 13*, 196–202.

(24) Mangiarini, L., Sathasivam, K., Seller, M., Cozens, B., Harper, A., Hetherington, C., Lawton, M., Trottier, Y., Lehrach, H., and Davies, S. W. (1996) Exon 1 of the< i> HD</i> Gene with an Expanded CAG Repeat Is Sufficient to Cause a Progressive Neurological Phenotype in Transgenic Mice. *Cell 87*, 493–506.

(25) Charvin, D., Vanhoutte, P., Pagès, C., Borelli, E., and Caboche, J. (2005) Unraveling a role for dopamine in Huntington's disease: the dual role of reactive oxygen species and D2 receptor stimulation. *Proc. Natl. Acad. Sci. U. S. A. 102*, 12218–12223.

(26) Li, J. Y., Popovic, N., and Brundin, P. (2005) The use of the R6 transgenic mouse models of Huntington's disease in attempts to develop novel therapeutic strategies. *NeuroRx 2*, 447–464.

(27) Hodgson, J. G., Agopyan, N., Gutekunst, C.-A., Leavitt, B. R., LePiane, F., Singaraja, R., Smith, D. J., Bissada, N., McCutcheon, K., and Nasir, J. (1999) A YAC mouse model for Huntington's disease with full-length mutant huntingtin, cytoplasmic toxicity, and selective striatal neurodegeneration. *Neuron 23*, 181–192.

(28) Van Raamsdonk, J. M. (2005) Selective degeneration and nuclear localization of mutant huntingtin in the YAC128 mouse model of Huntington disease. *Hum. Mol. Genet. 14*, 3823–3835.

(29) Van Raamsdonk, J. M. (2005) Cognitive Dysfunction Precedes Neuropathology and Motor Abnormalities in the YAC128 Mouse Model of Huntington's Disease. *J. Neurosci. 25*, 4169–4180.

(30) Levine, M. S., Cepeda, C., Hickey, M. A., Fleming, S. M., and Chesselet, M.-F. (2004) Genetic mouse models of Huntington's and Parkinson's diseases: illuminating but imperfect. *Trends Neurosci. 27*, 691–697.

(31) Khan, A. S., and Michael, A. C. (2003) Invasive consequences of using micro-electrodes and microdialysis probes in the brain. *TrAC Trends Anal. Chem. 22*, 503–508.

(32) Borland, L. M., Shi, G., Yang, H., and Michael, A. C. (2005) Voltammetric study of extracellular dopamine near microdialysis probes acutely implanted in the striatum of the anesthetized rat. *J. Neurosci. Methods 146*, 149–158.

(33) Westerink, B. H. (1995) Brain microdialysis and its application for the study of animal behaviour. *Behav. Brain Res. 70*, 103–124.

(34) Nandi, P., and Lunte, S. M. (2009) Recent trends in microdialysis sampling integrated with conventional and microanalytical systems for monitoring biological events: A review. *Anal. Chim. Acta 651*, 1–14.

(35) Petersén, å., Puschban, Z., Lotharius, J., NicNiocaill, B., Wiekop, P., O'Connor, W. T., and Brundin, P. (2002) Evidence for Dysfunction of the Nigrostriatal Pathway in the R6/1 Line of Transgenic Huntington's Disease Mice. *Neurobiol. Dis. 11*, 134–146.

(36) Fernandez-Gomez, F. J., Galindo, M. F., Gómez-Lázaro, M., Yuste, V. J., Comella, J. X., Aguirre, N., and Jordán, J. (2005) Malonate induces cell death *via* mitochondrial potential collapse and delayed swelling through an ROS-dependent pathway. *Br. J. Pharmacol. 144*, 528–537.

(37) Callahan, J. W., and Abercrombie, E. D. (2011) In vivo Dopamine Efflux is Decreased in Striatum of both Fragment (R6/2) and Full-Length (YAC128) Transgenic Mouse Models of Huntington's Disease. *Front. Syst. Neurosci. 5*.

(38) Hickey, M. A., Reynolds, G. P., and Morton, A. J. (2002) The role of dopamine in motor symptoms in the R6/2 transgenic mouse model of Huntington's disease. *J. Neurochem. 81*, 46–59.

(39) Johnson, M. A., Villanueva, M., Haynes, C. L., Seipel, A. T., Buhler, L. A., and Wightman, R. M. (2007) Catecholamine exocytosis is diminished in R6/2 Huntington's disease model mice. *J. Neurochem. 103*, 2102–2110.

(40) Ortiz, A. N., Kurth, B. J., Osterhaus, G. L., and Johnson, M. A. (2011) Impaired dopamine release and uptake in R6/1 Huntington's disease model mice. *Neurosci. Lett. 492*, 11–14.

(41) Carter, R. J., Lione, L. A., Humby, T., Mangiarini, L., Mahal, A., Bates, G. P., Dunnett, S. B., and Morton, A. J. (1999) Characterization of progressive motor deficits in mice transgenic for the human Huntington's disease mutation. *J. Neurosci. 19*, 3248–3257.

(42) Lüesse, H.-G., Schiefer, J., Spruenken, A., Puls, C., Block, F., and Kosinski, C. M. (2001) Evaluation of R6/2 HD transgenic mice for therapeutic studies in Huntington's disease: behavioral testing and impact of diabetes mellitus. *Behav. Brain Res. 126*, 185–195.

(43) Baur, J. E., Kristensen, E. W., May, L. J., Wiedemann, D. J., and Wightman, R. M. (1988) Fast-scan voltammetry of biogenic amines. *Anal. Chem. 60*, 1268–1272.

(44) Robinson, D. L., Venton, B. J., Heien, M. L., and Wightman, R. M. (2003) Detecting subsecond dopamine release with fast-scan cyclic voltammetry in vivo. *Clin. Chem. 49*, 1763–1773.

(45) Ortiz, A. N., Oien, D. B., Moskovitz, J., and Johnson, M. A. (2011) Quantification of reserve pool dopamine in methionine sulfoxide reductase A null mice. *Neuroscience 177*, 223–229.

(46) Voorn, P., Vanderschuren, L. J. M. ., Groenewegen, H. J., Robbins, T. W., and Pennartz, C. M. . (2004) Putting a spin on the dorsal–ventral divide of the striatum. *Trends Neurosci. 27*, 468–474.

(47) Zahm, D. S., Cheng, A. Y., Lee, T. J., Ghobadi, C. W., Schwartz, Z. M., Geisler, S., Parsely, K. P., Gruber, C., and Veh, R. W. (2011) Inputs to the midbrain dopaminergic complex in the rat, with emphasis on extended amygdala-recipient sectors. *J. Comp. Neurol. 519*, 3159–3188.

(48) Calipari, E. S., Huggins, K. N., Mathews, T. A., and Jones, S. R. (2012) Conserved dorsal–ventral gradient of dopamine release and uptake rate in mice, rats and rhesus macaques. *Neurochem. Int. 61*, 986–991.

(49) Volkow, N. D., Wang, G.-J., Fowler, J. S., Gatley, S. J., Logan, J., Ding, Y.-S., Hitzemann, R., and Pappas, N. (1998) Dopamine transporter occupancies in the human brain induced by therapeutic doses of oral methylphenidate. *Am. J. Psychiatry 155*, 1325–1331.

(50) Palmiter, R. D. (2008) *Dopamine Signaling in the Dorsal Striatum Is Essential for Motivated Behaviors*. *Ann. N. Y. Acad. Sci. 1129*, 35–46.

(51) Reep, R. L., Cheatwood, J. L., and Corwin, J. V. (2003) The associative striatum: Organization of cortical projections to the dorsocentral striatum in rats. *J. Comp. Neurol. 467*, 271–292.

(52) Jocham, G., Klein, T. A., and Ullsperger, M. (2011) Dopamine-Mediated Reinforcement Learning Signals in the Striatum and Ventromedial Prefrontal Cortex Underlie Value-Based Choices. *J. Neurosci. 31*, 1606–1613.

(53) Kelley, A. E. (2004) Ventral striatal control of appetitive motivation: role in ingestive behavior and reward-related learning. *Neurosci. Biobehav. Rev. 27*, 765–776.

(54) Lynd-Balta, E., and Haber, S. N. (1994) The organization of midbrain projections to the ventral striatum in the primate. *Neuroscience 59*, 609–623.

(55) Ortiz, A. N., Kurth, B. J., Osterhaus, G. L., and Johnson, M. A. (2010) Dysregulation of intracellular dopamine stores revealed in the R6/2 mouse striatum. *J. Neurochem. 112*, 755–761.

(56) Ortiz, A. N., Osterhaus, G. L., Lauderdale, K., Mahoney, L., Fowler, S. C., von Hörsten, S., Riess, O., and Johnson, M. A. (2012) Motor function and dopamine release measurements in transgenic Huntington's disease model rats. *Brain Res. 1450*, 148–156.

(57) Wayment, H. K., Schenk, J. O., and Sorg, B. A. (2001) Characterization of extracellular dopamine clearance in the medial prefrontal cortex: role of monoamine uptake and monoamine oxidase inhibition. *J. Neurosci. 21*, 35–44.

(58) Sesack, S. R., Hawrylak, V. A., Matus, C., Guido, M. A., and Levey, A. I. (1998) Dopamine axon varicosities in the prelimbic division of the rat prefrontal cortex exhibit sparse immunoreactivity for the dopamine transporter. *J. Neurosci. 18*, 2697–2708.

(59) Moghaddam, B., and Bunney, B. S. (1989) Differential effect of cocaine on extracellular dopamine levels in rat medial prefrontal cortex and nucleus accumbens: comparison to amphetamine. *Synapse 4*, 156–161.

(60) Giros, B., Jaber, M., Jones, S. R., Wightman, R. M., and Caron, M. G. (1996) Hyperlocomotion and indifference to cocaine and amphetamine in mice lacking the dopamine transporter. *Nature* 606–12.

(61) Kraft, J. C., Osterhaus, G. L., Ortiz, A. N., Garris, P. A., and Johnson, M. A. (2009) In vivo dopamine release and uptake impairments in rats treated with 3-nitropropionic acid. *Neuroscience 161*, 940–949.

(62) Kawagoe, K. T., Jankowski, J. A., and Wightman, R. M. (1991) Etched carbon-fiber electrodes as amperometric detectors of catecholamine secretion from isolated biological cells. *Anal. Chem. 63*, 1589–1594.

(63) Rice, M. E., and Nicholson, C. (1989) Measurement of nanomolar dopamine diffusion using low-noise perfluorinated ionomer-coated carbon fiber microelectrodes and high-speed cyclic voltammetry. *Anal. Chem. 61*, 1805–1810.

(64) Hashemi, P., Danoski, E., Petrovic, J., Keithley, R. B., and Wightman, R. M. (2009) Voltammetric Detection of 5-Hydroxytryptamine Release in the Rat Brain. *Anal. Chem. 81*, 9462–9471.

(65) Jackson, B. P., Dietz, S. M., and Wightman, R. M. (1995) Fast-scan cyclic voltammetry of 5-hydroxytryptamine. *Anal. Chem. 67*, 1115–1120.

(66) Coulter, C. L., Happe, H. K., Bergman, D. A., and Murrin, L. C. (1995) Localization and quantification of the dopamine transporter: comparison of [3 H] WIN 35,428 and [125 I] RTI-55. *Brain Res. 690*, 217–224.

(67) Paxinos, G., and Watson, C. H. (1986) The rat brain in stereotaxic coordinates 2nd edn. *Acad. Press N. Y. Rasoolijazi H Joghataie MT Roghani M Nobakht M2007 Benef. Eff. -- Epigallocatechin-3-Gallate Exp. Model Alzheimers Dis. Rat Behav. Anal. Iran Biomed J 11*, 237–243.

(68) Gerfen, C. R. (1992) The neostriatal mosaic: multiple levels of compartmental organization in the basal ganglia. *Annu. Rev. Neurosci. 15*, 285–320.

(69) Ferrante, R. J., Kowall, N. W., Beal, M. F., Richardson, E. P., Bird, E. D., and Martin, J. B. (1985) Selective sparing of a class of striatal neurons in Huntington's disease. *Science 230*, 561–563.

(70) Kowall, N. W., Ferrante, R. J., and Martin, J. B. (1987) Patterns of cell loss in Huntington's disease. *Trends Neurosci. 10*, 24–29.

(71) Ginovart, N., Lundin, A., Farde, L., Halldin, C., Bäckman, L., Swahn, C.-G., Pauli, S., and Sedvall, G. (1997) PET study of the pre-and post-synaptic dopaminergic markers for the neurodegenerative process in Huntington's disease. *Brain 120*, 503–514.

(72) Suzuki, M., Desmond, T. J., Albin, R. L., and Frey, K. A. (2001) Vesicular neurotransmitter transporters in Huntington's disease: initial observations and comparison with traditional synaptic markers. *Synapse 41*, 329–336.

(73) Neves, G., and Lagnado, L. (1999) The kinetics of exocytosis and endocytosis in the synaptic terminal of goldfish retinal bipolar cells. *J. Physiol. 515*, 181–202.

(74) Zucker, R. S., and Regehr, W. G. (2002) Short Term Synaptic Plasticity. *Annu. Rev. Physiol. 64*, 355–405.

(75) Rizzoli, S. O., and Betz, W. J. (2005) Synaptic vesicle pools. *Nat. Rev. Neurosci. 6*, 57–69.

(76) Harata, N., Ryan, T. A., Smith, S. J., Buchanan, J., and Tsien, R. W. (2001) Visualizing recycling synaptic vesicles in hippocampal neurons by FM 1-43 photoconversion. *Proc. Natl. Acad. Sci. 98*, 12748–12753.

(77) Kuromi, H., and Kidokoro, Y. (2003) Two synaptic vesicle pools, vesicle recruitment and replenishment of pools at the Drosophila neuromuscular junction. *J. Neurocytol. 32*, 551–565.

(78) Richards, D. A., Guatimosim, C., Rizzoli, S. O., and Betz, W. J. (2003) Synaptic vesicle pools at the frog neuromuscular junction. *Neuron 39*, 529–541.

(79) Heien, M., and Wightman, R. M. (2006) Phasic dopamine signaling during behavior, reward, and disease states. *Curr. Drug Targets-CNS Neurol. Disord. 5*, 99–108.

(80) Venton, B. J. (2006) Cocaine Increases Dopamine Release by Mobilization of a Synapsin-Dependent Reserve Pool. *J. Neurosci. 26*, 3206–3209.

(81) Cyr, M., Beaulieu, J.-M., Laakso, A., Sotnikova, T. D., Yao, W.-D., Bohn, L. M., Gainetdinov, R. R., and Caron, M. G. (2003) Sustained elevation of extracellular dopamine causes motor dysfunction and selective degeneration of striatal GABAergic neurons. *Proc. Natl. Acad. Sci. 100*, 11035–11040.

(82) Nuber, S., Petrasch-Parwez, E., Winner, B., Winkler, J., von Horsten, S., Schmidt, T., Boy, J., Kuhn, M., Nguyen, H. P., Teismann, P., Schulz, J. B., Neumann, M., Pichler, B. J., Reischl, G., Holzmann, C., Schmitt, I., Bornemann, A., Kuhn, W., Zimmermann, F., Servadio, A., and Riess, O. (2008) Neurodegeneration and Motor Dysfunction in a Conditional Model of Parkinson's Disease. *J. Neurosci. 28*, 2471–2484.

(83) Jones, S. R., Gainetdinov, R. R., Jaber, M., Giros, B., Wightman, R. M., and Caron, M. G. (1998) Profound neuronal plasticity in response to inactivation of the dopamine transporter. *Proc. Natl. Acad. Sci. 95*, 4029–4034.

(84) Park, S. S., Schulz, E. M., and Lee, D. (2007) Disruption of dopamine homeostasis underlies selective neurodegeneration mediated by α-synuclein: Disrupted dopamine homeostasis by α-synuclein. *Eur. J. Neurosci. 26*, 3104–3112.

Chapter 4. Application of Caged Compound Photoactivation with Fast-Scan Cyclic Voltammetry for Neurochemical Measurements

In this chapter we describe the development of a method to quantify the liberation of biologically active compounds from the photo-uncaging of pHP caged compounds. Of the results shown, Figure 2 and 4 contain data adapted from material we have published in *The Analyst.*

4.1 Introduction

Caged compounds are molecules that possess photoremovable protecting groups that, when exposed to light of the proper wavelength, intensity, and duration, are released from the parent molecule.[1] It is the ability to control precise spatially and temporally resolved concentration changes that make the use of caged compounds so attractive to research in biological systems that possess highly complex spatial diversity. In order to create a caged compound for biological research, the molecule of interest is synthesized with photoremovable groups that render the compound biologically inert and remain inert until photorelease occurs.[2] When applied to biological systems, a good photoreleasable group should satisfy four critera: 1) the compound must be pure, be stable in the desired media, and the addition of the photoreleasable group should render the molecule biologically inactive.[1] 2) the photoreleasable group must release the compound of interest with high yield. 3) the group must undergo photolysis with light that is not of sufficient energy to damage or destroy the biological material ($\lambda > 300$nm).[1] 4) the byproduct of the photorelease must not interact with the biological material.[3]

4.1.1 A Brief History of Caged Compounds

The use photoactivatable compounds for biological research was pioneered primarily by Kaplan et al. in the 1970s (no relation) when they successfully made photoprotected ATP analogues and coined the term "caged".[4] Since their introduction, a series of photoreleasable groups have been synthesized and evaluated as candidates to cage a series of biological molecules including carboxylic acids, phosphates, sulfates, alcohols, phenols, and acids.[5] The first photoreleasable group used by Kaplan et al. that continues to be the most widely used is the o-nitrobenzyl group.[6] Other photoreleasable groups that have been adapted for biological research are benzoins, phenacyl groups, and coumaryl groups.[5]

As previously stated, the most widely used photoremovable protecting groups used for such experimentation have been o-nitrobenzyl compounds.[5,6] The *o*-nitrobenzyl group has been most extensively used due to its relative ease of synthesis and its compatibility with multiple functional groups.[3] Despite the popularity of the *o*-nitrobenzyl group, it fails to meet one of our criteria regarding being an ideal photoremovable group for biological research. The byproduct of the photolysis of compounds caged with the *o*-nitrobenzyl group is 2-nitrosobenzaldehyde is toxic.[3,4] It is also the case that the photolysis of the o-nitrobenzyl group is relatively slow which renders it useless for researching rapid biological processes.[7] It has therefore been the goal of researchers to develop novel photoreleasable groups for application in biological research and has been extensively reviewed.[1,2,8–21] Specifically within the field of biological research, caged compounds have provided a useful means to study the brain, and have been used *in vivo* and *ex vivo*.[2,22–24]

4.1.2 The p-Hydroxyphenacyl protecting group

The *p*-hydroxyphenacyl group (pHP, Fig. 1) was developed as a promising alternative photoreleasable group for use in biological systems. One attractive attribute of the pHP photoremovable group is that its photochemical byproduct, *p*-hydroxyphenylacetic acid (4HPAA), is non-toxic.[5,25,26] In fact, 4HPAA is a naturally occurring byproduct of the metabolism of aromatic amino acids in humans and has gained interest as a biomarker for diseases involving nitrosative stress.[27,28] The pHP photoremovable protecting group also provides advantages over other commonly used moieties, including high quantum yields, rapid photorelease rates, biologically inert byproducts, and high aqueous solubility.[25] Another benefit to the pHP group is that the photolysis byproduct 4HPAA absorption is blue shifted from the incident light used for uncaging.[6] The generation of 4HPAA after uncaging therefore will not interfere with the ability to quantify release.

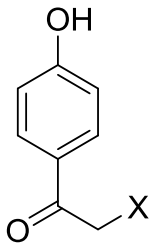

Figure 1. The structure of the pHP photoremovable group.

The photoreaction that leads to the release of both the biomolecule of interest and 4HPAA involves a Favorskii rearrangement (Scheme 1). This rearrangement occurs on the nanasecond scale,[1,26] which also lends to its appeal for studying rapid biological processes. The pHP photoremovable group's photochemistry[1,29] and application to biological systems[1,3,6,7,26,29–31] have been extensively reviewed.

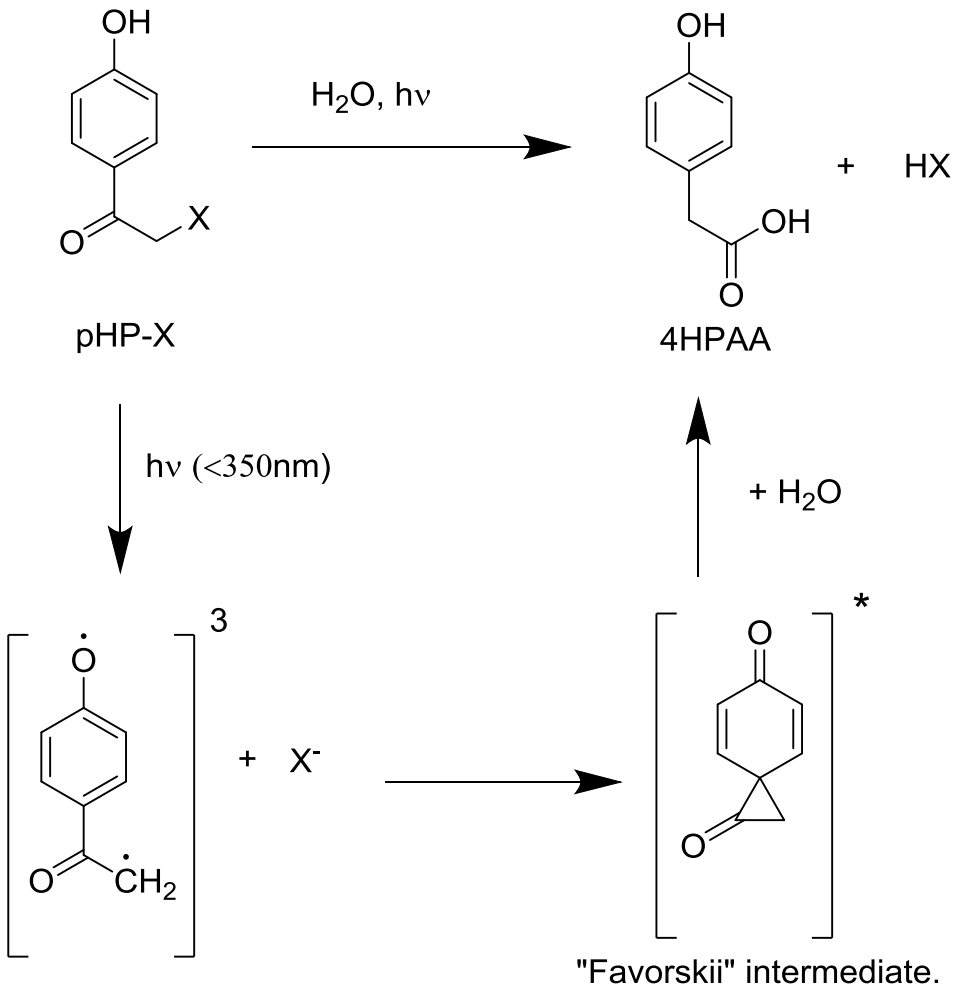

Scheme 1. The photorelease of X^- from pHP-X via the Favorskii rearrangement.

4.1.3 *p*-Hydroxyphenyl glutamate

The rapid rate of substrate release from the pHP cage ($k_r = 10^8$-10^9 s^{-1}) has made its use attractive to studying neurotransmission,[32] which as one would expect, occurs rapidly. Here, we demonstrate an analytical approach aimed at investigating neurotransmitter interactions that occur on fast timescales. We use *p*-hydroxyphenyl glutamate (pHP-Glu, Scheme 2) as a model system with the intent to be used to monitor real-time neurotransmitter actions *in-vivo.* pHP-Glu has successfully been used by Kandler et al. to study long term depression in hippocampal pyramidal cell populations.[33]

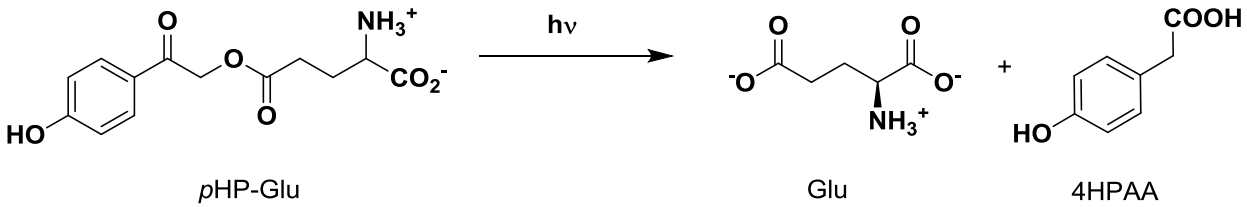

*p*HP-Glu Glu 4HPAA

Scheme 2. The photolysis of pHP-Glu to release glutamate and 4HPAA.

Glutamate (Glu) is an abundant, excitatory amino acid neurotransmitter in the central nervous system that is released by exocytosis and actively taken up by glutamate transporters.[34] Elevated levels of glutamate have been associated with a variety of neurological conditions and syndromes, including stroke,[35–40] Amyotrophic lateral sclerosis (ALS),[41–47] and Alzheimer's disease.[48–52] pHp-Glu therefore offers a means to study glutamate neurotransmission with high spatial and temporal resolution that could be applied to researching these neurological conditions.

4.1.4 Caged compound photoactivation in conjunction with FSCV

The ability to quantify the amount biomolecule generated in real time upon photorelease has proven to be a somewhat difficult task. Here, we have offered an analytical approach for the quantification of Glu release via the photolysis of pHP-Glu. The photolysis of pHP-Glu yields two products, biologically active Glu and 4HPAA. The structure of 4HPAA is similar to the neurotransmitters octopamine and tyramine, which are electroactive compounds and are detectable by FSCV. Fast-scan cyclic voltammetry (FSCV) at carbon-fiber microelectrodes is an electrochemical technique often used to measure sub-second concentration changes of neurotransmitters and neuromodulators in single cells,[53,54] brain slices,[53,55–58] and *in vivo*.[59] FSCV allows for the positive identification of electroactive species with high spatial and temporal resolution. There is therefore a spatial and temporal compatibility of FSCV and caged compound photoactivation.

This compatiblity between FSCV and caged compound photoactivation has been exploited previously. Lee *et. al.* were able to increase DA concentration via the photolysis of caged DA while measuring D2 receptor-mediated auto-inhibition of stimulated dopamine release with FSCV.[60] Although these studies are complicated by the fact that the CV generated by the caged form of dopamine was similar to that of uncaged dopamine, the feasibility of combining FSCV and caged compound photoactivation was successfully demonstrated. Here, we have applied this method combination as a means to indirectly quantify Glu release by quantifying 4HPAA generation upon the photolysis of pHP-glu with FSCV.

Additionally, recent evidence has suggested that glutamate modulates dopamine release with hydrogen peroxide acting as a mediator.[61–63] Because the CV of the photoreleased by-

product of pHP-Glu, 4HPAA, is easily distinguishable from that of DA, we are able to track this photoactivation process simultaneously with that of DA. This method can therefore provide the ability to measure neurotransmitter interaction with novel spatial and temporal resolution within the brain.

4.2 Materials and Methods

4.2.1 Materials and solutions

pHP-Glu was synthesized by Dr. Sanjeewa Senadheera, a member of Dr. Richard Givens' research group at The University of Kansas, Lawrence. All other compounds used were purchased from Sigma-Aldrich (St. Louis, MO, USA). All aqueous solutions were made with water purified to 18.2 MΩ resistances. Flow cell injection experiments were carried out in artificial cerebrospinal fluid (aCSF).

4.2.2 Animals

Mice (Charles River Laboratories, Inc., Wilmington, MA, USA), were housed 5 per cage in plastic cages with food and water available *ad libitum* in a temperature/humidity-controlled environment. Animals were placed on a 12 hour light/dark cycle. All experiments were carried out in accordance with the National Institutes of Health *Guide for the Care and Use of Laboratory Animals.* All procedures were approved by the University of Kansas Institutional Animal Care and Use Committee.

4.2.3 Electrode fabrication

Carbon-fiber cylindrical microelectrodes were fabricated as previously described.[59,64] Briefly, 7µm carbon-fiber purchased from Goodfellow Cambridge Ltd. (Huntingdon, England) was loaded into glass capillaries (4in, 1.2mm OD; A-M Systems, Inc. Carlsborg, WA, USA) and pulled using a heated coil puller (Narishige International USA, East Meadow, NY, USA). Carbon-fiber tips were then cut with a scalpel 25 µm from the end of the glass seal. Electrodes were then sealed by dipping into a well-mixed epoxy mixture of 0.24g EPI-CURE 3234 Curing Agent (lot FCXC4114/0886GG) and 2.00g EPON Resin 815C (lot HADN0003/1307GG). Excess resin was removed by dipping several times in toluene and electrodes were then baked for 1 hour at 100°C. The electrodes were back-filled with 0.5 M potassium acetate in order to establish an electrical connection between the carbon-fiber and the inserted silver wire.

4.2.4 Brain slices

Brain slices were harvested as previously described [57]. In summary, rats were deeply anesthetized by isofurane inhalation and decapitated. The brain was then immediately removed and placed into ice-cold artificial cerebral spinal fluid (aCSF). The aCSF solution contains the following concentrations: 2.5 mM KCl, 126 mM NaCl, 1.2 mM NaH_2PO_4, 25 mM $NaHCO_3$, 2.4 mM $CaCl_2$, 1.2 mM $MgCl_2$, 20 mM HEPES, 11 mM D-glucose. The pH was adjusted to the physiological pH 7.4. To ensure the tissue received ample oxygen, the aCSF was continuously bubbled with 95% O_2/5% CO_2 throughout the experiment. After chilling for one minute the cerebellum was removed and the brain was bisected using a sterile razor blade. One hemisphere of the brain was then glued to a plate against a cube of agar for support. 300 µm coronal brain slices were then obtained using a vibratome (Leica, Wetzlar, Germany). After obtaining a brain

slice containing striatal tissue, it was transferred to a perfusion chamber where oxygenated aCSF was perfused over the slice and was heated to 34 ºC. The slice was equilibrated for one hour before taking any measurements.

4.2.5 Uncaging set up

Our experimental setup was adapted for voltammetry from a previous design that had been used for electrophysiology.[32] A mercury lamp was used as a light source and the lamp output was gated using a shutter, under computer control, to a 100 μm diameter fiber optic cable (PolyMicro Technologies, Inc), Phoenix, AZ, held in the proper orientation by a micro-positioner. The fiber-optic cable was positioned near the tip of the carbon-fiber microelectrode by a micromanipulator.

4.2.6 Electrochemical detection of pHP-Glu photoactivation in a microliter reaction vessel

An Eppendorf pipette (epT.I.P.S.®) was inverted and clamped into position. An optical fiber was positioned in the pipette to allow for sample illumination. The 1mm optical fiber was high UV transmitting fused silica and was purchased from Polymicro Technologies. The microliter reaction vessel was fabricated with an inverted pipette tip that allowed for microliter volumes of pHP-Glu solution to be contained within the tip, held in place by the surface tension of the aqueous solution. This design allows for the positioning of a 1mm fiber optic cable directly beneath the pHP-Glu solution while inserting a CF working electrode and an Ag/AgCl reference electrode into the solution (Fig. 7) to allow for obtaining electrochemical measurements of the photo-uncaging of pHP-Glu. Once the photo-uncaging of pHP-Glu is

measured with FSCV, the electrodes can be removed and the sample can be removed from the reaction vessel for HPLC analysis. Each sample in the vessel contained 100μM pHP-Glu and 25μM 4-methoxyphenylacetic acid internal standard in αCSF.

4.2.7 HPLC analysis

An isocratic high performance liquid chromatography (HPLC) method was used on a Shimadzu Model LC 20 AD with a dual reciprocating pump and a DGV 20A3 degasser. The detector was a Simadzu SPD-201V UV-VIS detector set to the wavelengths of 220 nm and 240 nm for the detection of the pHP-Glu and 4-HPAA. The mobile phase components were (A) 99% water, 1% methanol and 0.06% formic acid; (B) 99% methanol, 1% water and 0.06% formic acid. The flow rate was set to 1 mL/min.

4.2.8 Fast scan cyclic voltammetry

4.2.8.1 Flow cell analysis

FSCV measurements were collected with a custom-modified ChemClamp potentiostat (Dagan, Minneapolis, MN, USA) and TarHeel CV software provided by R.M. Wightman and M. Heien (University of North Carolina, Chapel Hill, NC, USA). For measurements taken in a flow cell, a six-port sample injector with manual injection was used. A cylindrical carbon fiber microelectrode was placed in the flow cell or microliter reaction vessel for the detection of analyte. A triangular waveform starting at -0.4V, scanning up to 1.0V, and back to -.4V, was applied to the carbon fiber microelectrode at a scan rate of 300V/s and an update rate of 10Hz

against a Ag/AgCl reference electrode. The measured currents were then plotted versus applied potential to obtain CVs of the analytes of interest.

4.2.8.2 Brain slice analysis

Procedures for measuring DA release with background-subtracted FSCV in brain slices has been previously described in detail.[55, 65–67] Briefly, a pre-calibrated cylinder carbon-fiber microelectrode was inserted 100μm into the brain slice using micromanipulators and a stereoscope. The electrode was positioned between two biphasic stimulating electrodes (A-M Systems Inc, Carlsborg, WA, USA) in the striatum. For DA and 4HPAA detection, a triangular waveform starting at -0.4V, scanning up to 1.0V, and back to -0.4V, was applied to the carbon-fiber microelectrode at a scan rate of 300V/s and an update rate of 10 Hz. Dopamine release was evoked by applying a single, biphasic pulse (350 μA, 4 ms total duration). The peak current after stimulation was used for all release measurements, and there was a 5 minute recovery period between each measurement.

4.2.9 Simultaneous uncaging and measuring DA in brain slices

Harvested striatal brain slices were obtained as previously described. For voltammetric recordings, a carbon fiber microelectrode and biphasic stimulating electrode were embedded 100μm deep into the striatum. A 100 μm diameter fiber optic cable (PolyMicro Technologies, Inc) was then positioned via a micropositioner near the tip of the carbon-fiber microelectrode (Fig 10).

4.3 Results and discussion

4.3.1 Electrochemical detection of 4HPAA

The temporally resolved release of biologically active glutamate is dependent on the photo-uncaging of pHP-Glu. Upon UV (300nm) stimulation, pHP-Glu undergoes a Favorskii rearrangement to release biologically active glutamate and the photo-uncaging byproduct 4HPAA (Scheme 2). The pHP photoremovable group lends itself to use in biological systems due to its high quantum yield, rapid uncaging, and relative stability in biologically relevant solutions when compared to other conventional caged compounds.[25] The byproduct of photoactivation, 4HPAA, consists of a hydroxyl group situated para to the acetate group on a benzene ring. The chemical structure of this molecule prompted us to determine if we could measure it with FSCV. Molecules having this similar structural arrangement have been shown to reproducibly generate measurable cyclic voltammograms (CVs) when applying FSCV.[68]

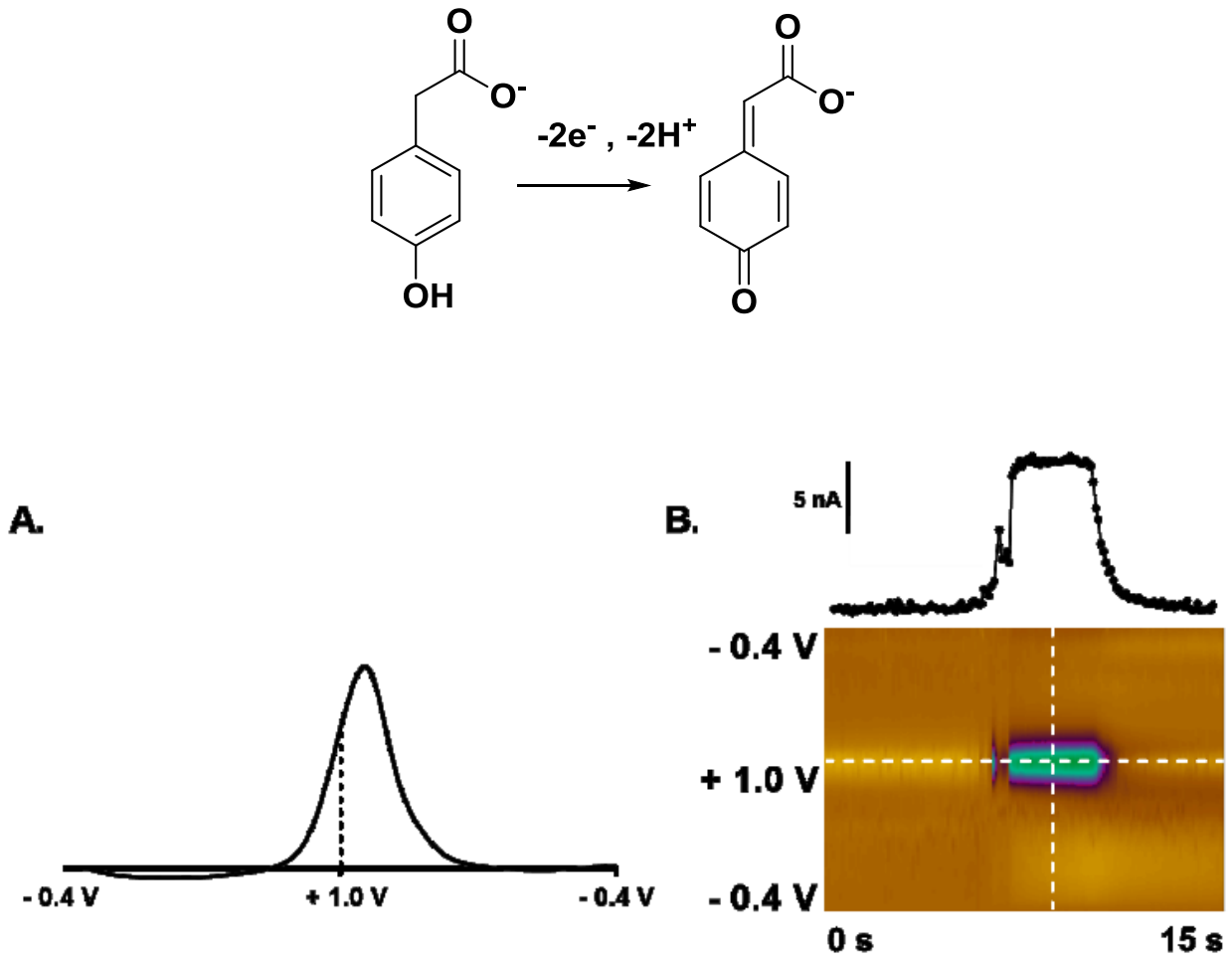

Figure 2. Fig. 1 Background subtracted cyclic voltammetry of the oxidation of 4HPAA (top). (A) Unfolded cyclic voltammogram of 100 µM 4HPAA in aCSF. The applied waveform was -0.4 V to +1.0 V to -0.4 V at 400 V/s and 10 scans/s. The oxidation peak of 4HPAA was detected around + 0.9 V on cathodic sweep. (B) The color plot (bottom) and oxidation current response (top), measured from the peak oxidation current of 4HPAA.This figure has been modified from Shin *et al*.[69]

It was determined *in vitro*, using flow injection analysis, that 4HPAA is readily detectable by FSCV and a representative cyclic voltammogram of 4HPAA can be seen in Figure 2. The cyclic voltammogram in Fig. 2A was unfolded as to clearly delineate the forward and reverse scan with the switching potential in the middle of the x axis. Using a typical triangular waveform (-0.4V → 1.0V → -0.4V; 400 V/s), 4HPAA undergoes an irreversible oxidation near the switching potential on the reverse potential sweep. Since beginning this research project, further optimization of the quantification of 4HPAA by FSCV has recently been reported by Shin *et al*.[69] A plot of the current response vs 4HPAA remains linear over a broad concentration range ($R^2 = 0.999$; Fig 3), which demonstrates that FSCV provides an accurate means to quantify 4HPAA.

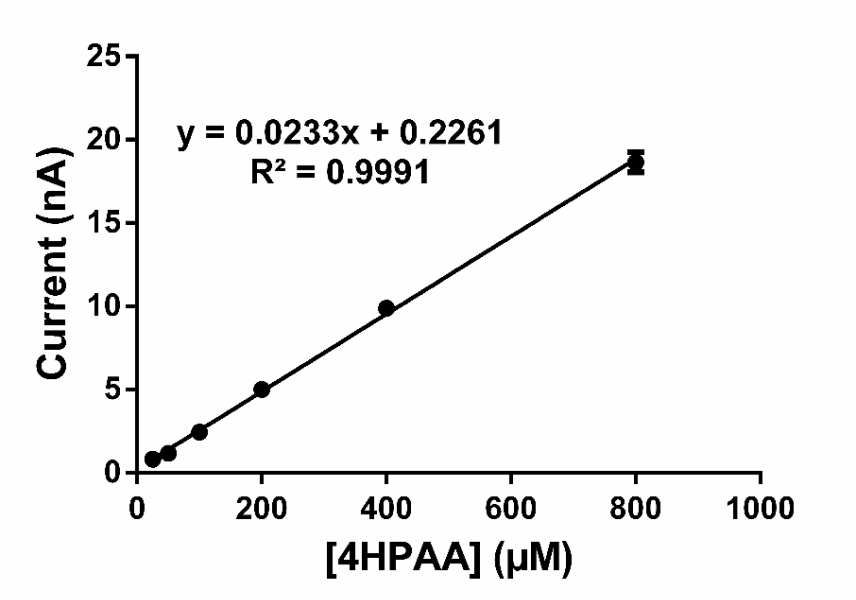

Figure 3. 4HPAA calibration curve as measured by FSCV.

4.3.2 The simultaneous detection of 4HPAA and dopamine

The ability to rapidly release, detect, and quantify the photo-uncaging of pHP-Glu by measuring 4HPAA release provides us with a novel means to measure the real time interaction of Glu mediation on DA release in the striatum. It was hypothesized that real time glutamate mediated DA release could be measured by the simultaneous detection of 4HPAA and DA upon the photo-uncaging of pHP-Glu. The oxidation currents obtained for 4HPAA and DA using FSCV were determined to be resolvable *in vitro* using flow injection analysis with a standard flow cell (Fig. 4). Note that the waveform used for the representative CV and, color plot, and current response in figure 4 was the optimized waveform developed by Shin *et al*. (-0.4 V to +1.3 V and back to -0.4 V at a scan rate of 600 V/s).[69] The DA oxidative peak is resolved from the 4HPAA oxidation peak and can therefore be quantified via FSCV. The detection of 4HPAA in the measured in the presence of DA remains linear over a broad range of concentrations (100nM - 100μM; Tabular results in Table 1; Fig 4. A,B).[69]

Table 1: Average current response vs concentration of 4HPAA in the presence of 1μM DA.

[4HPAA] (μM)	Average current (nA)
0.1	1.995 ± 0.231
0.5	2.483 ± 0.366
1	2.805 ± 0.379
10	4.217 ± 0.563
20	7.152 ± 1.280
50	12.314 ± 2.637
80	16.314 ± 2.671
100	17.666 ± 2.023

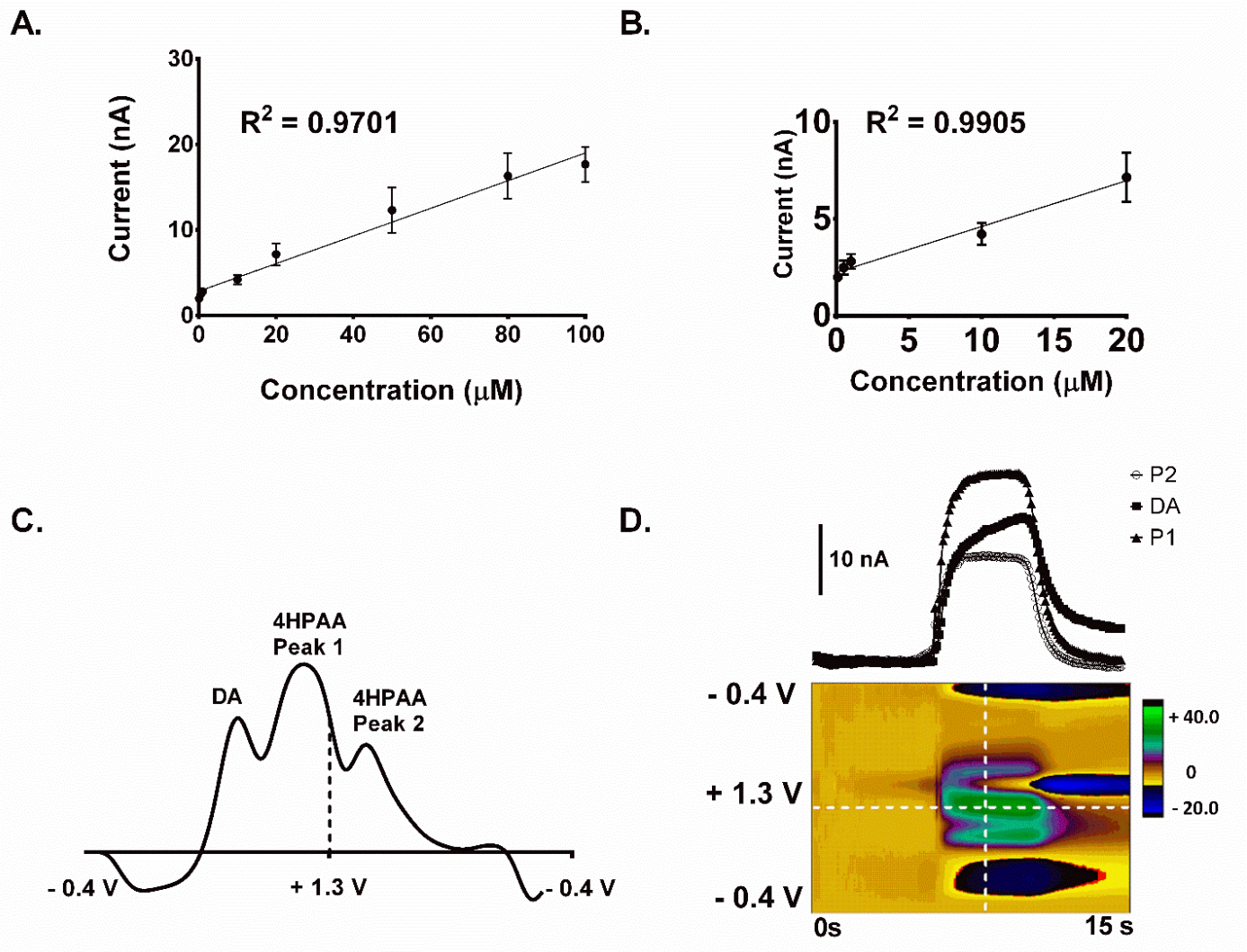

Figure 4. Cyclic voltammetry of 4HPAA in the presence of 1μM DA from optimized waveform (-0.4 V to +1.3 V and back to -0.4 V at a scan rate of 600 V/s). (A and B) Current vs concentration for 4HPAA showing linear ranges from 100nM to 100μM (A) and 100nM to 20 μM (B). Current response of the primary oxidation peak was plotted against 4HPAA concentration. (n=3, P=0.0091, t-test) (C) Unfolded CV of 4HPAA and DA. The three observed oxidation peaks include DA oxidation and two 4HPAA oxidative peaks. (D) Color plot and current traces of 4HPAA and DA were obtained from a flow cell. This figure has been modified from Shin *et al*.[69]

4.3.3 Addressing experimental concerns

4.3.3.1 Subtraction of pHP-Glu signal

Exploiting the electrochemical detection of 4HPAA upon the photo-uncaging of pHP-glutamate as a means to quantify the release of biologically active glutamate has provided certain challenges to be addressed. Firstly, the similarity of CVs from 4HPAA flow cell measurements and pHP-Glu photoactivation recordings suggested that 4HPAA liberated by the application of light can be effectively detected by FSCV as the reaction is occurring. Nevertheless, it is important to consider that pHP-Glu itself is electroactive and also generates a CV similar to that of 4HPAA. The CV resulting from the uncaging of pHP-Glu must, therefore, be the result of subtracting the averaged CV of pHP-Glu from that of 4HPAA. Since it is our goal to use FSCV as a means to quantify the amount of pHP-Glu has been photolyzed, it was necessary to confirm that the oxidation current from pHP-Glu could be successfully subtracted from that of 4HPAA. 4HPAA can be electrochemically detected in mobile phase containing pHP-Glu (Fig. 5, solid line), and therefore confirms the faradaic oxidation peak of pHP-Glu can be successfully subtracted from oxidation peak of 4HPAA (Fig. 5). We are therefore able to measure the formation of 4HPAA as a direct response to photoactivation of pHP-Glu.

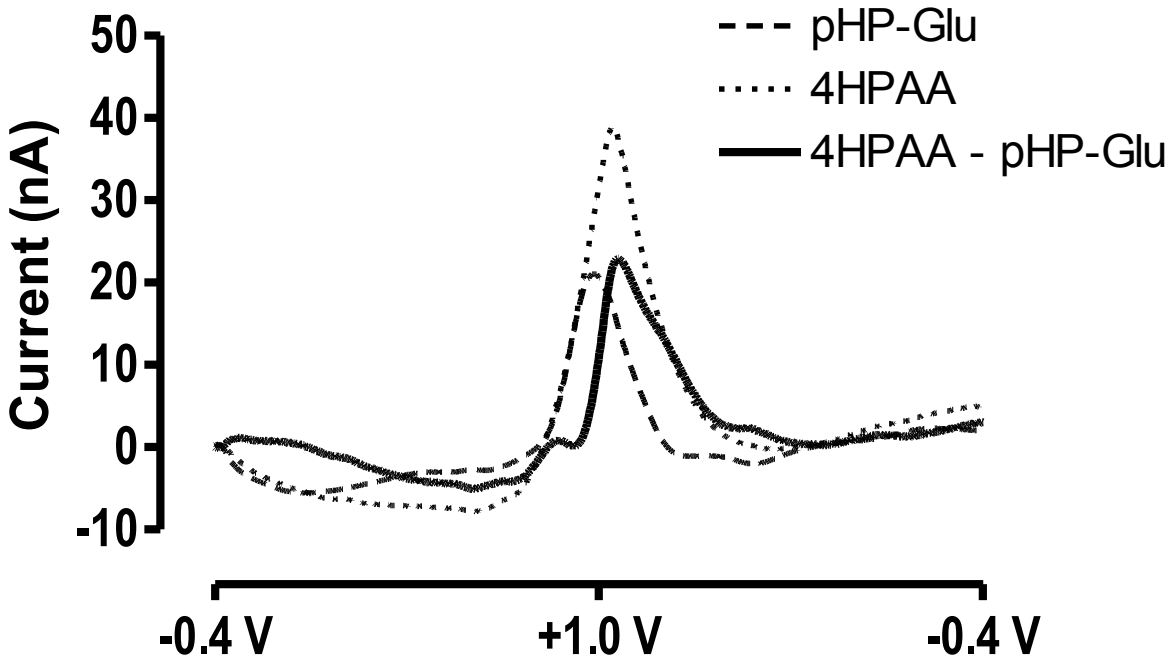

Figure 5. Flow injection analysis of the subtraction of pHP-Glu oxidative current from that 4HPAA. 100 μM pHP-Glu 100 μM 4HPAA solutions in aCSF were separately injected followed by an injection of 100 μM 4HPAA in the presence of 100 μM pHP-Glu (black line).

4.3.3.2 The light artifact

Another challenge to be addressed was that photo-uncaging of pHP-Glu is accompanied by a light artifact which can be seen in Figure 6. The light artifact is a measured current response resulting from the illumination of the electrode surface. This artifact therefore exists in the presence or absence of pHP-Glu. In order to quantify 4HPAA generation as a result of the photolysis of pHP-Glu the light artifact current response must be subtracted out. Possible interference due to the light artifact can be successfully subtracted out via background subtraction, therefore allowing for the direct detection of concentration changes of 4HPAA evolution (Figure 6). The current response attributed to a light artifact along with representative

CV and colorplot can be seen in Figure 6A. The light artifact must be subtracted from the total measured current (Fig. 6B) to obtain the desired linear current response to the evolution of 4HPAA resulting from the photolysis of pHP-Glu (Fig. 6C).

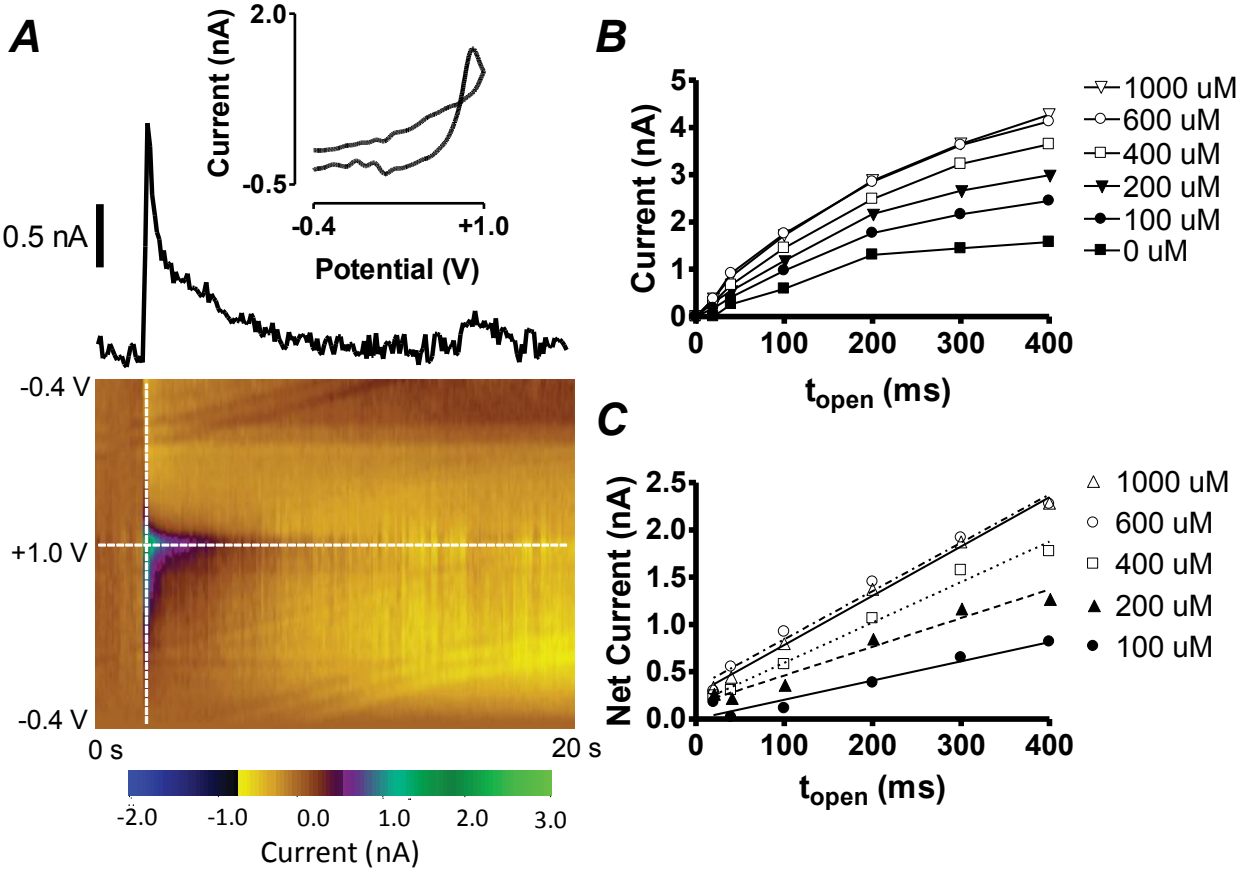

Figure 6. The light artifact is a current response measured as a resulting from solely illuminating the electrode surface. (A) Current response attributed to a light artifact along with representative CV and colorplot. (B) Plot of measured current vs time of light exposure for the uncaging of pHP-Glu solutions. (C) Current response after the subtraction of the current attributed to the light artifact (n = 4 electrodes).

4.3.4 Method validation using FSCV and HPLC

In order validate this method described, we have developed a microliter reaction vessel for measuring the photo-uncaging of pHP-Glu by FSCV followed by HPLC analysis. The experimental setup was adapted to voltammetry from a previous design developed by Kandler *et al.* [32] The microliter reaction vessel was fabricated with an inverted pipette tip that allowed for microliter volumes of pHP-Glu solution to be contained within the tip, held in place by the surface tension of the aqueous solution (Fig. 7). This design allows for the positioning of a 1mm diameter optical fiber using a micro-positioner directly beneath the pHP-Glu solution within the pipette tip. The optical fiber was interfaced to a mercury lamp that was gated by a shutter under computer control. After setting up the microliter reaction vessel, the working electrode and Ag/AgCl reference electrode into the solution to take electrochemical measurements of the photo-uncaging of pHP-Glu (Fig. 8A).

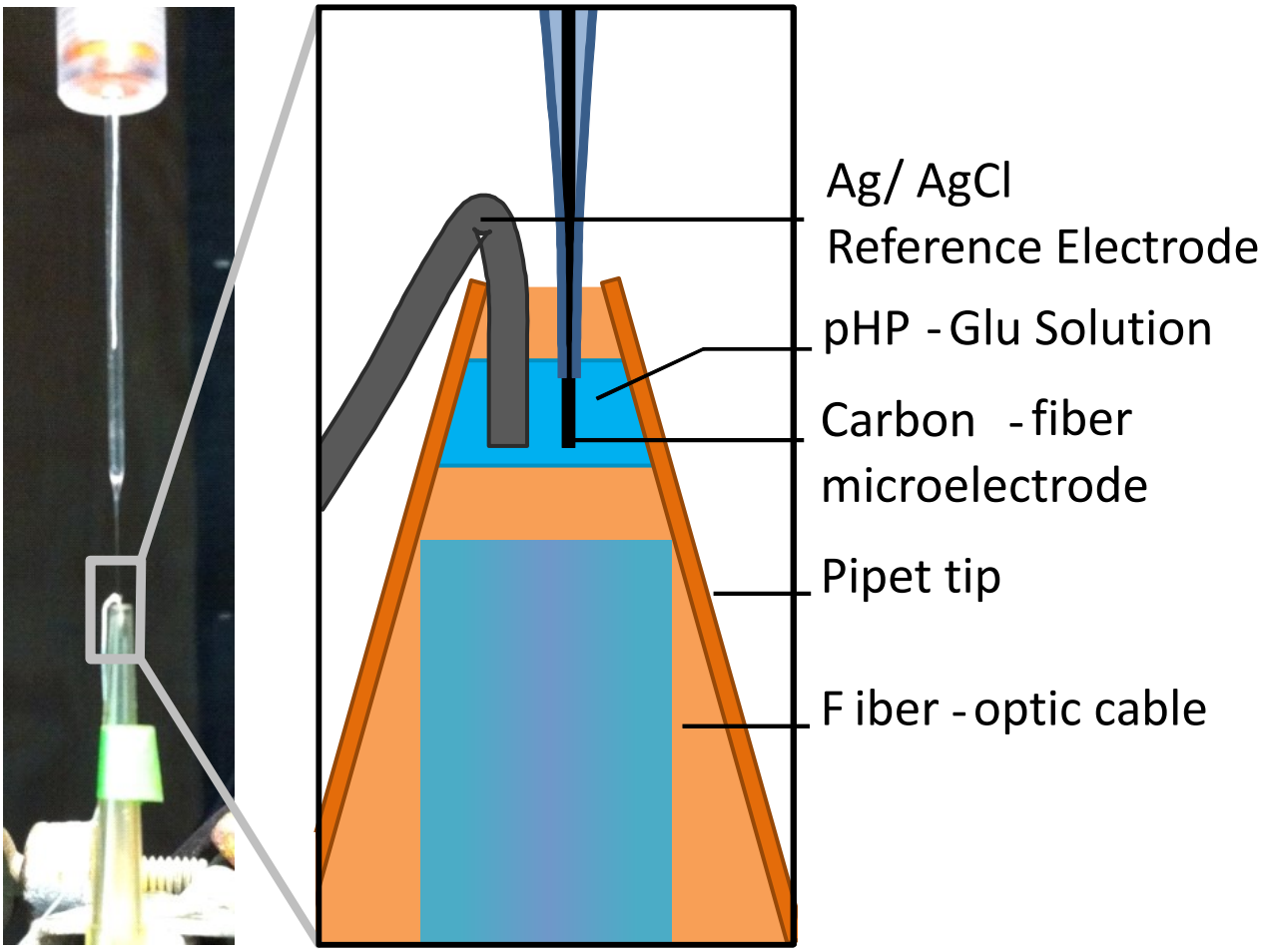

Figure 7. Photograph (left) and diagram of the fabricated microliter vessel for measuring the photo-uncaging of pHP-glutamate by FSCV followed by HPLC analysis. 5µL of pHP-Glu solution was pipetted into a pipette tip with a 1mm optical fiber place directly beneath. The working electrode and Ag/AgCl reference were then positioned into the solution.

Once the photo-uncaging of pHP-Glu is measured with FSCV, the electrodes were removed (Fig 8B) and the sample solution was carefully extracted with a pipette from the reaction vessel for HPLC analysis. 4HPAA concentration was measured as a function of UV exposure time by FSCV and HPLC analysis. The data from this analysis was used to generate two calibration curves relating current response measured via FSCV (Fig. 9A) and 4HPAA concentration via HPLC to exposure time(Fig 9B). These two calibration curves were then combined to generate a calibration curve directly relating current response to 4HPAA concentration (Fig. 9C). The direct quantification of 4HPAA by FSCV released by the photolysis of pHP-Glu can therefore be a means to indirectly quantify the release biologically active glutamate.

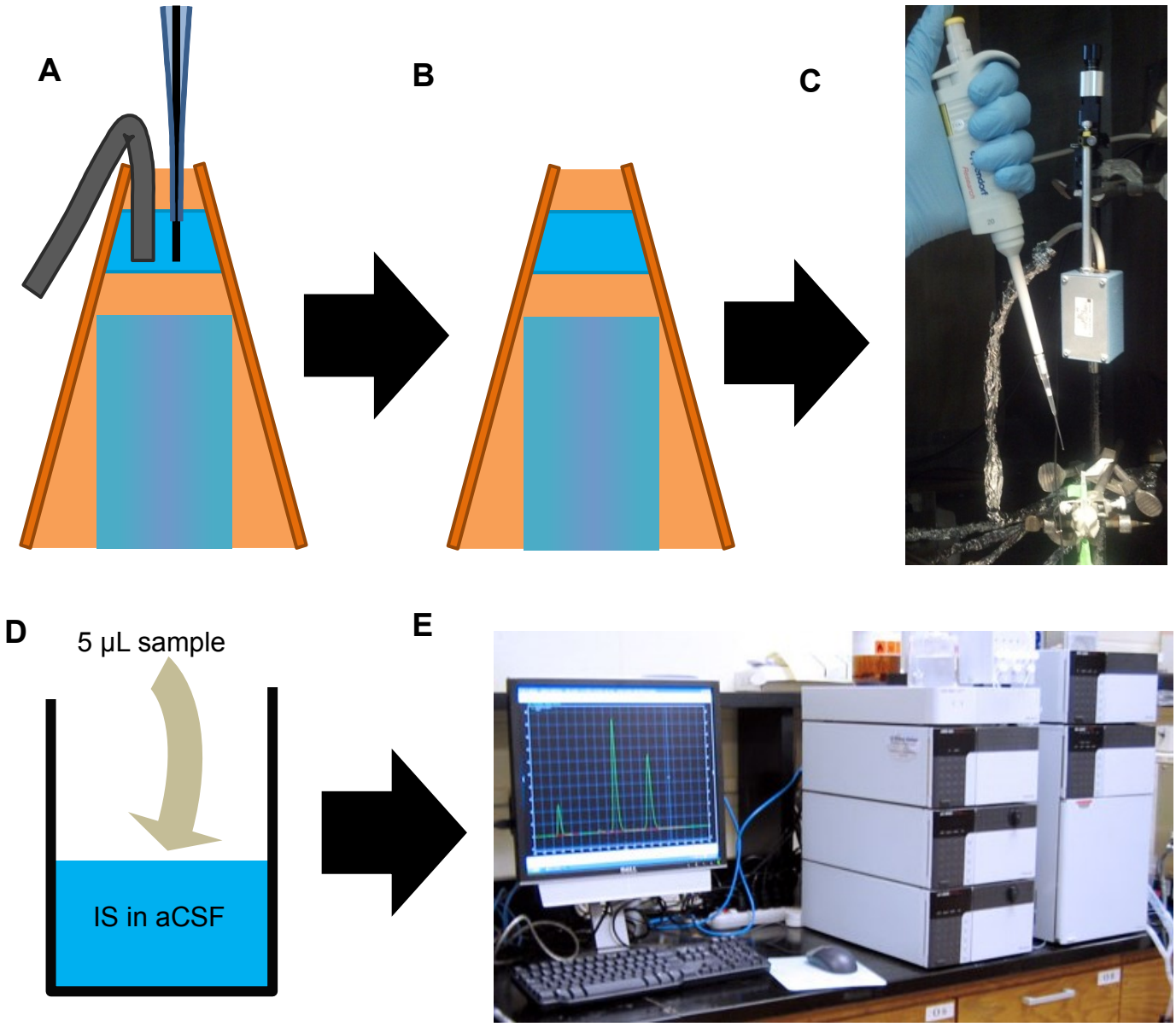

Figure 8. The process of using the microliter reaction vessel for FSCV measurements followed by HPLC Analysis. (A) The microliter reaction vessel with all components in place for FSCV measurements. (B) After taking FSCV measurements the working and reference electrodes are removed. (C) The sample is carefully extracted from the vessel by pipette. (D) the sample is transferred to an HPLC vial containing an internal standard in aCSF. (E) The sample is then analyzed by HPLC.

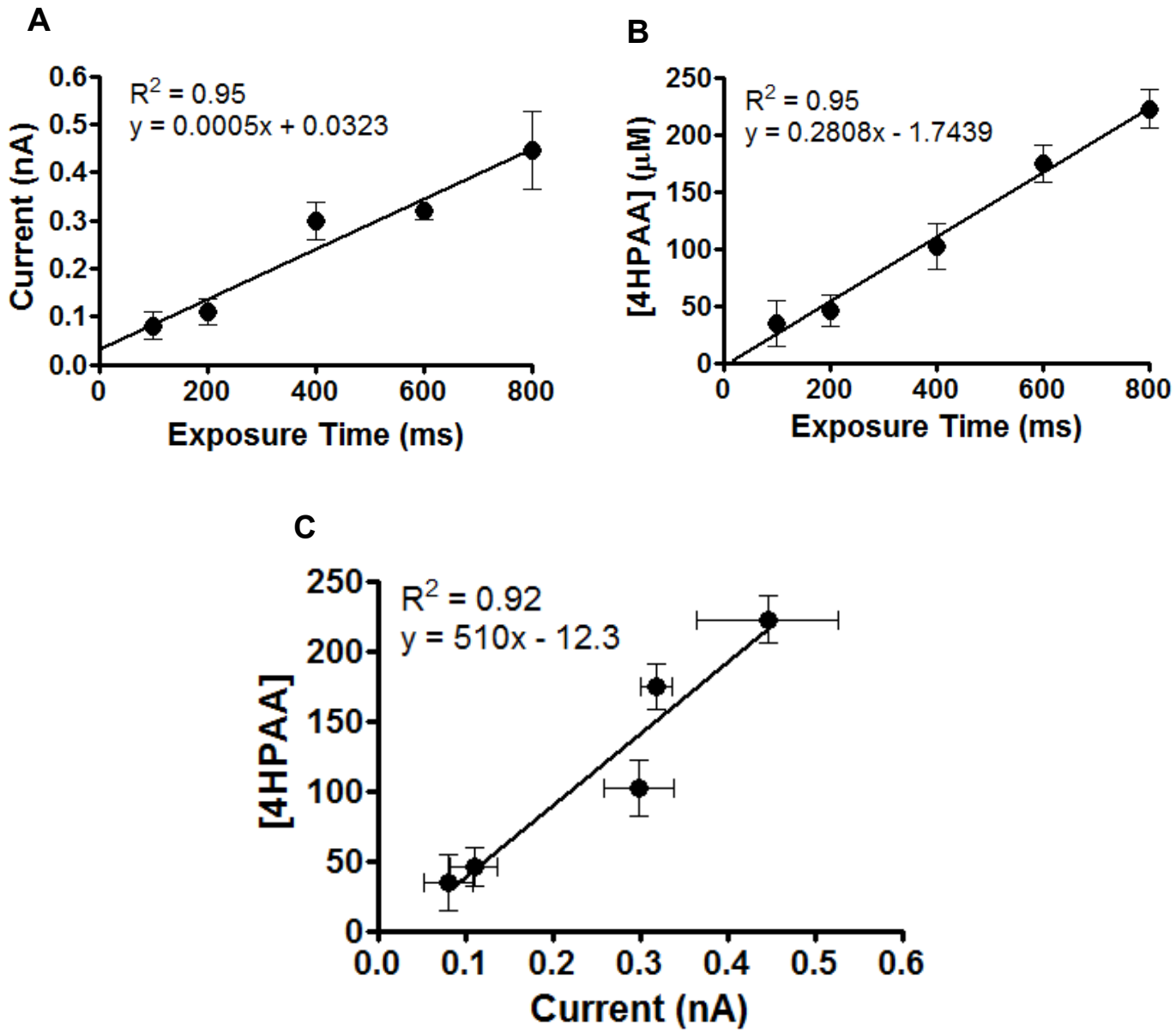

Figure 9. Generation of a calibration curve from the measuring the photo-uncaged of pHP-glutamate by FSCV followed by HPLC analysis. Two calibration curves relating current response measured via FSCV (Fig. 9A) and 4HPAA concentration via HPLC to exposure time (Fig 9B) were generated with sample from the microliter reaction vessel. These two calibration

curves were then combined to generate a calibration curve directly relating current response to 4HPAA concentration (Fig. 9C).

4.3.5 Application to brain slice experiments

It was the eventual goal of this study to apply this novel methodology to the brain. The high temporal and spatial resolution along with the ability to quantify the release of biologically active molecules can be applied to looking at real-time rapid biochemical interactions. Here we have successfully shown that we can simultaneously detect DA and 4HPAA with FSCV. As stated previously, it has recently been suggested that glutamate modulates dopamine release with hydrogen peroxide acting as a mediator.[61–63] Specifically, it has been suggested glutamate acts at AMPA receptors, inhibiting striatal DA release through a mechanism mediated by hydrogen peroxide (H_2O_2). One possible application of the methodology developed here would therefore be to elicit this response by photo-uncaging pHP-glutamate in the striatum while simultaneously detecting DA release.

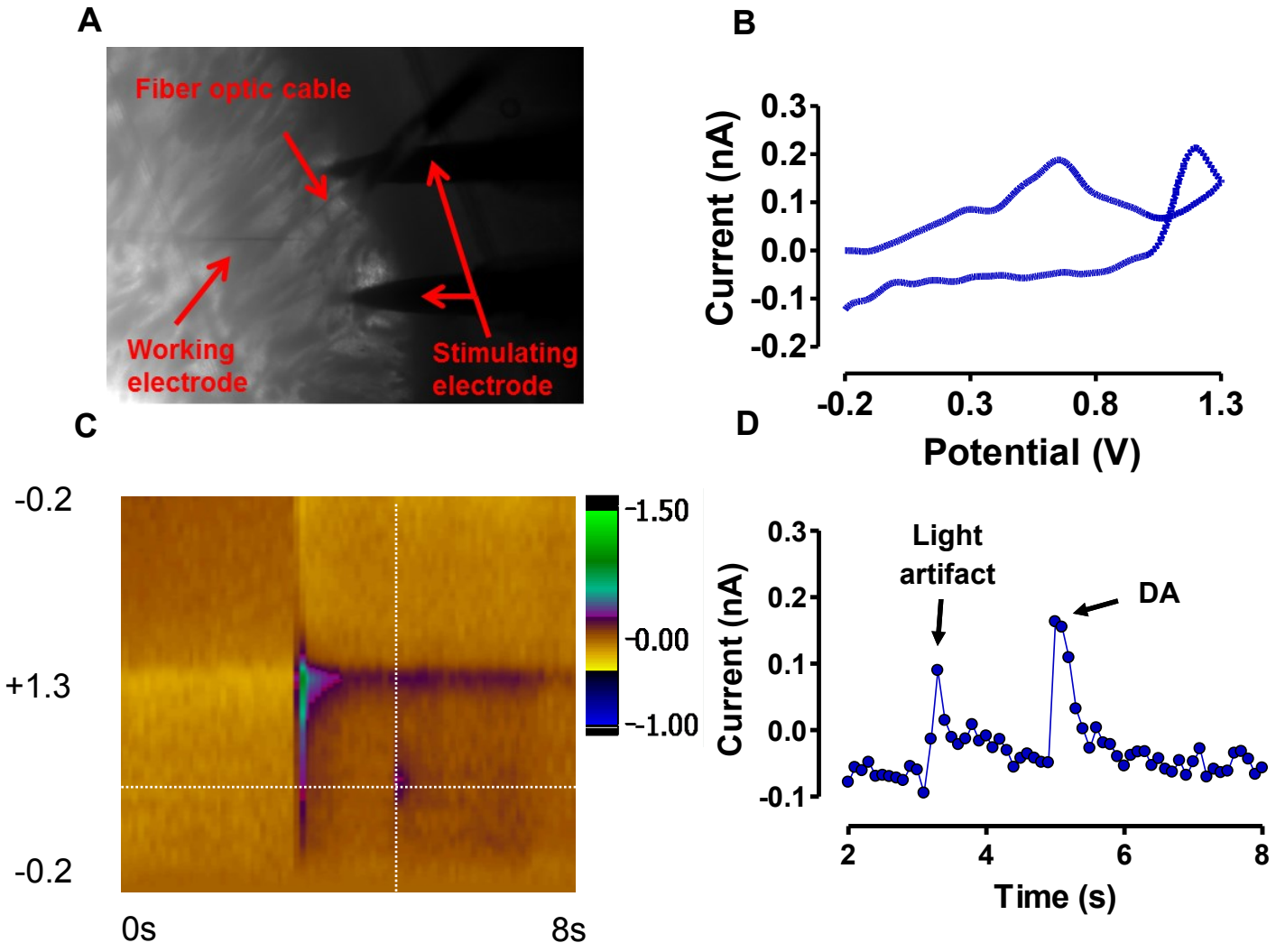

Figure 10. The uncaging of pHP-Glu and the simultaneous measurement of DA release in a brain slice. These measurements were taken in a coronal brain slice perfused with 200µM pHP-Glu in aCSF. (A) The stimulating electrode and working electrode were inserted 100µm deep into striatal tissue and an optical fiber was positioned to illuminate the tissue directly in contact with the working electrode active surface. (B) Representative cyclic voltammogram with both DA (at 0.6 V) and 4HPAA (at 1.1V) oxidation peaks present. (C) Representative color plot and (D) current response to the photo-uncaging of pHP-Glu followed by electrically-evoked DA release taken 2 seconds after the light pulse.

The next logical step was to expand upon this method and apply it to a brain slice experiment. Brain slices provide a nice bridge from *in vitro* to *in vivo* studies as they maintain much of the intact three dimensional neuroanatomical structure while providing ample surface area of the exposed region of interest to be accessed by our probes and solution. The simultaneous detection of DA and 4HPAA after the photo-uncaging of pHP-Glu was successfully carried out in a brain slice (Fig. 10). The light artifact from the light pulse at 5 seconds is clearly visible on the color plot (Fig. 10C) and is similar to what has been observed *in vitro*. DA release was stimulated two seconds after the light pulse. The simultaneous detection of stimulated DA release and 4HPAA released from the photo-uncaging of pHP-Glu is confirmed by the CV obtained (Fig 10B). The successful development of this method therefore provides a means to quantify sub-second neurotransmitter interactions.

It was and still is the goal of this study to apply the described method to look at Glu-DA interactions *in vivo*. Specifically, this method was applied to measure how the rapid release of biologically-active Glu via the photo-uncaging of pHP-Glu would impact stimulated DA release. Although we have successfully developed this methodology, further experiments examining how Glu modulates DA release in the striatum have failed to show a significant difference in stimulated DA release after the photo-uncaging of pHP-Glu. There are a number possibilities as to why we have yet to observe said result. The experiment itself is quite complex in that it includes the harvesting and maintenance of living tissue and the precise micropositioning of electrodes and optical fiber with limited space. The complexity of the experiment has also made it difficult to limit the amount of material (pHP-GLu) used to complete these studies. Despite these difficulties mentioned, we remain optimistic that this methodology will be used to successfully quantify the spatially resolved sub-second neurotransmitter interaction. Experiments

are currently being performed and optimized to look at the modulation of DA by Glu in the striatum.

4.4 Conclusion

We have successfully developed a method to quantify the liberation of biologically active comounds from the photo-uncaging of pHP caged compounds. FSCV was successfully employed to quantify 4HPAA release in response to the photo-uncaging of pHP-Glu. The quantification of 4HPAA indirectly allows for the quantification of the biomolecule (Glu here) release as a result of the photolysis. It was also demonstrated that the quantification of the liberated biomolecule as a result of the photo-uncaging of pHP-Glu could be measured while simultaneously quantifying DA concentration. This ability was demonstrated by performing *in vitro* studies in a microliter reaction vessel. The ability to quantify 4HPAA released from the photo-uncaging of pHP-Glu and DA by FSCV was confirmed via HPLC. This method was then successfully applied to a brain slice, where it was demonstrated that electrically-evoked DA release could be quantified while simultaneously measuring 4HPAA release after the photo-uncaging of pHP-Glu. We have therefore developed a novel method and provided a framework to electrochemically measure the interaction of biomolecules with extremely high spatial and temporal resolution.

4.5 References

(1) Klán, P., Šolomek, T., Bochet, C. G., Blanc, A., Givens, R., Rubina, M., Popik, V., Kostikov, A., and Wirz, J. (2013) Photoremovable Protecting Groups in Chemistry and Biology: Reaction Mechanisms and Efficacy. *Chem. Rev. 113*, 119–191.

(2) Ellis-Davies, G. C. R. (2007) Caged compounds: photorelease technology for control of cellular chemistry and physiology. *Nat. Methods 4*, 619–628.

(3) Adams, S. R., and Tsien, R. Y. (1993) Controlling cell chemistry with caged compounds. *Annu. Rev. Physiol. 55*, 755–784.

(4) Kaplan, J. H., Forbush III, B., and Hoffman, J. F. (1978) Rapid photolytic release of adenosine 5'-triphosphate from a protected analog: utilization by the sodium: potassium pump of human red blood cell ghosts. *Biochemistry (Mosc.) 17*, 1929–1935.

(5) Givens, R. S., Conrad, P. G., Yousef, A. L., Lee, J. I., Horspool, W. M., and Lenci, F. (2004) CRC Handbook of Organic Photochemistry and photobiology. *CRC Press Boca Raton*.

(6) Pelliccioli, A. P., and Wirz, J. (2002) Photoremovable protecting groups: reaction mechanisms and applications. *Photochem. Photobiol. Sci. 1*, 441–458.

(7) Park, C.-H., and Givens, R. S. (1997) New Photoactivated Protecting Groups. 6. p-Hydroxyphenacyl: A Phototrigger for Chemical and Biochemical Probes1, 2. *J. Am. Chem. Soc. 119*, 2453–2463.

(8) Lawrence, D. S. (2005) The preparation and in vivo applications of caged peptides and proteins. *Curr. Opin. Chem. Biol. 9*, 570–575.

(9) Kramer, R. H., Chambers, J. J., and Trauner, D. (2005) Photochemical tools for remote control of ion channels in excitable cells. *Nat. Chem. Biol. 1*, 360–365.

(10) Mayer, G., and Heckel, A. (2006) Biologically active molecules with a “light switch.” *Angew. Chem. Int. Ed. 45*, 4900–4921.

(11) Gorostiza, P., and Isacoff, E. Y. (2008) Optical switches for remote and noninvasive control of cell signaling. *Science 322*, 395–399.

(12) Lee, H.-M., Larson, D. R., and Lawrence, D. S. (2009) Illuminating the chemistry of life: design, synthesis, and applications of “caged” and related photoresponsive compounds. *ACS Chem. Biol. 4*, 409–427.

(13) Yu, H., Li, J., Wu, D., Qiu, Z., and Zhang, Y. (2010) Chemistry and biological applications of photo-labile organic molecules. *Chem. Soc. Rev. 39*, 464–473.

(14) Specht, A., Bolze, F., Omran, Z., Nicoud, J.-F., and Goeldner, M. (2009) Photochemical tools to study dynamic biological processes. *HFSP J. 3*, 255–264.

(15) Schatzschneider, U. (2010) Photoactivated biological activity of transition-metal complexes. *Eur. J. Inorg. Chem. 2010*, 1451–1467.

(16) Priestman, M. A., and Lawrence, D. S. (2010) Light-mediated remote control of signaling pathways. *Biochim. Biophys. Acta BBA-Proteins Proteomics 1804*, 547–558.

(17) Riggsbee, C. W., and Deiters, A. (2010) Recent advances in the photochemical control of protein function. *Trends Biotechnol. 28*, 468–475.

(18) Krauss, U., Drepper, T., and Jaeger, K.-E. (2011) Enlightened enzymes: strategies to create novel photoresponsive proteins. *Chem.- Eur. J. 17*, 2552–2560.

(19) Givens, R. S., Rubina, M., and Wirz, J. (2012) Applications of p-hydroxyphenacyl (pHP) and coumarin-4-ylmethyl photoremovable protecting groups. *Photochem. Photobiol. Sci. 11*, 472.

(20) Civillico, E. F., Rickgauer, J. P., and Wang, S. S.-H. (2011) Targeting and excitation of photoactivatable molecules: design considerations for neurophysiology experiments, in *Photosensitive Molecules for Controlling Biological Function*, pp 7–37. Springer.

(21) Brieke, C., Rohrbach, F., Gottschalk, A., Mayer, G., and Heckel, A. (2012) Light-controlled tools. *Angew. Chem. Int. Ed. 51*, 8446–8476.

(22) Callaway, E. M., and Katz, L. C. (1993) Photostimulation using caged glutamate reveals functional circuitry in living brain slices. *Proc. Natl. Acad. Sci. 90*, 7661–7665.

(23) Wang, S. S.-H., and Augustine, G. J. (1995) Confocal imaging and local photolysis of caged compounds: dual probes of synaptic function. *Neuron 15*, 755–760.

(24) Nerbonne, J. M. (1996) Caged compounds: tools for illuminating neuronal responses and connections. *Curr. Opin. Neurobiol. 6*, 379–386.

(25) Givens, R. S., and Lee, J.-I. (2003) The p-hydroxyphenacyl photoremovable protecting group. *J. Photoscience 10*, 37–48.

(26) Givens, R. S., Heger, D., Hellrung, B., Kamdzhilov, Y., Mac, M., Conrad, P. G., Cope, E., Lee, J. I., Mata-Segreda, J. F., Schowen, R. L., and Wirz, J. (2008) The Photo-Favorskii Reaction of *p* -Hydroxyphenacyl Compounds Is Initiated by Water-Assisted, Adiabatic Extrusion of a Triplet Biradical. *J. Am. Chem. Soc. 130*, 3307–3309.

(27) Ischiropoulos, H. (1998) Biological tyrosine nitration: a pathophysiological function of nitric oxide and reactive oxygen species. *Arch. Biochem. Biophys. 356*, 1–11.

(28) Takahama, U., Oniki, T., and Murata, H. (2002) The presence of 4-hydroxyphenylacetic acid in human saliva and the possibility of its nitration by salivary nitrite in the stomach. *FEBS Lett. 518*, 116–118.

(29) Givens, R. S., Rubina, M., and Wirz, J. (2012) Applications of p-hydroxyphenacyl (pHP) and coumarin-4-ylmethyl photoremovable protecting groups. *Photochem. Photobiol. Sci. 11*, 472.

(30) Goeldner, M., and Givens, R. (2005) Dynamic studies in biology: phototriggers, photoswitches and caged biomolecules. Wiley-VCH, Weinheim.

(31) Corrie, J. E., Furuta, T., Givens, R., Yousef, A. L., and Goeldner, M. (2005) Photoremovable protecting groups used for the caging of biomolecules. *Dyn. Stud. Biol. Phototriggers Photoswitches Caged Biomol.* 1–94.

(32) Kandler, K., Nguyen, T., Noh, J., and Givens, R. S. (2013) An Optical Fiber-Based Uncaging System. *Cold Spring Harb. Protoc. 2013*, pdb.top072900–pdb.top072900.

(33) Kandler, K., Katz, L. C., and Kauer, J. A. (1998) Focal photolysis of caged glutamate produces long-term depression of hippocampal glutamate receptors. *Nat. Neurosci. 1*, 119–123.

(34) Iversen, L., Iversen, S., Bloom, F. E., and Roth, R. H. (2008) Introduction to neuropsychopharmacology. Oxford University Press.

(35) Castillo, J., Dávalos, A., Naveiro, J., and Noya, M. (1996) Neuroexcitatory amino acids and their relation to infarct size and neurological deficit in ischemic stroke. *Stroke 27*, 1060–1065.

(36) Dávalos, A., Castillo, J., Serena, J., and Noya, M. (1997) Duration of glutamate release after acute ischemic stroke. *Stroke 28*, 708–710.

(37) Besancon, E., Guo, S., Lok, J., Tymianski, M., and Lo, E. H. (2008) Beyond NMDA and AMPA glutamate receptors: emerging mechanisms for ionic imbalance and cell death in stroke. *Trends Pharmacol. Sci. 29*, 268–275.

(38) Sun, D. A., Sombati, S., and DeLorenzo, R. J. (2001) Glutamate Injury–Induced Epileptogenesis in Hippocampal Neurons An In Vitro Model of Stroke-Induced "Epilepsy." *Stroke 32*, 2344–2350.

(39) Bullock, R. (1995) Strategies for neuroprotection with glutamate antagonists. *Ann. N. Y. Acad. Sci. 765*, 272–278.

(40) Castillo, J., Davalos, A., and Noya, M. (1998) Aggravation of acute ischemic stroke by hyperthermia is related to an excitotoxic mechanism. *Cerebrovasc. Dis. Basel Switz. 9*, 22–27.

(41) Kawahara, Y., Ito, K., Sun, H., Aizawa, H., Kanazawa, I., and Kwak, S. (2004) Glutamate receptors: RNA editing and death of motor neurons. *Nature 427*, 801–801.

(42) Bruijn, L. I., Miller, T. M., and Cleveland, D. W. (2004) Unraveling the mechanisms involved in motor neuron degeneration in ALS. *Annu Rev Neurosci 27*, 723–749.

(43) Trotti, D., Rolfs, A., Danbolt, N. C., Brown, R. H., and Hediger, M. A. (1999) SOD1 mutants linked to amyotrophic lateral sclerosis selectively inactivate a glial glutamate transporter. *Nat. Neurosci. 2*, 427–433.

(44) Cleveland, D. W., and Rothstein, J. D. (2001) From Charcot to Lou Gehrig: deciphering selective motor neuron death in ALS. *Nat. Rev. Neurosci. 2*, 806–819.

(45) Guo, H., Lai, L., Butchbach, M. E., Stockinger, M. P., Shan, X., Bishop, G. A., and Lin, C. G. (2003) Increased expression of the glial glutamate transporter EAAT2 modulates excitotoxicity and delays the onset but not the outcome of ALS in mice. *Hum. Mol. Genet. 12*, 2519–2532.

(46) Howland, D. S., Liu, J., She, Y., Goad, B., Maragakis, N. J., Kim, B., Erickson, J., Kulik, J., DeVito, L., and Psaltis, G. (2002) Focal loss of the glutamate transporter EAAT2 in a transgenic

rat model of SOD1 mutant-mediated amyotrophic lateral sclerosis (ALS). *Proc. Natl. Acad. Sci. 99*, 1604–1609.

(47) Vogels, O. J. M., Oyen, W. J. G., Van Engelen, B. G. M., Padberg, G., and Horstink, M. (1999) Decreased striatal dopamine-receptor binding in sporadic ALS: Glutamate hyperactivity? *Neurology 52*, 1275–1275.

(48) Sheldon, A. L., and Robinson, M. B. (2007) The role of glutamate transporters in neurodegenerative diseases and potential opportunities for intervention. *Neurochem. Int. 51*, 333–355.

(49) Hynd, M. R., Scott, H. L., and Dodd, P. R. (2004) Glutamate-mediated excitotoxicity and neurodegeneration in Alzheimer's disease. *Neurochem. Int. 45*, 583–595.

(50) Maragos, W. F., Greenamyre, J. T., Penney, J. B., and Young, A. B. (1987) Glutamate dysfunction in Alzheimer's disease: an hypothesis. *Trends Neurosci. 10*, 65–68.

(51) Minoshima, S., Giordani, B., Berent, S., Frey, K. A., Foster, N. L., and Kuhl, D. E. (1997) Metabolic reduction in the posterior cingulate cortex in very early Alzheimer's disease. *Ann. Neurol. 42*, 85–94.

(52) Hyman, B. T., Van Hoesen, G. W., and Damasio, A. R. (1987) Alzheimer's disease: glutamate depletion in the hippocampal perforant pathway zone. *Ann. Neurol. 22*, 37–40.

(53) Heien, M. L. A. V., Johnson, M. A., and Wightman, R. M. (2004) Resolving Neurotransmitters Detected by Fast-Scan Cyclic Voltammetry. *Anal. Chem. 76*, 5697–5704.

(54) Troyer, K. P., and Wightman, R. M. (2002) Dopamine Transport into a Single Cell in a Picoliter Vial. *Anal. Chem. 74*, 5370–5375.

(55) Ortiz, A. N., Kurth, B. J., Osterhaus, G. L., and Johnson, M. A. (2010) Dysregulation of intracellular dopamine stores revealed in the R6/2 mouse striatum. *J. Neurochem. 112*, 755–761.

(56) Ortiz, A. N., Oien, D. B., Moskovitz, J., and Johnson, M. A. (2011) Quantification of reserve pool dopamine in methionine sulfoxide reductase A null mice. *Neuroscience 177*, 223–229.

(57) Johnson, M. A., Rajan, V., Miller, C. E., and Wightman, R. M. (2006) Dopamine release is severely compromised in the R6/2 mouse model of Huntington's disease. *J. Neurochem. 97*, 737–746.

(58) Johnson, M. A., Villanueva, M., Haynes, C. L., Seipel, A. T., Buhler, L. A., and Wightman, R. M. (2007) Catecholamine exocytosis is diminished in R6/2 Huntington's disease model mice. *J. Neurochem. 103*, 2102–2110.

(59) Kraft, J. C., Osterhaus, G. L., Ortiz, A. N., Garris, P. A., and Johnson, M. A. (2009) In vivo dopamine release and uptake impairments in rats treated with 3-nitropropionic acid. *Neuroscience 161*, 940–949.

(60) Lee, T. H., Gee, K. R., Ellinwood, E. H., and Seidler, F. J. (1996) Combining "caged-dopamine" photolysis with fast-scan cyclic voltammetry to assess dopamine clearance and release autoinhibition in vitro. *J. Neurosci. Methods 67*, 221–231.

(61) Avshalumov, M. V., Patel, J. C., and Rice, M. E. (2008) AMPA Receptor-Dependent H2O2 Generation in Striatal Medium Spiny Neurons But Not Dopamine Axons: One Source of a Retrograde Signal That Can Inhibit Dopamine Release. *J. Neurophysiol. 100*, 1590–1601.

(62) Avshalumov, M. V., Chen, B. T., Marshall, S. P., Peña, D. M., and Rice, M. E. (2003) Glutamate-dependent inhibition of dopamine release in striatum is mediated by a new diffusible messenger, H2O2. *J. Neurosci. 23*, 2744–2750.

(63) Bao, L., Avshalumov, M. V., Patel, J. C., Lee, C. R., Miller, E. W., Chang, C. J., and Rice, M. E. (2009) Mitochondria Are the Source of Hydrogen Peroxide for Dynamic Brain-Cell Signaling. *J. Neurosci. 29*, 9002–9010.

(64) Kawagoe, K. T., Jankowski, J. A., and Wightman, R. M. (1991) Etched carbon-fiber electrodes as amperometric detectors of catecholamine secretion from isolated biological cells. *Anal. Chem. 63*, 1589–1594.

(65) Ortiz, A. N., Osterhaus, G. L., Lauderdale, K., Mahoney, L., Fowler, S. C., von Hörsten, S., Riess, O., and Johnson, M. A. (2012) Motor function and dopamine release measurements in transgenic Huntington's disease model rats. *Brain Res. 1450*, 148–156.

(66) Jackson, B. P., Dietz, S. M., and Wightman, R. M. (1995) Fast-scan cyclic voltammetry of 5-hydroxytryptamine. *Anal. Chem. 67*, 1115–1120.

(67) Hashemi, P., Danoski, E., Petrovic, J., Keithley, R. B., and Wightman, R. M. (2009) Voltammetric Detection of 5-Hydroxytryptamine Release in the Rat Brain. *Anal. Chem. 81*, 9462–9471.

(68) Cooper, S. E., and Venton, B. J. (2009) Fast-scan cyclic voltammetry for the detection of tyramine and octopamine. *Anal. Bioanal. Chem. 394*, 329–336.

(69) Shin, M., Kaplan, S. V., Raider, K. D., and Johnson, M. A. (2015) Simultaneous measurement and quantitation of 4-hydroxyphenylacetic acid and dopamine with fast-scan cyclic voltammetry. *The Analyst 140*, 3039–3047.

Chapter 5: Conclusions and Future Directions

5.1 Chemobrain Conclusions and Future Directions.

It has been revealed that striatal DA release is attenuated in chemotherapy-treated rats. It is our hypothesis that this attenuated release is at least partially responsible for the negative effects associated with chemobrain. It was found that this impaired neurotransmitter release was generalized across all regions of the striatum. However, there was no significant difference in total DA tissue content, which suggests that DA release attenuation is not simply the result of massive neurodegeneration but is actually an impairment in the mechanism of release itself. We looked at vesicular storage by isolating and mobilizing reserve pool DA using pharmacological manipulation; however, no significant difference was found.

We have begun to elucidate the underlying physiological mechanism of chemobrain by studying how real-time neurotransmission may be altered by chemotherapy treatment. One question that can be proposed is whether or not impaired release occurs in other neurotransmitter systems. We have since expanded our research to look at how serotonin (5HT) release in the dorsal raphe nucleus may be altered in chemobrain. These first experiments have revealed that 5HT release is also attenuated in carboplatin treated rats. There should therefore be further research regarding how other neurotransmitter systems may be implicated in chemobrain.

It should also be the goal of researchers investigating chemobrain to elucidate the mechanism leading to release impairments. It is interesting that a variety of chemotherapeutic agents cause chemobrain although many of them do not cross the blood brain barrier.[1] Both blood brain barrier permeable and impermeable can induce programmed cell death and inhibit

neuronal repair. Whether or not metabolites enter the blood brain barrier or if changes in blood brain barrier permeability occur during or after chemotherapy treatment should be addressed.

Another possibility is that chemotherapeutic agents can inhibit neuronal signaling by affecting myelination. In fact, it has been found that some chemotherapeutic agents can destroy oligodendrocytes, which are responsible for proper myelination.[2] investigating how chemotherapy may affect myelination *in vitro* would therefore be interesting.

Here, I have presented behavior measurements that involve general locomotion. It is imperative that more complex and rigorous behavior paradigms be completed in future studies, possibly in conjunction with *in vivo* measurements to establish that measured cognitive impairments correspond to electrochemical measurements. A series of behavioral paradigms involving learning and memory could be informative with or without simultaneous electrochemical measurements and include open field habituation, passive avoidance task, the Morris water maze, object recognition task, and differential reinforcement at lower rates.

The research presented here should be continued with the intention to find possible points of intervention regarding the alleviation or elimination of chemobrain. For instance, it is possible that exogenous treatment with glucocorticoid could raise endogenous DA levels in the striatum and could therefore could be used to alleviate or counteract the cognitive impairments associated with chemobrain. Oxidative stress may also play an important role in chemobrain and the ability for antioxidants to prevent or eliminate such cognitive impairments should be investigated.

5.2 Regional differences in striatal DA release in R6/2 mice conclusions and future directions.

In the work presented here, it was shown that electrically-evoked DA release is progressively attenuated in the striatum of R6/2 mice and that this attenuation is more severe in the dorsal striatum. Moreover, when applying a 120 stimulation pulse-train, it was found that DA release was only significantly attenuated in the dorsal striatum, suggesting that the ventral striatum is less vulnerable to the mechanism of impairment caused by the HD mutation. It was also found that the amount of dopamine transporter (DAT) is present in the striatum is significantly lower in R6/2 mice in comparison to their wild type controls. There was no regional difference found in DAT distribution, however. These data collectively suggest that the genetic mutation involved in HD leads to the increased vulnerability of the dorsal striatum in comparison to the ventral striatum, therefore providing insight into the disease mechanism.

These novel findings indeed suggest that the dorsal striatum is more vulnerable to the deleterious effects of HD. The next logical question would be, 'Why?' I believe *in vivo* studies that are sensitive to could be integral in determining why these region specific susceptibilities occur in HD model rodents. *In vivo* studies would allow for the investigation of intact neuronal pathways that differentially innervate the striatum.

5.3 Caged compound photo-activation and FSCV conclusions and future directions.

We have successfully developed a method to quantify the liberation of biologically active compounds from the photo-uncaging of pHP caged compounds with FSCV. FSCV was successfully employed to quantify 4HPAA release in response to the photo-uncaging of pHP-

Glu.[3] It was also demonstrated that the quantification of the liberated biomolecule as a result of the photo-uncaging of pHP-Glu could be measured while simultaneously quantifying DA concentration. This method was validated with HPLC via our fabricated microliter reaction vessel. We then have successfully applied this method to a brain slice experiment.

I could not begin to address all of the potential future directions of this developed method. The ability to apply, release and quantify biologically active material with such high spatial and temporal resolution could offer nearly limitless application to future biological research. Although I have reported the successful development of this novel method, it is our initial goal is to monitor how glutamate modulates striatal DA release in real time and this work is currently being done in our lab.

5.4 References

(1) Ginos, J. Z., Cooper, A. J., Dhawan, V., Lai, J. C., Strother, S. C., Alcock, N., and Rottenberg, D. A. (1987) [13N]cisplatin PET to assess pharmacokinetics of intra-arterial versus intravenous chemotherapy for malignant brain tumors. *J. Nucl. Med. Off. Publ. Soc. Nucl. Med. 28*, 1844–1852.

(2) Dietrich, J., Han, R., Yang, Y., Mayer-Pröschel, M., and Noble, M. (2006) CNS progenitor cells and oligodendrocytes are targets of chemotherapeutic agents in vitro and in vivo. *J. Biol. 5*, 22.

(3) Shin, M., Kaplan, S. V., Raider, K. D., and Johnson, M. A. (2015) Simultaneous measurement and quantitation of 4-hydroxyphenylacetic acid and dopamine with fast-scan cyclic voltammetry. *The Analyst 140*, 3039–3047.